MECHANISM OF THE HYDROXYLATION REACTIONS CATALYZED BY 4-HYDROXYPHENYLPYRUVATE DIOXYGENASE AND HYDROXYMANDELATE SYNTHASE

by

Dhara D. Shah

A Dissertation Submitted in

Partial Fulfillment of the

Requirements for the Degree of

Doctor of Philosophy

in Chemistry

at

The University of Wisconsin-Milwaukee

August 2014

ABSTRACT

MECHANISM OF THE HYDROXYLATION REACTIONS CATALYZED BY 4-HYDROXYPHENYLPYRUVATE DIOXYGENASE AND HYDROXYMANDELATE SYNTHASE

by

Dhara D. Shah

The University of Wisconsin-Milwaukee, 2014
Under the Supervision of Dr. Graham R. Moran

4-Hydroxyphenylpyruvate dioxygenase (HPPD) and Hydroxymandelate synthase (HMS) carry out highly similar complex dioxygenation reactions using the substrates, 4-hydroxyphenylpyruvate (HPP) and dioxygen. HPPD catalyzes decarboxylation, aromatic hydroxylation and substituent migration (NIH shift) in a single catalytic cycle to form homogentisate (HG), whereas HMS catalyzes decarboxylation and aliphatic hydroxylation to give hydroxymandelate (HMA). Wild-type HPPD, HPPD variants and HMS variants produce both native and non-native products. Based on this observation, we have employed a product analysis method with HPP deuterium substitutions (ring or benzylic) that reveal kinetic isotope effects from intermediate partitioning ratios. In this study we offer evidence for the 1) oxygenation intermediates for HPPD and HMS pathways and 2) mechanism of NIH shift in HPPD. Our data with ring-deutero HPP suggest that the native hydroxylation reaction of HPPD to form HG occurs via a ring epoxide intermediate whereas secondary normal KIEs with 3',3'-diduetero HPP in HPPD indicate that bond cleavage in the substituent shift step occurs via a homolytic biradical mechanism (biradical). HMS variants show a small normal KIE with 3',3'-diduetero

HPP, indicating displacement of a benzylic deuteron in the hydroxylation step which has a multiplicative component from geometry changes for the non-abstracted deuterium. When R-3′-monodeutero-HPP is used as a substrate for HMS reaction, the secondary KIE observed indicates sp^3 geometry at the benzylic carbon in the transition state for the hydroxylation step.

TABLE OF CONTENTS

LIST Of FIGURES

LIST OF SCHEMES

LIST OF TABLES

ACKNOWLEDGMENTS

I would like to thank my advisor Dr. Graham R. Moran, my thesis committee members, colleagues in the laboratory, my family and friends for their support and encouragement during my Ph.D. This work could not have been possible without all of them.

Dr. Graham R. Moran has been a constant source of valuable laboratory and life skills throughout my Ph.D. His motivation, enthusiasm and scientific discussions have been very useful during difficult experiments. I am very thankful to Dr. Moran for introducing me to the wonderful world of enzymes.

I would like to thank my committee members, Dr. A. Andy Pacheco, Dr. David N. Frick, Dr. Nicholas R. Silvaggi and Dr. Guilherme L. Indig for their constant direction and inputs during committee meetings and all their support.

This work could not have been completed without the help of my current and former lab members. Dr. June M. Brownlee, Dr. Judith M. Bates and Dr. John A. Conrad helped me on this project initially. Thank you Brett A. Beaupure and Matthew R. Hoag, you guys have been really good lab colleagues.

I would like to thank my family for being so wonderful and supporting me through every step of my life. I would not have been able to accomplish this without you. Thank you mom, dad and my dear sister, Nira. I would like to thank my husband, Abhishek for his immense support and love throughout my Ph.D. You have been a great friend, colleague, and a wonderful listener. I thank you very much for listening to my endless research and lab talks so patiently for hours. Your constructive criticisms and your motivation have helped me a lot. Thank you for everything.

Chapter 1

4-Hydroxyphenylpyruvate Dioxygenase and Hydroxymandelate Synthase: Two-substrate α-Keto Acid Dependent Oxygenases

1.1 Introduction

Although oxygen reduction is thermodynamically favored, kinetically it occurs slowly. This can be attributed to the spin-triplet ground state of the molecular oxygen, which has to react with singlet-state biological molecules. Oxygenases catalyze formation of reactive oxygen species from dioxygen and add one or both oxygen atoms to a specific molecule. Oxygenases make the reduction of dioxygen rapid by utilizing a cofactor (generally a metal ion with paramagnetic properties or an organic prosthetic group capable of one-electron chemistry), which bridges the reaction of singlet-state molecules with triplet-state oxygen. Fe(II) is the most commonly found cofactor utilized by oxygenases. Among the non-heme Fe(II)-dependent oxygenases, α-ketoglutarate (αKG) is the most prevalent source of electrons for dioxygen activation (1). These α-keto acid dependent oxygenases (α-KAOs) utilize a ferrous ion and the oxidative power of dioxygen to collectively perform an extremely broad set of chemistries throughout secondary metabolism. Some examples are enzymes involved in protein modifications, alkylated DNA/RNA repair, antibiotic biosynthesis, biosynthesis of plant products, lipid metabolism and oxygen sensing (2). The majority of the α-KAOs utilize three substrates: molecular oxygen, αKG, and a substrate that is specific to each enzyme. These enzymes typically catalyze two half-reactions, initial decarboxylation of the αKG and then oxidation of the specific substrate. Grouped within the α-KAOs family are two important enzymes that require only two substrates; i.e., 4-hydroxyphenylpyruvate dioxygenase (HPPD) and hydroxymandelate synthase (HMS). These sister enzymes accomplish the fundamental catalytic chemistry observed in essentially all α-KAO family members without requiring αKG. For these enzymes, the requisite α-keto acid is supplied from the

pyruvate substituent of 4-hydroxyphenylpyruvate (HPP), the organic substrate common to both enzymes. The decarboxylation half-reaction is thought to be largely equivalent in HPPD and HMS, while the oxidation/hydroxylation half-reactions differ in regioselectivity and complexity. HPPD induces oxidative decarboxylation of HPP followed by aromatic hydroxylation and substituent migration (known as the NIH shift), whereas HMS accomplishes only decarboxylation and aliphatic hydroxylation at the benzylic carbon (Scheme 1.1).

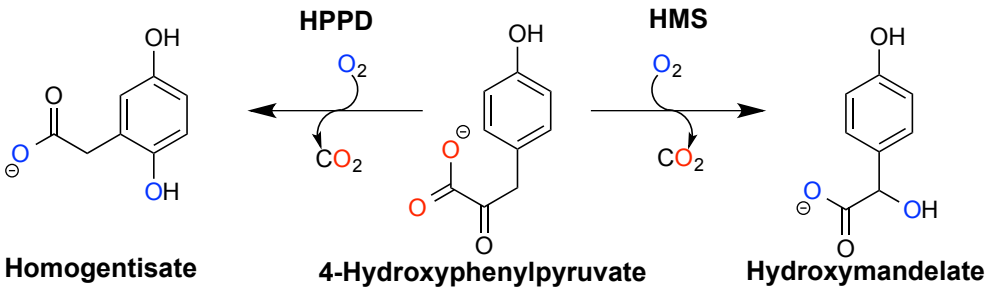

Scheme 1.1 Reactions catalyzed by HPPD and HMS

The ubiquity of the HPPD reaction has meant that it has been enlisted to participate in important added roles in a variety of organisms. This has resulted in its inhibition having unique significance in each kingdom of life and has become the basis for the development of herbicides and therapeutics.

1.2 Natural Context

Both HPPD and HMS acquire HPP from the first step of tyrosine catabolism (Scheme 1.2), a pathway that comprises five enzyme activities common to essentially all aerobes that yields acetoacetate and fumarate for use in energy-yielding metabolism (Scheme 1.2-black structures).

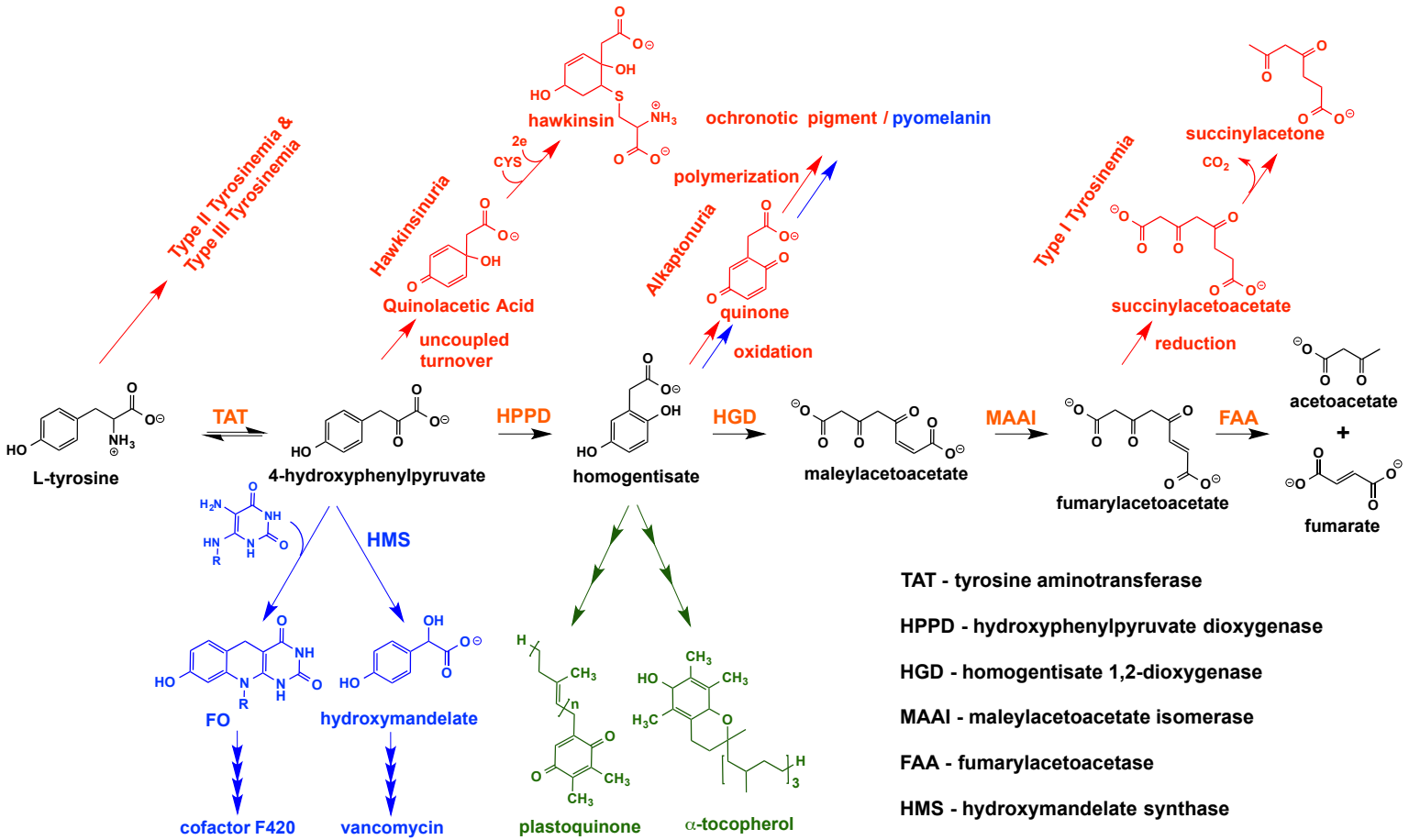

Scheme 1.2 Tyrosine catabolism. Reactions shown in black depict the typical steps of the tyrosine catabolism pathway. Reactions shown in red are mammalian metabolic disorders. Reactions depicted in blue are from bacteria and archaea. Reactions in green occur in photosynthetic organisms.

HPPD catalyzes the committed second step of this pathway in which HPP is converted to 2,5-dihydroxyphenylacetate (homogentisate, HG) (3). It was believed that, HPP to homogentisate conversion was catalyzed by two separate proteins until in 1957 Hager et al., demonstrated that this transformation was in fact catalyzed by a single protein HPPD (3). Since its discovery the HPPD reaction has generated a great deal of interest due to the curious chemical transformation catalyzed, but also as inhibition of this chemistry has unique important outcomes. The reason for this is that tyrosine catabolism metabolites provide biosynthetic stocks for the production of various physiologically important molecules that are unique in each kingdom. Examples are plastoquinone and tocopherols in photosynthetic organisms (4), melanin in fungi and bacteria (5), and cofactor F420 in mycobacteria and archaea (6). A relatively new branch from tyrosine catabolism was identified with the discovery of a protein having a similar sequence to that of HPPD, but that acted only on the pyruvate substituent of HPP (Scheme 1.1) to form 4-hydroxymandelate (HMA) (7). It transpired that this enzyme, HMS, catalyzes the initial step in the biosynthesis of 4-hydroxyphenylglycine, a building block of various peptide antibiotics (8).

1.2.1 Role in Photosynthesis

In 1968, Hellyer et al identified oils secreted from 24 plant species that contained leptospermone, a 1,3,3'-triketone that is secreted as an allelopathic agent (9). Usnic acid is a second example of a naturally occurring molecule that has this triketone arrangement and also serves to inhibit plant growth (Scheme 1.3A). Plants exposed to these compounds produce chlorophyll and carotenoids in decreased amounts that results in

bleaching and necrosis and eventual death (9-13). Synthetic derivatives based on the leptospermone scaffold have brought new and more effective herbicides (Scheme 1.3). It was initially believed that these triketones blocked carotenoid biosynthesis pathway by inhibiting phytoene desaturase. It was later discovered that rats fed with the synthetic triketone, NTBC, showed increased levels of tyrosine in blood and HPP in urine. This indicated a negative influence in the tyrosine catabolism pathway. Later studies established that NTBC blocked the first committed step of tyrosine catabolism inhibiting HPPD (14). In early 2000, the mode of action for a natural triketone - usnic acid was also confirmed to be HPPD inhibition (11). Since then this observation has been validated with both in vivo and in vitro inhibition of plant derived HPPDs by various triketone inhibitors (14). In photosynthetic organisms the HPPD reaction provides HG for the biosynthesis of plastoquinone (a redox cofactor that bridges the photosystems), and tocopherols (antioxidant lipophilic plant hormones) (15); HPPD is therefore required for photosynthesis. 2-(2-nitro-4-fluoromethylbenzoyl)-1,3-cyclohexanedione (NTBC) was one of the earliest synthetic HPPD herbicides identified and has remained the paradigm HPPD inhibitor despite never being marketed for agricultural use (*vide infra*) (14). Sulcotrione, mesotrione, isoxaflutole, and tembotrione are a few examples of highly successful pre- and post-emergent broadleaf herbicides that target HPPD.

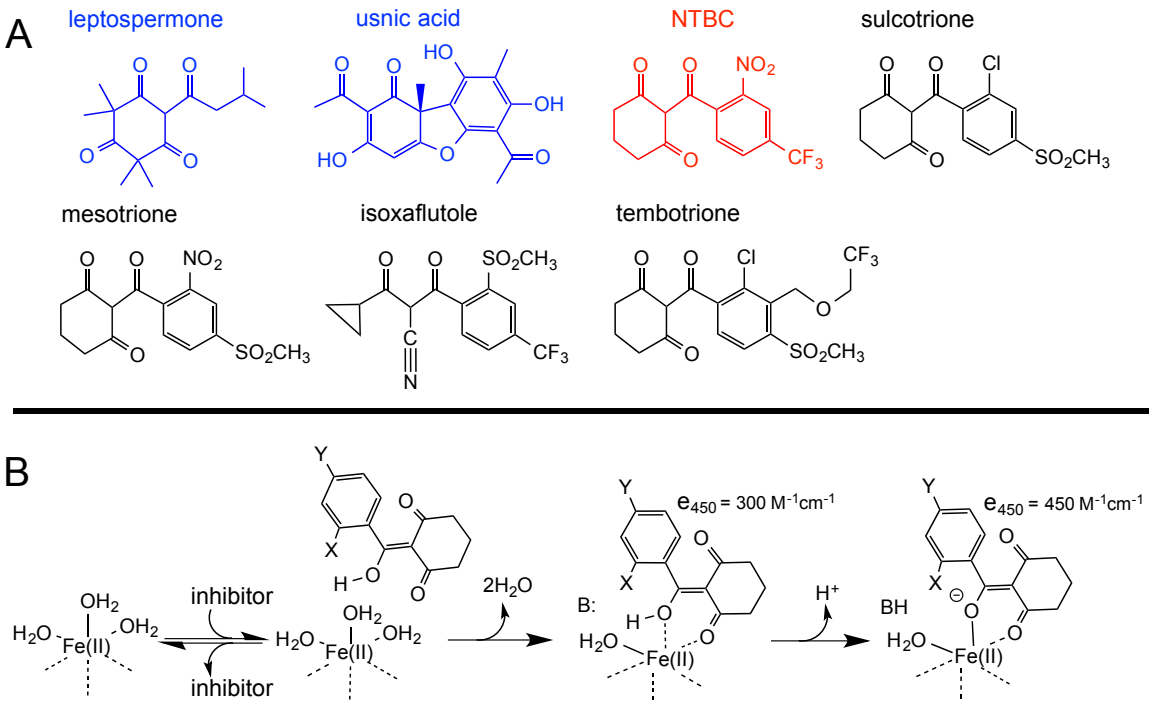

Scheme 1.3 (A) Examples of HPPD inhibitors. Molecules in blue are naturally occurring. NTBC, in red, is used for therapeutic purposes. Inhibitors shown in black are the active components of commercially available herbicides. (B) A minimal kinetic mechanism for association of inhibitors with HPPD.

1.2.2 Role in Mammals

In mammals tyrosine catabolism is required to diminish blood concentrations of this highly insoluble amino acid. Five inborn errors of tyrosine catabolism result in metabolic disorders (Scheme 1.2, red structures). Type II tyrosinemia is caused by a lack of tyrosine aminotransferase activity. Elevated blood tyrosine levels are observed in patients with this disease resulting in mild intellectual impairment, corneal opacities, and palmoplantar hyperkeratosis (16). Mutations in the gene encoding HPPD cause type III tyrosinemia and hawkinsinuria. Type III tyrosinemia, arises from mutations that render HPPD inactive. Due to the reversibility of the tyrosine aminotransferase reaction, this leads to elevated blood tyrosine and large excretion of tyrosine derivatives in urine (17).

As such, patients with type II and type III tyrosinemias have similar pathologies. Type III tyrosinemia is an autosomal recessive disorder because one of the alleles would produce functional HPPD and only a homozygote would show clinical symptoms. Hawkinsinuria results from a specific mutation in the gene coding for HPPD that expresses an active enzyme that catalyzes an abortive reaction (17,18). This disease is thought to be an autosomal dominant disorder, as only one mutated allele is required for the symptoms of the disease to manifest. This disease is characterized by quiescence and a general inability to thrive during infancy as a consequence of persistent acidosis, vomiting, diarrhea, hair growth abnormalities and liver enlargement in some cases (19). Curiously, the condition seems to self-correct at approximately two years of age for reasons that are unknown (20,21). The disorder is diagnosed by the presence of hawkinsin in the urine. In addition to hawkinsin, the unusual metabolites quinolacetic acid (QAA), 4-hydroxyphenyllactic acid, 4-hydroxyphenylacetic acid (HPA), 4-hydroxycyclohexylacetic acid, and 5-oxoproline are also excreted (22). The causative mutation for the occurrence of hawkinsinuria was thought to be an N-terminal alanine to threonine change (A33T) from the case studies of two patients in early 2000 (17). This was later shown to be a frequent polymorphism (23). Recently, the causative mutation for hawkinsinuria was shown to be a missense mutation resulting in an Asn to Ser variant (N241S in human HPPD) (18). This Asn is conserved in HPPD primary structure and the mutation at this position was later explored with the structurally equivalent *Rattus norvegicus* N241S HPPD and *Streptomyces avermitilis* N245S HPPD variants. In place of HG, the variant enzymes form QAA that is prone to react via a Michael addition with cellular thiols to form a two-electron oxidized form of hawkinsin (Scheme 1.2) (24-26).

In this abortive reaction of HPPD, oxidative decarboxylation and ring hydroxylation occur efficiently but the shift reaction does not occur resulting in the dissociation of a premature product, QAA. HPPD variants with this mutation are subject to NTBC inhibition in a similar manner to wild-type HPPD, suggesting a role for HPPD inhibitors as therapeutics for hawkinsinuria patients (24).

Alkaptonuria is the oldest known inherited metabolic disorder. In 1902, Garrod coined the term 'inborn error of metabolism' and speculated that alkaptonuria is caused by inactivity or deficiency of the enzyme involved in the cleavage of the HG aromatic ring (27,28). In 1958, La Du *et al*. established the deficiency of homogentisate 1,2-dioxygenase (HGD) activity, the third enzyme in the tyrosine catabolism pathway, in the manifestation of the disease (29). Patients with alkaptonuria excrete dark, melanin-laden urine arising from the oxidation and polymerization of HG. These pigments also accumulate in tissues where they cause ochronosis, a darkening of cartilage and bones, and lead to arthritic joint destruction and deterioration of cardiac valves (30). HPPD inhibition by NTBC has been tested successfully as a therapy for alkaptonuria patients, causing pronounced abatement of symptoms (30-32).

The fourth step of the tyrosine catabolism pathway is catalyzed by maleylacetoacetate isomerase. Any deficiency in the activity of this enzyme is not deleterious as maleylacetoacetate can be converted to fumarylacetoacetate and succinylacetone via a glutathione-mediated nonenzymatic bypass (33), and both of these molecules are reported as substrates for the last enzyme in the pathway, fumarylacetoacetase. The most severe and morbid tyrosinemia is type I. The primary pathological signature is early onset of liver cirrhosis, renal tubular defects and ultimately

hepatocellular carcinoma (34). Type 1 tyrosinemia is caused by the deficiency of fumarylacetoacetase activity. As such, fumarylacetoacetate accumulates and leads to the formation of succinylacetoacetate and succinylacetone, which have been linked with liver and kidney damage possibly due to facile reactions with cellular thiols (35). Liver transplantation was once the only effective therapy to treat patients with type I tyrosinemia (36); however, in 1977 inhibition of HPPD activity was suggested as an alternative approach (35). Patients treated with NTBC for several months show a marked decrease in the plasma succinylacetoacetate and succinylacetone concentrations and improved liver function. These initial trials established the current era of FDA approved herbicidal treatment of type I tyrosinemia (37).

In summary, inhibition of HPPD by NTBC has provided established or potential therapies for three of the five inborn errors of tyrosine catabolism. The therapeutic use of NTBC, however, can lead to type II and III tyrosinemia-like symptoms including high blood tyrosine levels, which can result in corneal opacities and suppression of IQ (38-40).

1.2.3 Role in Microorganisms

In Scheme 1.2, the blue reactions represent tyrosine catabolism branches that are known to occur in bacteria and archaea. These branches function in pathogenesis, redox reactions (coenzymes), and competition (antibiotic production). It was in this latter function that HMS was discovered (7,8). HMS diverts HPP from the tyrosine catabolism pathway and catalyzes the first step in the biosynthesis of 4-hydroxyphenylglycine. Based on the sequence similarity of HMS to HPPD, it was hypothesized that HMS might be involved in the biosynthesis of 4-hydroxyphenylglycine. The incubation of this protein

with the substrates for HPPD showed 4-hydroxymandelate as a product and not homogentisate and thus was named 4-hydroxymandelate synthase (8). The early labeling studies confirmed that tyrosine was incorporated into the 4-hydroxyphenylglycine structure of vancomycin (8,41). In 2000, Hubbard et al studied the four activities that comprise the pathway for the formation of 4-hydroxyphenylglycine in the chloroeremomycin biosynthetic cluster of *Amycolatopsis orientalis* (Scheme 1.4). The first activities yield 4-hydroxyphenylpyruvate from both prephenate and tyrosine via respective dehydrogenase and aminotransferase activities. 4-Hydroxyphenylglycine is a non-proteinogenic amino acid and a substructure for many macrocyclic non-ribosomal peptide antibiotics including vancomycin, complestatin, and chloroeremomycin.

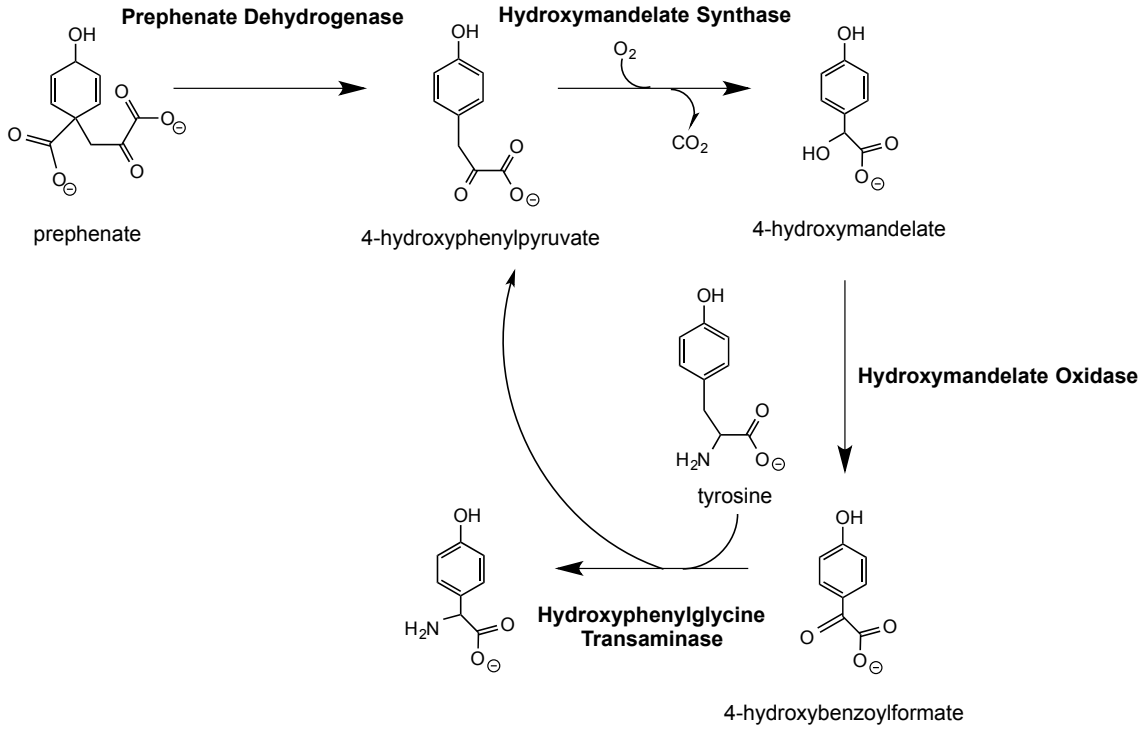

Scheme 1.4 The metabolic cycle for the formation of 4-hydroxyphenylglycine (7)

In another synthetic branch that occurs in mycobacteria and methanogenic archaea, HPP is diverted from tyrosine catabolism and condensed with a pyrimidine dione to form FO, the redox active portion of cofactor F420 (42,43). F420 is a cofactor for F420 dependent glucose-6-phosphate dehydrogenase in *mycobacterium* species, whereas in *archaea* it is necessary for the reactions catalyzed by hydrogenase, formate dehydrogenase, methylene-tetrahydromethanopterin dehydrogenase, alcohol dehydrogenase, methylene-tetrahydromethanopterin reductase and quinone oxidoreductase (44). Numerous pathogenic bacteria (e.g. *Legionella*, *Shewanella*, and *Pseudomonas* spp.) are known to produce pyomelanin to aid virulence, and HPPD has been identified as the virulence factor associated with pigment production (45). It is believed that HG oxidation and polymerization yield pyomelanin and that this over-production is selected for when the bacterial population experiences environmental stresses such as the oxidative onslaught brought on by the immune system (46). In clinical isolates from cystic fibrosis patients with persistent *P. aeruginosa* infections, bacteria exhibit increased extracellular pyomelanin production resulting from mutation in the *HGD* gene (47). Increased pyomelanin production is linked to the increased persistence of infecting bacteria (5,48). Another study on *P. aeruginosa* showed a development of small diverse subpopulations inside the biofilm. One of these subpopulations produced increased pyomelanin, which may be a structural component of the biofilm (49). *B. cenocepacia* is an opportunistic pathogen for cystic fibrosis (CF) patients. This bacterium targets lungs of CF patients and causes persistent inflammation, deteriorates the lung function and in extreme cases, develops a sepsis-like syndrome. This infection causes increased inflammatory response to produce large quantities of reactive

oxygen species in CF patients. *B. cenocepacia* producing increased pyomelanin is known to survive in phagocytic vesicles within macrophage cells by scavenging free radicals with the aid of pyomelanin. HPPD inhibition through NTBC, however, causes reduced pigment production and increases clearance of pathogens by macrophages (50).

Tyrosine catabolism and HPPD have been linked to the establishment of specific fungal infections. For the fungus *Paracoccidioides brasiliensis* the mycelium-to-yeast morphological transition occurring inside the pulmonary epithelium is crucial to establishing the infection in humans. HPPD is overexpressed during this transition, and in vitro studies demonstrate that NTBC prevents the change in morphology and halts infection, opening a door to the treatment of dimorphic fungal infections by HPPD inhibition (51).

1.3 Structure

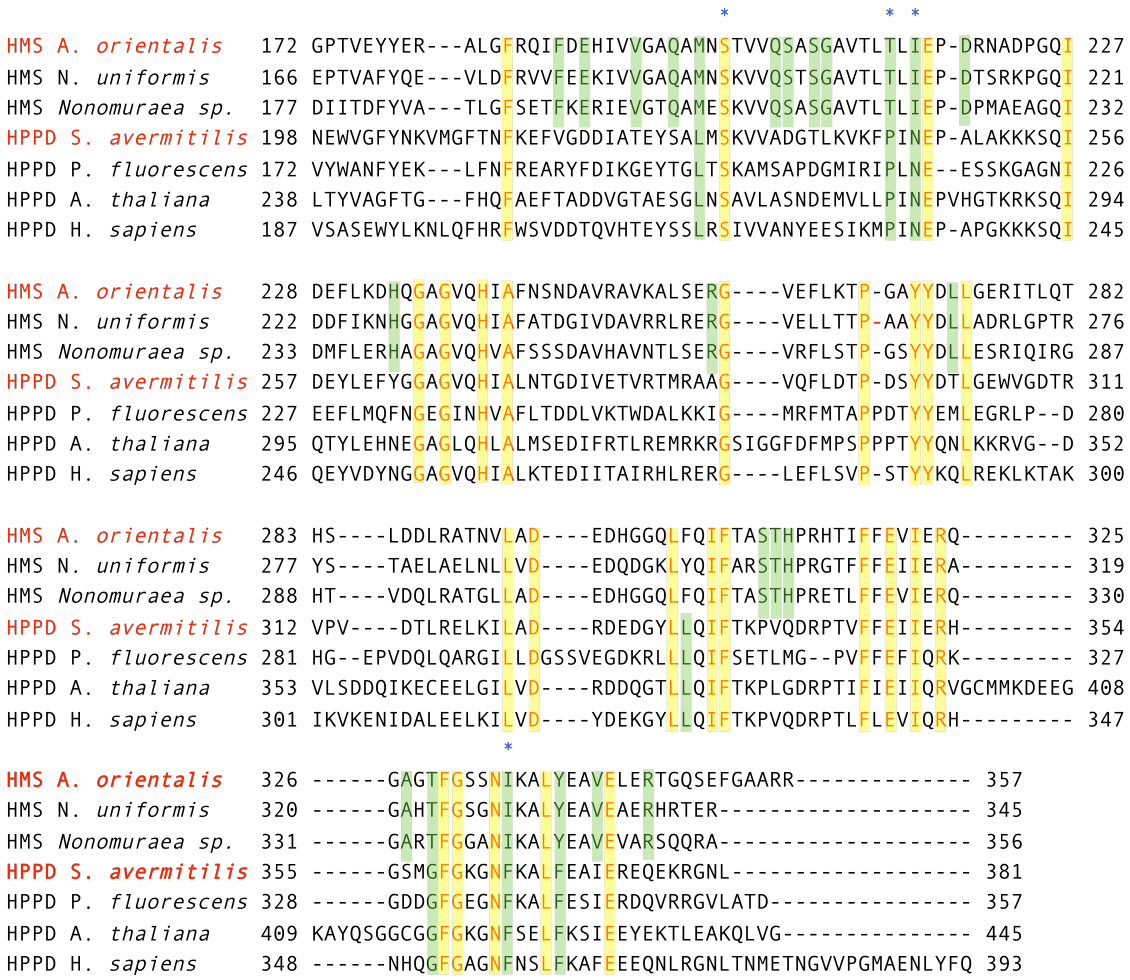

Figure 1.1 Primary structure sequence alignment of C-terminal domains of HPPD and HMS. HPPD and HMS sources for this study are highlighted in red. Conserved residues are highlighted in yellow, residues that are either only conserved in HPPD or HMS (distinct residues) are highlighted in green. The residues targeted for mutation in this study have been indicated with blue stars.

HPPD is found in almost all aerobic life forms, whereas HMS is found only in specific bacteria. Moreover, organisms that express HMS also express HPPD. These factors suggest that the gene encoding HPPD is the progenitor of that for HMS. HPPDs from bacteria are generally found as tetramers as opposed to mammalian HPPDs, which

are dimeric in nature. Secondary structural elements of HPPD and HMS are highly superimposable (Figure 1.3A) despite modest (~35%) sequence identity (Figure 1.1). Both enzymes contain two structural domains, a conserved *C*-terminal domain that includes all residues of the active site plus the ferrous ion cofactor and a less well conserved *N*-terminal domain with apparent vestigial structural functionality (52,53). Plant HPPD sequences are found to contain an insertion at carboxy terminus (54,55). The *N*- and the *C*-terminal domains of each enzyme are also largely superimposable.

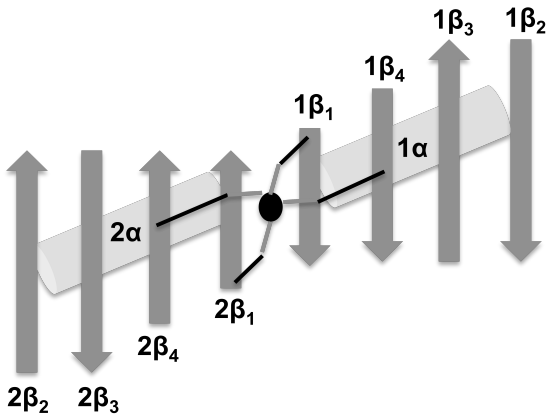

Figure 1.2 Topology of the vicinal oxygen chelate fold. Two βαββββ units are depicted. β-strands are presented as arrows (dark gray) and α-helices are presented as cylinders (light gray). In the middle of two βαββββ units, is a metal ion. The positions of residues chelating metal ions from different β-strands have been depicted as lines. This figure has been regenerated from reference (56).

Each domain forms an incomplete β-barrel comprised of tandem βαββββ units. This overall bi-symmetrical topology suggests two successive gene duplications were required to form the overall structure. This domain topology is that of the vicinal oxygen chelate fold (Figure 1.2) (56,57), which has no topological resemblance to the structures

of other α-KAOs that have modifications to the more common jelly roll fold (58). This difference in topology indicates separate evolutionary lineages that yielded independent mechanistic convergence.

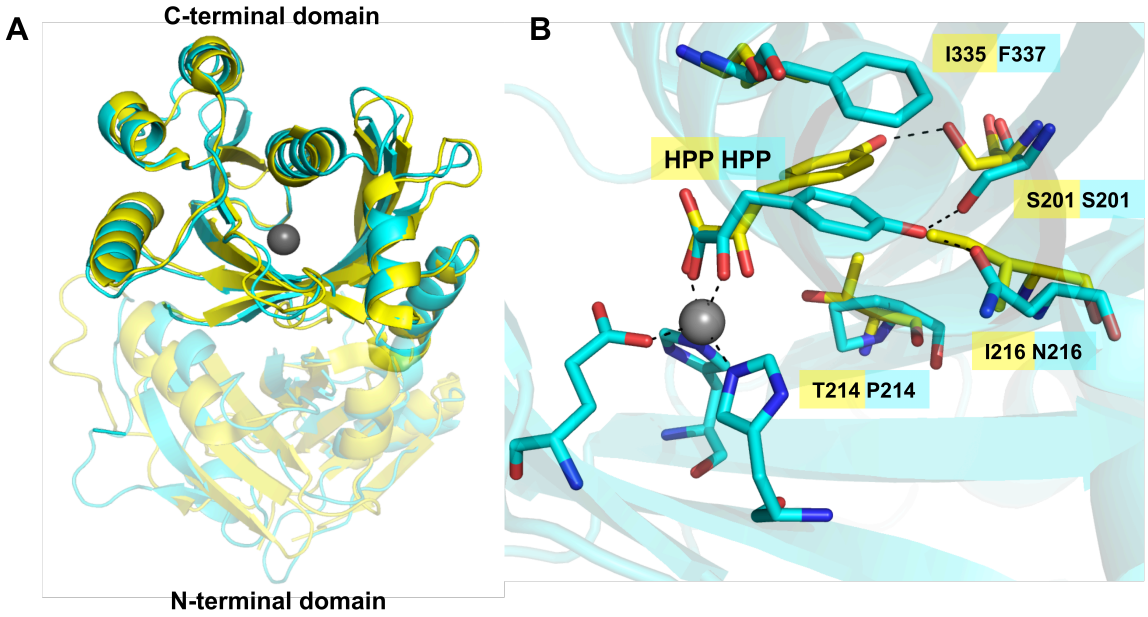

Figure 1.3 (A) Superimposed tertiary structures of *P. fluorescens* HPPD (cyan, PDB ID: 1CJX) and *A. orientalis* HMS (yellow, PDB ID: 2R5V). (B) Unique and mechanistically important residues, including the facial triad, in the active site of HPPD and HMS, with substrate HPP modeled. The positions for the substrate were taken from reference (53).

As might be expected the majority of sequence conservation in HPPD and HMS occurs in the catalytic *C*-terminal domain (Figure 1.1) and that many of these conserved residues extend inward toward the approximate center of the β-barrel structure, arrayed toward the metal ion (Figure 1.3B). Three of these residues comprise a common structural motif, coined the 2-His-1-carboxylate facial triad, that is present in almost all known mononuclear non-heme Fe(II)-dependent oxygenases (59,60). This motif, which functions in coordinating Fe(II), has the general spacing of $HX(D/E)X_{50\text{-}210}H$ in αKG-dependent oxygenases, whereas in HPPD and HMS a spacing of $HX_{\sim 80}HX_{\sim 80}E$ is

observed, consistent with their very different structures (2). The *N*-terminal domains in both enzymes show few conserved residues as compared to the *C*-terminal domain. These conserved residues are thought to be useful in connecting secondary structures for proper folding of the polypeptide chain. The protein surface does not show any conservation of residues in domains in either enzyme or between enzymes (52,53,56).

1.3.1 The Active Site

As might be expected, HPPD and HMS have numerous active site residues in common; equally expected is that they possess residues that are conserved in only HPPD or HMS sequences (Figure 1.1) (53). The structural conservation and the similarity of the reactions catalyzed has been the basis of attempts to interconvert HPPD and HMS by directed mutation (61,62). Figure 1.3B shows a select group of residues (conserved and distinct in these structures) that have been the primary focus of hydroxylation regiospecificity studies. In this figure, HPP is modeled into the substrate-binding pocket to provide reference. This position for the substrate is based on the density observed for HMA in the HMS•Co(II)•HMA structure, as no structure of the HPPD or HMS•Fe(II)•HPP complex has yet been solved (53). While mutational studies have helped elucidate the chemical mechanisms of HPPD and HMS (*vide infra*), few active site residues have been assigned an unambiguous discrete catalytic function (24,61-64). It was also observed that residues within the 10 Å distance of a metal ion in the active site of HPPD and HMS make few ligand interactions and seem to have auxiliary indirect functions (53). In HMS, a catalytic tolerance to mutation is observed; i.e., variants of HMS with alterations to residues hypothesized to play a key role in catalysis and/or

hydroxylation regioselectivity do not exhibit substantially altered catalytic chemistry. The HPPD reaction coordinate, however, proved less durable in that active site variants are observed to frequently uncouple in turnover and accumulate non-native products from abortive pathways. This difference in response to mutation has been suggested to be a consequence of the larger active site cavity in HPPD (~60 $Å^3$ vs 30 $Å^3$) whose shape confines the phenol ring to a lesser extent than that of HMS (Figure 1.4) (53).

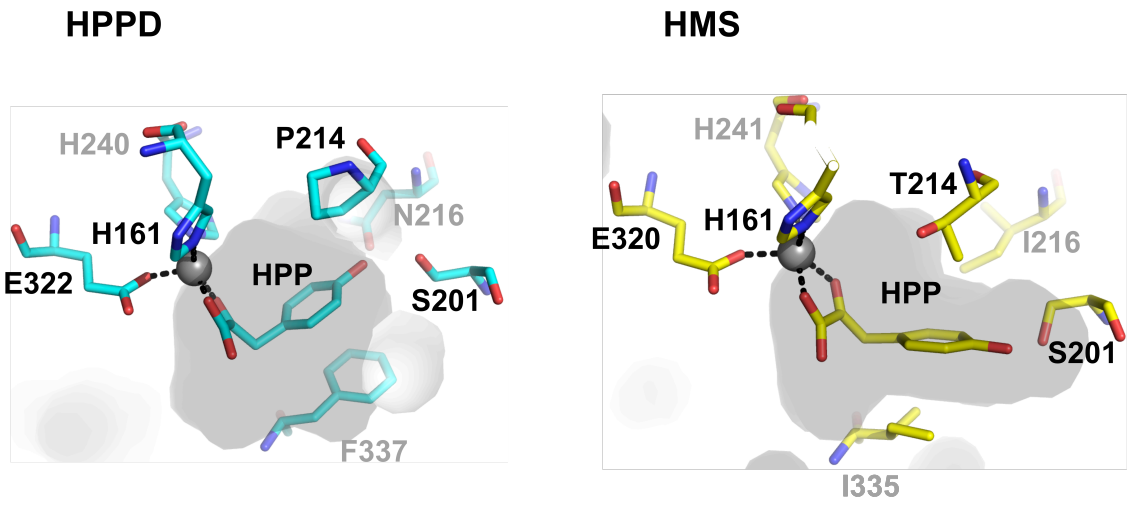

Figure 1.4 HPP modeled into the substrate-binding pocket of HPPD and HMS. The shape of the active site cavity is shown for both. Substrate-binding pocket of HPPD is shown in cyan and for HMS is shown in yellow. Residue numbering is based on the HPPD from *P. fluorescens* and HMS from *A. orientalis*. The figure was regenerated using the data from references (53,65).

A select number of α-KAOs have been investigated using magnetic circular dichroism (MCD) spectroscopy to reveal the geometry about the Fe(II) (66-68). Complexes with liganding α-keto acids typically exhibit low-lying metal-to-ligand charge-transfer (MLCT) transitions arising from the coordination of the Fe(II) ion with

the carboxylate and keto groups (66,69-71). Analysis of the near-IR MCD data for α-keto acid dependent oxygenases indicate that resting enzymes show predominantly a six-coordinate (6C) Fe(II) center (with three endogenous and three water ligands) which remains 6C upon binding αKG, but switches to five-coordinate (5C) Fe(II) (with three endogenous and two αKG ligands) upon binding of the specific substrate, thus opening an attack site for dioxygen (66,72). The resting state HPPD/HMS•Fe(II) and HPPD/HMS•Fe(II)•HPP complexes have similar MLCT transitions centered around ~500 nm, characteristic of bidentate association of the α-keto acid moiety to the metal ion (73-75). Analysis of the resting HPPD/HMS•Fe(II) complex shows a mixture of both 5C (10%) and 6C (90%) ferrous ion geometry. Substrate bound forms of HPPD and HMS largely retain this 5C:6C ratio, suggesting that for these enzymes predominant 5C is not required to support their observed rates of reaction with dioxygen (69,76).

As stated above, no crystal structure of the HPP complex of either HPPD or HMS has been solved. Similar bidentate Fe(II) coordination of HPP occurs in both enzymes, but a curious reversal of transitions was noted in circular dichroism spectra of the HPPD•Fe(II)•HPP and HMS•Fe(II)•HPP complexes (76). This result suggests unique positions for the HPP phenol in the enzymes and promoted the notion that orientation of the aromatic ring relative to the hydroxylating species is principally responsible for the two observed activities (76). The structure of the HMS product complex, (HMS•Co(II)•HMA), coupled with the shape similarities of HMA and HPP, aided computer modeling of HPP into the active site of both enzymes (Figure 1.3B) (53). In the modeled complex, HMS•Fe(II)•HPP, the 4-hydroxyl group of HPP is a hydrogen bond donor to Ser-201, while in the HPPD•Fe(II)•HPP complex a 4.5 Å displacement of the 4-

hydroxyl group allows it to act as a hydrogen bond donor to the amide group of Asn-216 and a hydrogen bond acceptor from Ser-201, simultaneously (53). This pivot of the aromatic ring presumably dictates proximity of the benzylic carbon with respect to the hydroxylating intermediate after decarboxylation. In HMS•Co(II)•HMA complex, Thr214 exhibits an additional hydrogen bond with the newly added benzylic hydroxyl group of the product HMA. This residue is only conserved in all HMS sequences. These separate hydrogen bonding interactions in HPPD (Ser-201 and Asn-216) and HMS (Ser-201 and Thr-214) may also contribute the different orientation of the reaction intermediates in the active site and thus might be playing role in the regiospecificity of the reactions catalyzed by HPPD and HMS. Density functional theory calculations suggest unique conformations of the phenol are a result of differing conformations of Ser-201 in the HPPD/HMS•Fe(IV)=O•HPA complex that then dictate the separate reactivities (77,78).

As described in detail below, a pivot of the *C*-terminal α-helix in response to inhibitor association suggests an active site gating function. All α-KAOs form highly reactive oxygen species during the course of the catalyzed reaction. If these reactive intermediates decay in an uncontrolled manner, the active site or external cellular structures could incur oxidative damage (79). α-KAOs seem to employ a strategy of sealing the active site with a variety of mobile secondary structures to confine the chemistry and exclude the solvent from access to reactive species. Some examples are mobile otherwise disordered loops in alkylsulfatase, proline 3-hydrogenase and clavaminate synthase and α-helices in taurine dioxygenase, and HPPD (80-86). In HPPD, this *C*-terminal helix has a number of disordered residues at the terminus. Truncation of

these residues by mutation slows catalytic activity without affecting HPP binding. This finding strongly suggests that these residues function to define the balance of open and closed forms in solution (87).

1.4 Inhibition of HPPD and HMS

In terms of cumulative research activity, the catalytic chemistry of HPPD and HMS has been partially eclipsed by the chemistry of HPPD inhibition. While both HPPD and HMS are inhibited by 1,3,3'-triketones, only inhibition of the former has agricultural and medical implications (*vide supra*) (88). With one exception (carrot HPPD (89)), all other earlier inhibition studies for HPPD with triketone inhibitors for the measurement of K_i and IC_{50} values came from crude enzyme preparations and with the assumption of rapid single step binding and release. The corelation of IC_{50} and K_d is acceptable only if these assumptions hold (90). Also for an irreversible inhibitor displaying a slow time-dependent inhibition, IC_{50} value would not be helpful in determining the inhibition potency. The reason being that the concentration of an active enzyme varies for any given inhibitor concentration depending upon the pre-incubation time of enzyme-inhibitor complex. Thus it is crucial to establish the kinetics of inhibitor interaction such that conditions are selected that measure the true binding isotherm.

Despite clear herbicidal potency, one of the earliest inhibitors discovered, NTBC, was not formulated for crop use due to the apparent complications of a long metabolic half-life and limited long-term toxicity data. NTBC, nonetheless, remains the paradigm HPPD inhibitor and has since been shown to have low toxicity and the pharmacological advantage of an extended metabolic half-life (114). HPPD binds the exocyclic enol of

NTBC, with the native ferrous state appearing to bind the inhibitor irreversibly (negating the rapid equilibrium assumption used in IC50 determinations). While both HPPD•Fe(II) and HPPD•Fe(II)•HPP complexes react with molecular oxygen, the HPPD•Fe(II)•NTBC complex does not. This observation was confirmed with no loss in the MLCT transition for HPPD•Fe(II)•NTBC complex over long incubation periods (91). This might be a result of the blockage of the entry of molecular oxygen in the catalytic site of HPPD because of the presence of NTBC. Using the kinetics associated with the development of MLCT absorption transitions that arise in the inhibitor complex, a minimal three-step kinetic mechanism for NTBC association was proposed (Scheme 1.3B) (91).

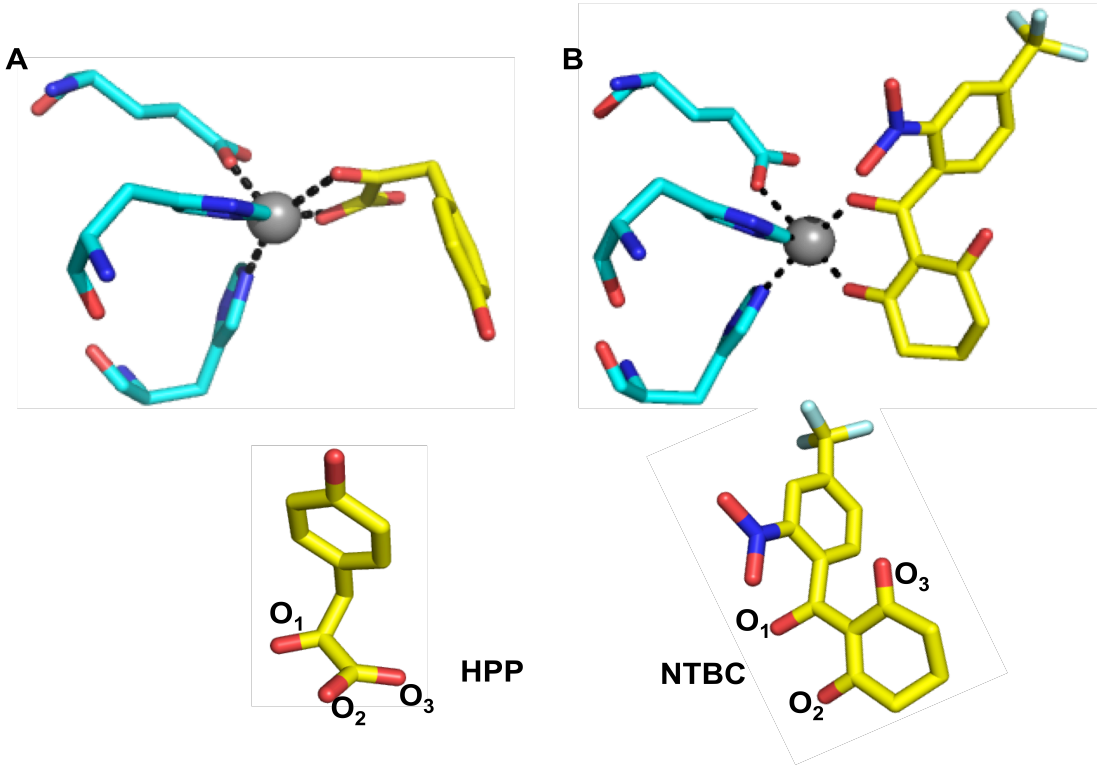

Figure 1.5 Bidentate association of HPP and NTBC to HPPD metal center. Similarity of the available positions for Fe(II) coordianation for (A) HPP and (B) NTBC are depicted.

The inhibitor made bidentate association with the active site metal ion to give primarily five-coordinate, distorted square pyramidal complex (Figure 1.5B) (84). In the first step NTBC binds weakly in a non-metal-centered complex. In the second step association of NTBC to the metal ion is observed as an accumulation of MLCT transitions centered about 450 nm. The final and slowest step is proposed to entail an irreversible deprotonation of the exocyclic enol group of the inhibitor to form the enolate complex with more intense MLCT at 450 nm (91). MCD spectra of the HPPD•Fe(II)•NTBC complex indicate that, despite its apparent extremely high affinity for HPPD, NTBC association with the active site Fe(II) is weaker than HPP association with the metal ion by ~12 kJ/mol (92). As such, it was concluded that bidentate association of the inhibitor to the active site metal ion (Figure 1.5) does not appreciably contribute to the binding energy for the inhibitor complex. The interaction of NTBC with the sister enzyme HMS from *A. orientalis* was explored later (88). The mechanism of NTBC association with HMS differs only slightly from HPPD, in which three-charge transfer species were observed for HMS•Fe(II)•NTBC complex after initial reversible step. All three charge-transfer species observed in HMS depicted no spectrophotometric difference except the change in the extinction coefficients at 450 nm. However in HPPD, the last charge-transfer complex exhibits a very significant difference in the extinction coefficient at 380 nm together with 450 nm. While the minimal kinetic mechanisms for the association of NTBC to HMS•Fe(II) and HPPD•Fe(II) complexes revealed some differences, both enzyme complexes with NTBC were equally unreactive to molecular oxygen. This confirmed NTBC as an irreversible inhibitor for HMS (88).

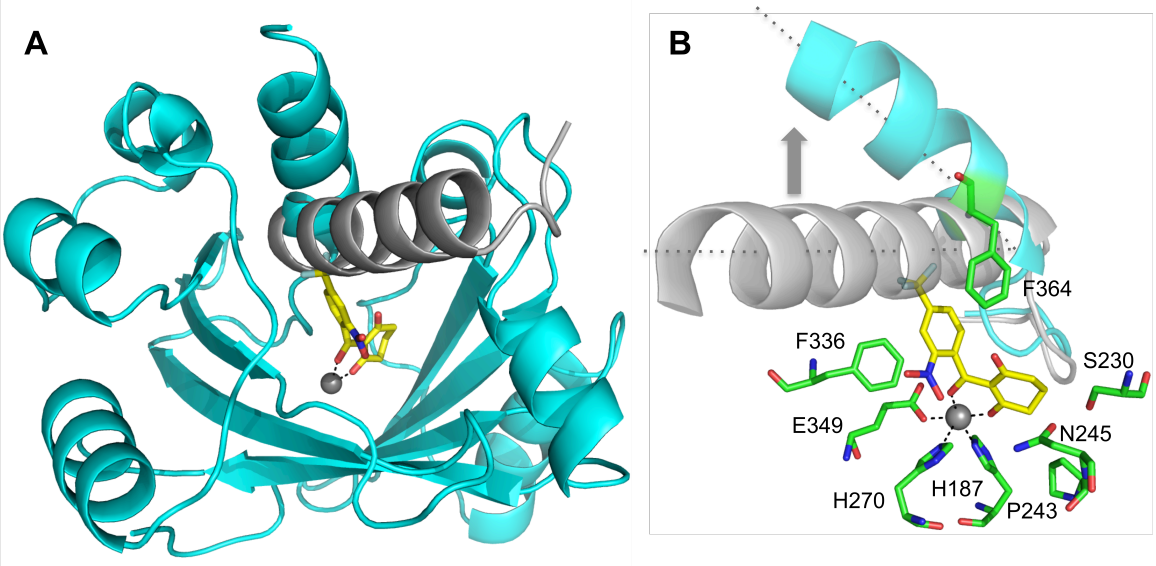

Figure 1.6 Structure of the HPPD•Fe(II)•NTBC complex. (A) The open *C*-terminal domain of HPPD from *S. avermitilis* in complex with NTBC (cyan, PDB ID: 1T47) overlaid with the closed position for the C-terminal α-helix from the *P. fluorescens* HPPD structure solved in the presence of an acetate ligand (grey, PDB ID: 1CJX). (B) The NTBC complex with the active site of HPPD. The residues shown are from the *S. avermitilis* HPPD•Fe(II)•NTBC complex (cyan, PDB ID: 1T47) and are those that contact the metal ion and/or the inhibitor. The displacement of the *C*-terminal α-helix is indicated relative to the position observed in the closed structure from *P. fluorescens* HPPD (grey, PDB ID: 1CJX).

The first inhibitor-bound HPPD structure reported was for *S. avermitilis* HPPD crystallized in the ferrous oxidation state in complex with NTBC (84). This complex reveals that the inhibitor makes the previously predicted bidentate interactions to the metal ion via its 1-ketone and 3-enol moieties (Figure 1.5B). While the overall fold reveals a high degree of similarity to the earlier solved *P. fluorescens* HPPD•Fe(III)•acetate structure (52), the *C*-terminal α-helix was pivoted about its *N*-terminal end to a position that places it at a ~40° angle compared to the earlier observed position (Figure 1.6). The other major difference between two structures came from the different packing of the β-strands and the intervening turn (residues 130-143 in *S.*

avermitilis HPPD, residues 106-116 in *P. fluorescens* HPPD) because of the increased length of the β-structure and the different position of the adjacent turn (84).

The *C*-terminal α-helix includes Phe-364 that, in combination with Phe-336, makes a staggered π-stacking interaction with the aromatic ring of NTBC (Figure 1.6B). Other mammalian HPPD inhibitor complexes have been solved since that show similar *C*-terminal α-helix displacement and stacking arrangements (55). Such π-stacking interactions are typically very low-energy associations and unlikely to account for the observed affinity. Since no additional electrostatic or hydrogen bonding interactions are observed in the HPPD•Fe(II)•NTBC complex, the basis for the extremely high affinity is largely unknown; however, it would appear that NTBC has excellent shape complementarity and makes near uniform van der Waals contact with the active site cavity (Figure 1.7) (65).

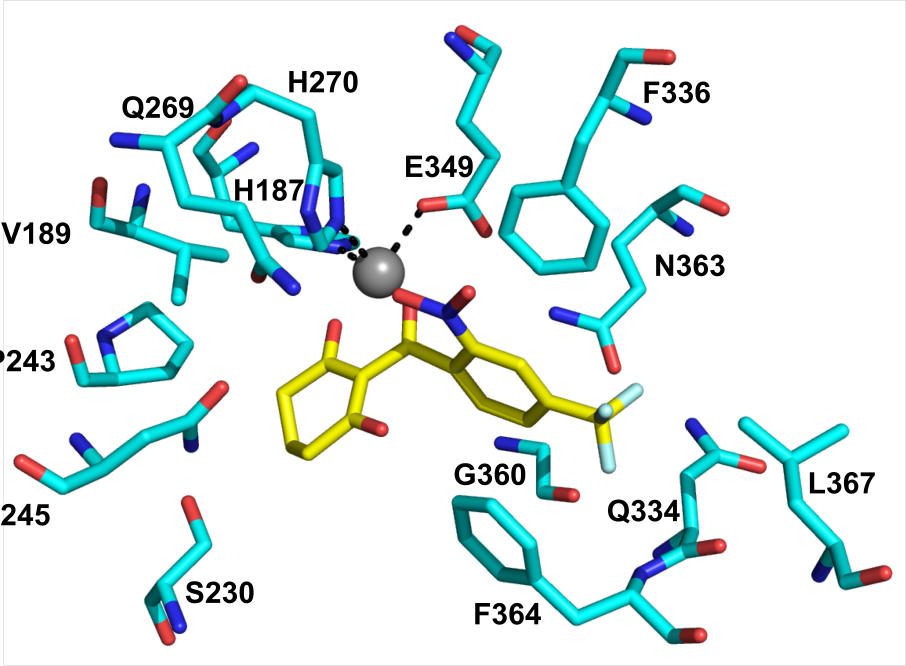

Figure 1.7 Active site residues in van der Waals contact with NTBC

1.5 The Reaction Catalyzed

HPPD and HMS catalyze two half reactions, decarboxylation and a hydroxylation. Decarboxylation half reactions in both are thought to be the same, while the hydroxylation reactions diverge to form unique products. In the decarboxylation half-reaction dioxygen reduction occurs after HPP association, and oxidative decarboxylation of the α-keto acid moiety yields the reactive Fe(IV)=O (ferryl) intermediate. There is scant experimental evidence for the events of this half-reaction. What is known has been assembled from computational studies and suggests that an Fe(III) superoxo species attacks the α-keto carbon atom to initially form a bridged peroxo species that then liberates carbon dioxide and forms a peracid intermediate. Severing of the peroxy bond forms the highly electron deficient ferryl species coordinated to HPA. From this point the hydroxylation half reaction ensues. As stated, it is thought that proximity dictates where the Fe(IV)=O species will hydroxylate; in HMS, the benzylic carbon of HPA has greater proximity, while in HPPD it is the aromatic C1 position, each as a direct consequence of the position of the phenol moiety (Figure 1.3B).

1.5.1 The Mechanism of Decarboxylation

The decarboxylation half-reaction starts with ordered substrate binding, a commonly observed feature in α-KAOs (1). For the three-substrate α-KAOs, the catalytic cycle starts with the binding of αKG, followed by the addition of the specific substrate to form a ternary complex that has heightened reactivity toward molecular oxygen (70) as a consequence of the switch from 6C to 5C geometry at the metal ion (66,72). HPPD and HMS also exhibit ordered substrate addition with HPP being the first

substrate to bind followed by molecular oxygen. Relative to the HPPD/HMS•Fe(II) complexes, the HPPD/HMS•Fe(II)•HPP complexes show reactivities towards molecular oxygen that are several thousand fold more rapid (73,75). The basis for these changes in reactivity appears to derive from the conformation of the HPP α-keto acid. The absorption spectrum of unliganded HPP shows an n→π* transition at ~31,500 cm^{-1} that shifts to ~28,000 cm^{-1} when bound in the active site of HPPD or HMS. The difference in energy of the α-keto acid n and π* orbitals is evidence of the dihedral angle between the carbonyl and carboxyl groups (θ) and this energy difference reaches a minimum when the two groups are coplanar (Figure 1.3B) (66). The planar conformation of the α-keto acid maximizes conjugation between the coordinating moieties and the ferrous ion, facilitating metal to dioxygen charge delocalization. The energy of the n→π* transition of HPPD/HMS•Fe(II)•phenylpyruvate complexes indicates flattening of the α-keto acid only in HMS, consistent with the observation that phenylpyruvate is a substrate only for HMS (77).

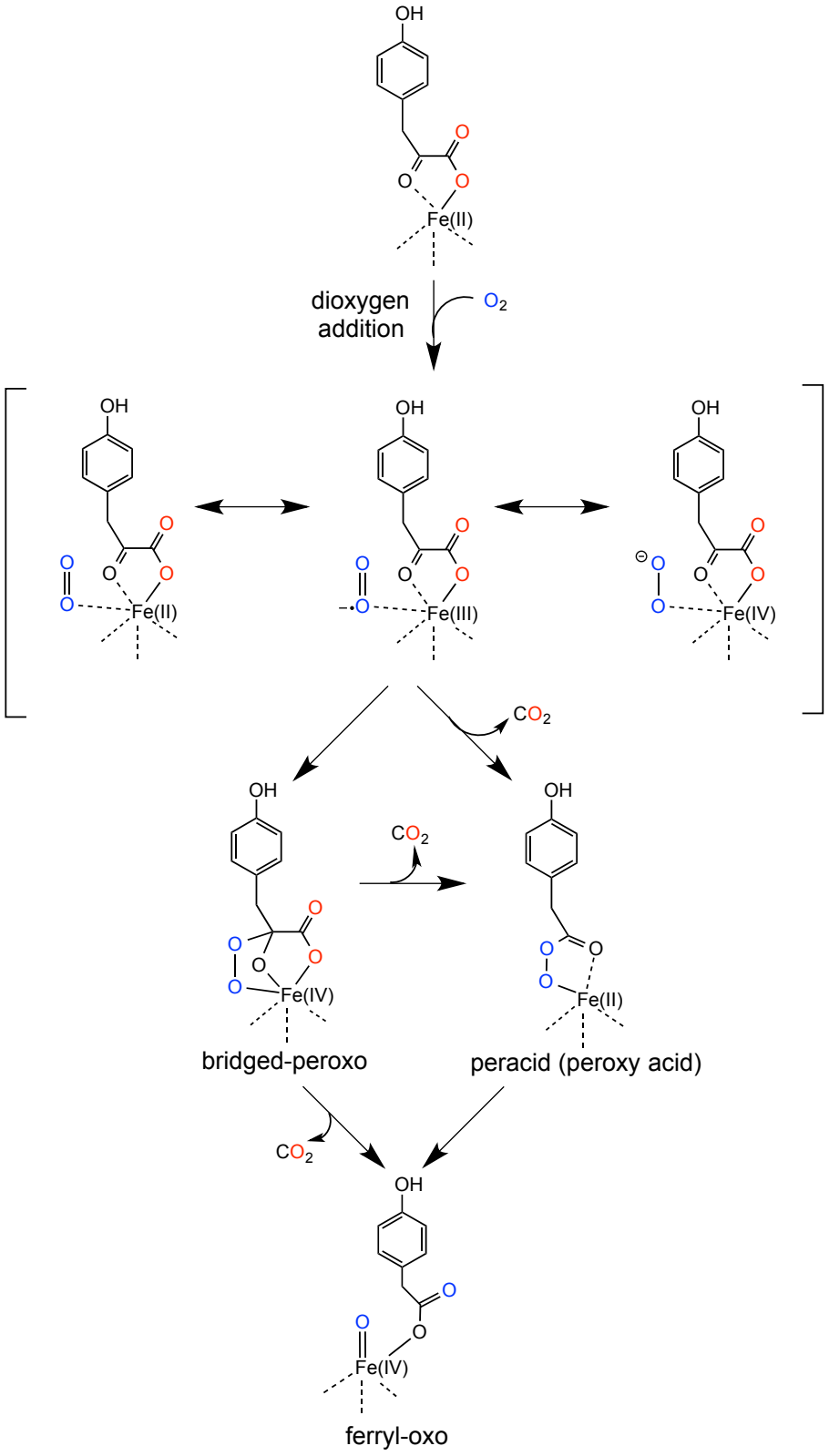

Scheme 1.5 Common decarboxylation half reaction in HPPD and HMS

The decarboxylation half-reaction is largely kinetically obscured in single turnover reactions of HPPD and HMS. While an early intermediate can be observed to accumulate to some extent, no evidence has yet been offered for the identity of this species (73-75). Computational data have provided detailed descriptions of the possible mechanisms for the decarboxylation chemistry (Scheme 1.5) (93-95). From such studies it was proposed that the first step after addition of HPP is the stepwise reduction of dioxygen to first form the ferric-superoxo species. Attack on the α-keto carbon forms a Fe(IV)-peroxo bridged species that decays with concomitant release of CO_2 to give a ferrous peracid intermediate. This peracid then undergoes heterolytic cleavage of the O–O bond to yield the E•Fe(IV)=O•HPA intermediate. In a variation of this sequence it has also been suggested that the ferric superoxo species can decay to the peracid via a single transition state (Scheme 1.5) (94). The Fe(IV)=O species accumulates in three-substrate α-KAOs as the first intermediate concomitant with CO_2 production (96-100). The identity of the intermediate was revealed by Mössbauer spectroscopy in conjunction with rapid freeze-quench, facilitated by enhanced accumulation of the intermediate that occurs when a deuterium is substituted at the site of the hydroxylation (98-101). Understanding the timing of the CO_2 release, was attempted using ^{14}C labeled substrate, which did not clearly establish if the release occur before, after or together with Fe(IV)=O intermediate (97). Fe(IV)=O is a highly electrophilic species that oxidizes a variety of proximal centers and thereby can be used for a range of different chemistries (1,2); however, the extreme electrophilicity of the ferryl species makes it unruly and prone to hydroxylate nearby active site residues. This phenomenon of self-hydroxylation has been observed in a variety of α-KAO type enzymes, including HPPD (102-104).

For HPPD and HMS, multiple intermediates have been observed in rapid mixing, single-turnover reactions (Scheme 1.6). The available data suggest that the ferryl species does not accumulate in these enzymes due to the formation and decay of this intermediate being fast relative to prior and later steps (73,74,105). Nonetheless, wild-type HPPD and variants of both enzymes make HPA as one of the products in an abortive pathway, consistent with a common decarboxylation half-reaction and indirectly implying the presence of a ferryl species (24,63,64).

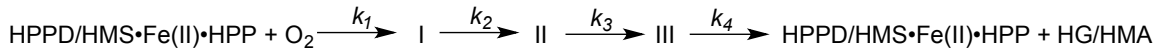

Scheme 1.6 Four-step model for the single turnover reactions of HPPD and HMS

1.5.2 The Mechanisms of Hydroxylation

The fate of the oxygen atom of the ferryl species defines the hydroxylation reactions of HPPD and HMS. Compared to the α-KAOs, the HMS hydroxylation half-reaction is rather conventional. The available data are consistent with the ferryl species abstracting a hydrogen atom from the benzylic carbon of HPA, forming an Fe(III)-OH intermediate. This species is able to quench the benzylic radical formed in the initial abstraction by transfer of •OH in a rebound reaction that restores the Fe(II) state of the metal ion (Scheme 1.8). In contrast to HMS, hydroxylation of the relatively electron replete aromatic ring of HPA by the Fe(IV)=O species of HPPD induces the quite remarkable displacement of the aceto substituent to the adjacent ring C2 carbon. As such, the overall hydroxylation/rearomatization half-reaction of HPPD is considerably more

chemically intricate and numerous hypotheses, based on experiment and/or intuition, have been put forward to account for the chemistry (Scheme 1.7) (3,62-64,94,106-108).

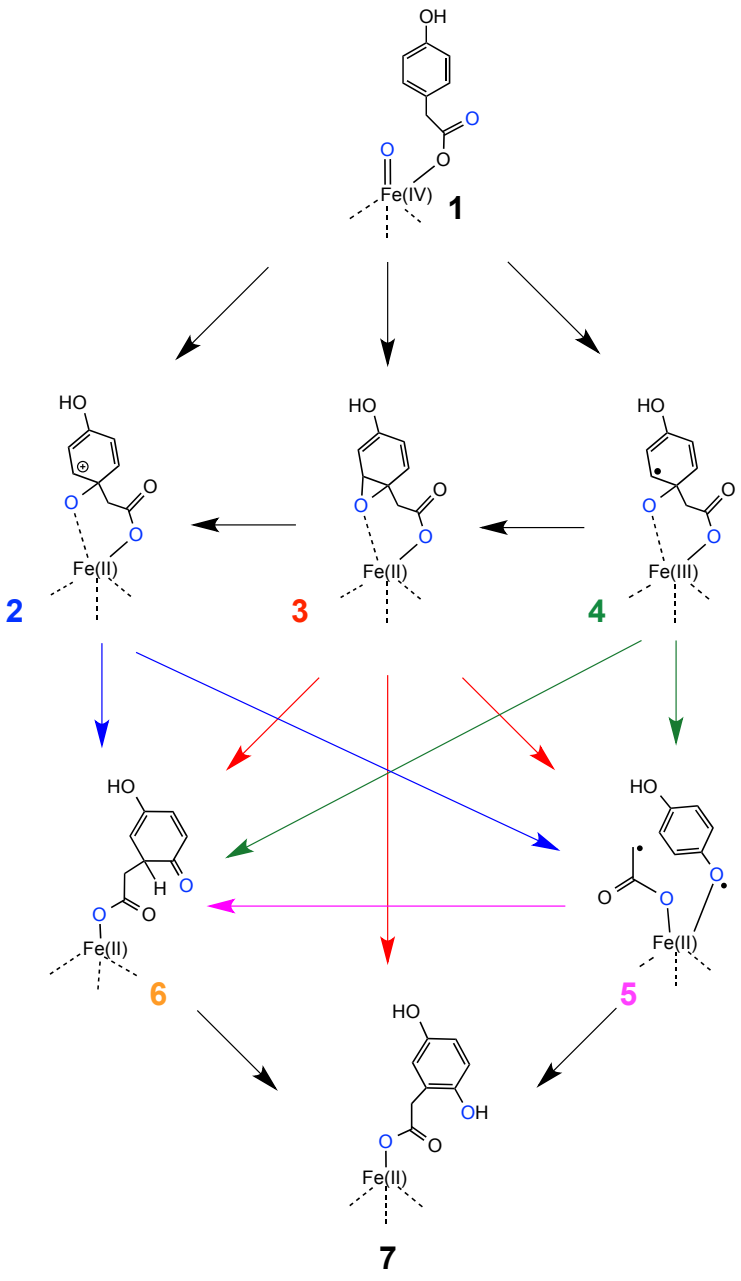

Scheme 1.7 Hydroxylation half-reaction in HPPD depicting all proposed intermediates.

Since the first observations of aromatic shift chemistry in the pterin-dependent hydroxylases, there has been a debate over the participation of either a benzylic cation (Scheme 1.7, structure 2) or a 1,2-epoxide (Scheme 1.7, structure 3) as the immediate intermediate arising from oxygenation of an aromatic ring (109-112). However, this narrow set of possibilities was presumably defined from precedent for ring oxygen substitutions in organic synthesis studies. Hybrid density functional calculations were used to explore a more extensive set of reaction paths for the attack on the ring C1 carbon by the Fe(IV)=O species, where oxygen addition forms either a radical σ complex, a biradical, an epoxide (arene oxide), or a benzylic cation (Scheme 1.7, structures 4,5,3 and 2) (94). In these calculations, the radical σ complex having the Fe(III) state is preferred over the ring cation or the epoxide intermediate. In a separate study, the epoxide was claimed as the first intermediate of the hydroxylation half-reaction based on the accumulation of an oxepinone from turnover of an HPPD active site variant that was thought to be a direct rearrangement of the product epoxide (62); however, it was later shown that the oxepinone is actually derived from QAA that was rearranged by the inclusion of trifluoroacetic acid during the HPLC identification (24).

Quite recently methodologies have been applied that successfully probe the hydroxylation half-reactions of both enzymes. Directed active site variants of either enzyme commonly induce some degree of uncoupling to form both native and non-native products. This outcome has enabled the use of intermediate partitioning to measure kinetic isotope effects (KIEs) on specific steps (63,113) (see chapters 2 & 3). The products monitored were HG (decarboxylated, doubly oxygenated and rearranged), HMA (decarboxylated and doubly oxygenated), HPA (decarboxylated and singly oxygenated),

and QAA (decarboxylated and doubly oxygenated) (24,63). KIEs are derived from the change in ratio of the products in the presence of a strategically placed heavy atom label, the ratio of ratios thus providing the KIE (Figure 1.8).

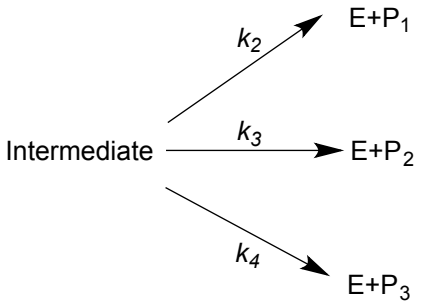

$$^{D}k_{obs} = \frac{(P_1/(P_1+P_2+P_3))^{H}}{(P_1/(P_1+P_2+P_3))^{D}}$$

Figure 1.8 Intermediate partitioning kinetic isotope effect calculation.

Intermediate partitioning KIEs have provided direct insight into both the initial oxygenation by HPPD and HMS and the ensuing NIH shift steps of HPPD. The KIE on the initial oxygenation step of wild-type HPPD when ring deuterons are added to HPP was an inverse value of 0.84, suggesting an sp^2 to sp^3 hybridization change. This hybridization change is predicted only for the formation of a ring epoxide (63). The ensuing NIH shift must then transiently severe the bond to the aceto substituent in either a heterolytic or homolytic mechanism. The earliest evidence for the mechanism of NIH shift came from the lack of scrambling or inversion at the benzylic carbon when 3'-monodeutero HPP is used as a substrate, and this result was recently confirmed (64,107). While this lack of scrambling is seemingly consistent with a heterolytic mechanism in which the in-flight benzylic carbon is anionic (sp^3) in character, it was later suggested by calculation to be an inconclusive result. Borowoski *et al.* determined that the barrier to

bond rotation to give scrambling is substantially greater than that for recombination and a lack of scrambling cannot by itself be evidence of the mechanism for the shift. 3',3'-dideutero HPP yields a KIE of unity for wild-type and most variants of HPPD (64); however, an N245S variant (corresponding to Asn-216 in Figure 1.3) gives a normal KIE of 1.4 for the formation of HG, suggesting a late transition state moving to sp^2 geometry with this variant. It was therefore concluded that in wild-type HPPD the shift occurs via a minimally advanced transition state toward a homolytic mechanism (64), consistent with the earlier conclusions from computational studies (94).

Recombination of the aceto group with the aromatic ring forms a dienone (Scheme 1.7, structure 6) that can rearomatize through tautomerization to yield HG. The activation energy barrier calculated for this tautomerization indicates this process could take place either within the enzyme or in solution (94). Single turnover studies of HPPD (Scheme 1.6) have shown that the highly fluorescent HG product (Scheme 1.7, structure 7) forms as the third intermediate ahead of the rate limiting dissociation of the product, indicating that rearomatization occurs within the active site. Moreover, the rate constant for the formation of this signal exhibits a KIE of 1.7 when ring-perdeutero-HPP is used as a substrate, consistent with a modest primary isotope effect for displacement of a deuteron from the ring 2-carbon during rearomatization (74). Decay of the third intermediate (Scheme 1.7, structure 7) is sensitive to deuterons derived from the solvent. In HPPD (and HMS) the product release rate constant (k_4) exhibits a solvent kinetic isotope effect of ~2 suggesting a role for an active site base in product release (73,74).

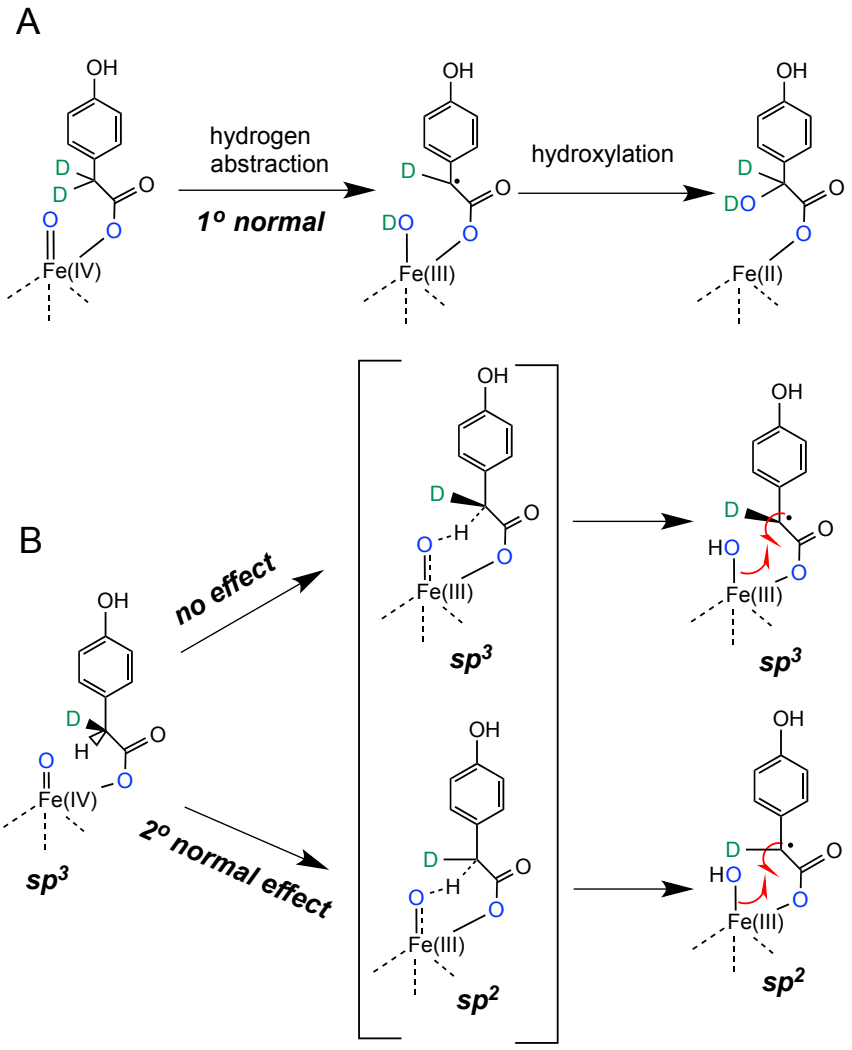

Scheme 1.8 Hydroxylation reaction in HMS depicting all possible intermediates. (A) Evidence for the hydrogen atom abstraction in HMS with 3',3'-dideutero HPP as a substrate. (B) Evidence for the geometry of the remaining atom after initial H-atom abstraction with R-3'-monodeutero HPP as a substrate.

Hydroxylation in HMS occurs at the benzylic carbon of HPA to give product HMA. Unfortunately, substitution of a deuterium atom(s) at the benzylic position of HPP does not slow any of the steps observed in single-turnover reactions of HMS (73). This result suggests that the hydroxylation reaction of HMS is fast and unable to be observed directly by conventional kinetic approaches. In HMS, the ferryl species abstracts only the

pro-S hydrogen atom to form a ferric-hydroxyl species (73). This Fe(III)-OH then attacks the benzylic radical via an oxygen rebound mechanism to form HMA (Scheme 1.8A). Like HPPD, HMS variants also show product partitioning, but they form just two products, HPA and HMA. When 3',3'-dideutero HPP is used as a substrate, the intermediate partitioning KIE is 2.2-2.6. This outcome suggests an H-atom abstraction that is largely devoid of tunneling (63). The KIE measured with the dideutero substrate is expected to include a multiplicative component from the non-abstracted deuteron (Scheme 1.8A). To dissect each component, the equivalent experiment was carried out with R-3'-monodeutero HPP and the KIE measured (Scheme 1.8B). This experiment gave a KIE of 1.06 indicating little geometry change in the transition state during abstraction (64). The F364I HPPD variant is able to form HMA as a product in 20% of turnovers. The R-3'-monodeutero HPP substrate shows a KIE of 1.92 with this variant, a significantly normal secondary effect, suggesting a hybridization change from sp^3 to sp^2 consistent with a less optimized reaction for the production of HMA in this variant.

1.6 Concluding Remarks

HPPD and HMS are the outliers of the α-KAO family. While they catalyze a mechanistically equivalent set of reactions to those observed in the majority of the enzyme family, they have evolved independently and exhibit unique characteristics that have in some cases elucidated parts of the catalytic cycle that remain obscured in all other family members. The ubiquity of the HPPD reaction has meant that its inhibition has a collectively broad set of consequences. Inhibitors have been found to be highly successful herbicides, targeted therapeutics for in-born errors in tyrosine catabolism, and have shown potential to augment the treatment of microbial infections.

For some considerable time there has been conjecture pertaining to the mechanism(s) of hydroxylation reactions catalyzed by Fe(II) dependent oxygenases (109-112). This chapter presented a summary and most up to date mechanistic chemistry of HPPD and HMS. Parts of this chapter have been published as a chapter in a book titled 2-Oxoglutarate-Dependent Oxygenases (Schofield C. J. and Hausinger R. P. Eds., In press). Chapter 2 of this thesis provides an evidence for the participation of an epoxide as the immediate intermediate with the oxygenation of an aromatic ring in HPPD. In the same chapter we show that in HMS benzylic hydroxylation occurs with hydrogen atom abstraction. This chapter was published as an article in Biochemistry (63). Chapter 3 of this thesis focuses on defining the transition state geometries that arise during the NIH shift in HPPD and hydrogen atom abstraction steps in HMS. From this chapter we conclude that, NIH shift in HPPD occurs through homolytic mechanism and in HMS hydrogen atom abstraction occurs without the geometry change at the benzylic carbon. This chapter was published as an article in Biochemistry (64). Chapter 4 of this thesis

details initial attempts to identify HPPD variants that have substantially altered kinetics in order to reveal new parts of the catalytic cycle and define the function of active site residues in HPPD.

1.7 References

1. Purpero, V., and Moran, G. R. (2007) The diverse and pervasive chemistries of the alpha-keto acid dependent enzymes. *J Biol Inorg Chem* **12**, 587-601
2. Hausinger, R. P. (2004) FeII/alpha-ketoglutarate-dependent hydroxylases and related enzymes. *Crit Rev Biochem Mol Biol* **39**, 21-68
3. Hager, S. E., Gregerman, R. I., and Knox, W. E. (1957) p-Hydroxyphenylpyruvate Oxidase of Liver. *J. Biol. Chem.* **225**, 935-947
4. Goodwin, T. W., and Mercer, E. I. (1983) *Introduction to Plant Biochemistry*, 2nd ed ed., Pergamon Press, Sydney
5. Nosanchuk, J. D., and Casadevall, A. (2003) The contribution of melanin to microbial pathogenesis. *Cellular microbiology* **5**, 203-223
6. Graham, D. E., Xu, H., and White, R. H. (2003) Identification of the 7,8-didemethyl-8-hydroxy-5-deazariboflavin synthase required for coenzyme F(420) biosynthesis. *Arch Microbiol* **180**, 455-464
7. Hubbard, B. K., Thomas, M. G., and Walsh, C. T. (2000) Biosynthesis of L-p-hydroxyphenylglycine, a non-proteinogenic amino acid constituent of peptide antibiotics. *Chemistry & Biology* **7**, 931-942
8. Choroba, O. W., Williams, D. H., and Spencer, J. B. (2000) Biosynthesis of the vancomycin group of antibiotics: Involvement of an unusual dioxygenase in the pathway to (S)-4-hydroxyphenylglycine. *Journal of the American Chemical Society* **122**, 5389-5390
9. Hellyer, R. (1968) The Occurrance of Beta-Triketones in the Steam-Volatile Oils of Some Myrtaceous Australian Plants. *Australian Journal of Chemistry* **21**, 2825-2828

10. Dayan, F. E., Duke, S. O., Sauldubois, A., Singh, N., McCurdy, C., and Cantrell, C. (2007) p-Hydroxyphenylpyruvate dioxygenase is a herbicidal target site for beta-triketones from Leptospermum scoparium. *Phytochemistry* **68**, 2004-2014
11. Romagni, J. G., Meazza, G., Nanayakkara, N. P., and Dayan, F. E. (2000) The phytotoxic lichen metabolite, usnic acid, is a potent inhibitor of plant p-hydroxyphenylpyruvate dioxygenase. *FEBS Lett* **480**, 301-305.
12. Schindler, H. (1957) [Ingredients of various usnea species with special reference to usnic acid]. *Arzneimittel-Forschung* **7**, 69-72
13. Cocchietto, M., Skert, N., Nimis, P. L., and Sava, G. (2002) A review on usnic acid, an interesting natural compound. *Naturwissenschaften* **89**, 137-146
14. Beaudegnies, R., Edmunds, A. J., Fraser, T. E., Hall, R. G., Hawkes, T. R., Mitchell, G., Schaetzer, J., Wendeborn, S., and Wibley, J. (2009) Herbicidal 4-hydroxyphenylpyruvate dioxygenase inhibitors--a review of the triketone chemistry story from a Syngenta perspective. *Bioorganic & medicinal chemistry* **17**, 4134-4152
15. Maeda, H., and DellaPenna, D. (2007) Tocopherol functions in photosynthetic organisms. *Curr Opin Plant Biol* **10**, 260-265
16. Huhn, R., Stoermer, H., Klingele, B., Bausch, E., Fois, A., Farnetani, M., Di Rocco, M., Boue, J., Kirk, J. M., Coleman, R., and Scherer, G. (1998) Novel and recurrent tyrosine aminotransferase gene mutations in tyrosinemia type II. *Human Genetics* **102**, 305-313
17. Tomoeda, K., Awata, H., Matsuura, T., Matsuda, I., Ploechl, E., Milovac, T., Boneh, A., Scott, C. R., Danks, D. M., and Endo, F. (2000) Mutations in the 4-hydroxyphenylpyruvic acid dioxygenase gene are responsible for tyrosinemia type III and hawkinsinuria. *Mol Genet Metab* **71**, 506-510
18. Item, C. B., Mihalek, I., Lichtarge, O., Jalan, A., Vodopiutz, J., Muhl, A., and Bodamer, O. A. (2007) Manifestation of hawkinsinuria in a patient compound heterozygous for hawkinsinuria and tyrosinemia III. *Mol Genet Metab* **91**, 379-383
19. Endo, F. (1998) [Hawkinsinuria]. *Ryoikibetsu Shokogun Shirizu* **18**, 141-143

20. Lehnert, W., Stogmann, W., Engelke, U., Wevers, R. A., and van den Berg, G. B. (1999) Long-term follow up of a new case of hawkinsinuria. *Eur J Pediatr* **158**, 578-582

21. Wilcken, B., Hammond, J. W., Howard, N., Bohane, T., Hocart, C., and Halpern, B. (1981) Hawkinsinuria: a dominantly inherited defect of tyrosine metabolism with severe effects in infancy. *N Engl J Med* **305**, 865-868

22. Hocart, C. H., Halpern, B., Hick, L. A., and Wong, C. O. (1983) Hawkinsinuria--identification of quinolacetic acid and pyroglutamic acid during an acidotic phase. *J Chromatogr* **275**, 237-243

23. Ruetschi, U., Cerone, R., Perez-Cerda, C., Schiaffino, M. C., Standing, S., Ugarte, M., and Holme, E. (2000) Mutations in the 4-hydroxyphenylpyruvate dioxygenase gene (HPD) in patients with tyrosinemia type III. *Hum Genet* **106**, 654-662

24. Brownlee, J. M., Heinz, B., Bates, J., and Moran, G. R. (2010) Product analysis and inhibition studies of a causative Asn to Ser variant of 4-hydroxyphenylpyruvate dioxygenase suggest a simple route to the treatment of Hawkinsinuria. *Biochemistry* **49**, 7218-7226

25. Niederwieser, A., Wadman, S. K., and Danks, D. M. (1978) Excretion of cis- and trans-4-hydroxycyclohexylacetic acid in addition to hawkinsin in a family with a postulated defect of 4-hydroxyphenylpyruvate dioxygenase. *Clin Chim Acta* **90**, 195-200

26. Niederwieser, A., Matasovic, A., Tippett, P., and Danks, D. M. (1977) A new sulfur amino acid, named hawkinsin, identified in a baby with transient tyrosinemia and her mother. *Clin Chim Acta* **76**, 345-356

27. Garrod, E. A. (1902) The Incidence of Alkaptonuria: A Study in Clinical Individuality. *Lancet* **ii**, 1616-1620

28. Garrod, A. E. (1908) The Croonian Lectures on Inborn Errors of Metabolism. Lecture II. Alkaptonuria. *Lancet* **ii**, 73-79

29. Zannoni, V. G., and La Du, B. N. (1959) The Tyrosine Oxidation System of Liver. *J. Biol. Chem.* **234**, 2925-2931

30. Phornphutkul, C., Introne, W. J., Perry, M. B., Bernardini, I., Murphey, M. D., Fitzpatrick, D. L., Anderson, P. D., Huizing, M., Anikster, Y., Gerber, L. H., and Gahl, W. A. (2002) Natural history of alkaptonuria. *N Engl J Med* **347**, 2111-2121

31. Introne, W. J., Perry, M. B., Troendle, J., Tsilou, E., Kayser, M. A., Suwannarat, P., O'Brien, K. E., Bryant, J., Sachdev, V., Reynolds, J. C., Moylan, E., Bernardini, I., and Gahl, W. A. (2011) A 3-year randomized therapeutic trial of nitisinone in alkaptonuria. *Molecular Genetics and Metabolism* **103**, 307-314

32. Suwannarat, P., O'Brien, K., Perry, M. B., Sebring, N., Bernardini, I., Kaiser-Kupfer, M. I., Rubin, B. I., Tsilou, E., Gerber, L. H., and Gahl, W. A. (2005) Use of nitisinone in patients with alkaptonuria. *Metabolism* **54**, 719-728

33. Fernandez-Canon, J. M., Baetscher, M. W., Finegold, M., Burlingame, T., Gibson, K. M., and Grompe, M. (2002) Maleylacetoacetate isomerase (MAAI/GSTZ)-deficient mice reveal a glutathione-dependent nonenzymatic bypass in tyrosine catabolism. *Mol Cell Biol* **22**, 4943-4951

34. Gentz, J., Jagenburg, R., and Zetterström, R. (1965) Tyrosinemia: an inborn error of tyrosine metobolism with cirrhosis of the liver and multiple renal tubular defects. *J. Pediatr.* **66**, 670-696

35. Lindblad, B., Lindstedt, S., and Steen, G. (1977) On the enzymic defects in hereditary tyrosinemia. *Proceedings of the National Academy of Sciences of the United States of America* **74**, 4641-4645

36. Mohan, N., McKiernan, P., Preece, M. A., Green, A., Buckels, J., Mayer, A. D., and Kelly, D. A. (1999) Indications and outcome of liver transplantation in tyrosinaemia type 1. *Eur J Pediatr* **158 Suppl 2**, S49-54

37. McKiernan, P. J. (2006) Nitisinone in the treatment of hereditary tyrosinaemia type 1. *Drugs* **66**, 743-750

38. Ahmad, S., Teckman, J. H., and Lueder, G. T. (2002) Corneal opacities associated with NTBC treatment. *Am J Ophthalmol* **134**, 266-268

39. Wisse, R. P., Wittebol-Post, D., Visser, G., and van der Lelij, A. (2012) Corneal depositions in tyrosinaemia type I during treatment with Nitisinone. *BMJ case reports* **2012**

40. Thimm, E., Richter-Werkle, R., Kamp, G., Molke, B., Herebian, D., Klee, D., Mayatepek, E., and Spiekerkoetter, U. (2012) Neurocognitive outcome in patients with hypertyrosinemia type I after long-term treatment with NTBC. *Journal of inherited metabolic disease* **35**, 263-268

41. Chiu, H. T., Hubbard, B. K., Shah, A. N., Eide, J., Fredenburg, R. A., Walsh, C. T., and Khosla, C. (2001) Molecular cloning and sequence analysis of the complestatin biosynthetic gene cluster. *Proceedings of the National Academy of Sciences of the United States of America* **98**, 8548-8553

42. Guerra-Lopez, D., Daniels, L., and Rawat, M. (2007) Mycobacterium smegmatis mc2 155 fbiC and MSMEG_2392 are involved in triphenylmethane dye decolorization and coenzyme F420 biosynthesis. *Microbiology* **153**, 2724-2732

43. Eirich, L. D., Vogels, G. D., and Wolfe, R. S. (1979) Distribution of coenzyme F420 and properties of its hydrolytic fragments. *J Bacteriol* **140**, 20-27

44. Choi, K. P., Kendrick, N., and Daniels, L. (2002) Demonstration that fbiC is required by Mycobacterium bovis BCG for coenzyme F(420) and FO biosynthesis. *J Bacteriol* **184**, 2420-2428

45. Wintermeyer, E., Flugel, M., Ott, M., Steinert, M., Rdest, U., Mann, K. H., and Hacker, J. (1994) Sequence determination and mutational analysis of the lly locus of Legionella pneumophila. *Infection and immunity* **62**, 1109-1117

46. Kotob, S. I., Coon, S. L., Quintero, E. J., and Weiner, R. M. (1995) Homogentisic acid is the primary precursor of melanin synthesis in Vibrio cholerae, a Hyphomonas strain, and Shewanella colwelliana. *Applied and environmental microbiology* **61**, 1620-1622

47. Ernst, R. K., D'Argenio, D. A., Ichikawa, J. K., Bangera, G. M., Selgrade, S., Burns, J. L., Hiatt, P., McCoy, K., Brittnacher, M., Kas, A., Spencer, D. H., Olson, M. V., Ramsey, B. W., Lory, S., and Miller, S. I. (2003) Genome mosaicism is conserved but not unique in Pseudomonas aeruginosa isolates from the airways of young children with cystic fibrosis. *Environmental Microbiology* **5**, 1341-1349

48. Rodriguez-Rojas, A., Mena, A., Martin, S., Borrell, N., Oliver, A., and Blazquez, J. (2009) Inactivation of the hmgA gene of Pseudomonas aeruginosa leads to

pyomelanin hyperproduction, stress resistance and increased persistence in chronic lung infection. *Microbiology* **155**, 1050-1057

49. Boles, B. R., Thoendel, M., and Singh, P. K. (2004) Self-generated diversity produces "insurance effects" in biofilm communities. *Proceedings of the National Academy of Sciences of the United States of America* **101**, 16630-16635
50. Keith, K. E., Killip, L., He, P., Moran, G. R., and Valvano, M. A. (2007) Burkholderia cenocepacia C5424 produces a pigment with antioxidant properties using a homogentisate intermediate. *J Bacteriol* **189**, 9057-9065
51. Nunes, L. R., Costa de Oliveira, R., Leite, D. B., da Silva, V. S., dos Reis Marques, E., da Silva Ferreira, M. E., Ribeiro, D. C., de Souza Bernardes, L. A., Goldman, M. H., Puccia, R., Travassos, L. R., Batista, W. L., Nobrega, M. P., Nobrega, F. G., Yang, D. Y., de Braganca Pereira, C. A., and Goldman, G. H. (2005) Transcriptome analysis of Paracoccidioides brasiliensis cells undergoing mycelium-to-yeast transition. *Eukaryot Cell* **4**, 2115-2128
52. Serre, L., Sailland, A., Sy, D., Boudec, P., Rolland, A., Pebay-Peyroula, E., and Cohen-Addad, C. (1999) Crystal structure of Pseudomonas fluorescens 4-hydroxyphenylpyruvate dioxygenase: an enzyme involved in the tyrosine degradation pathway. *Structure Fold Des* **7**, 977-988
53. Brownlee, J., He, P., Moran, G. R., and Harrison, D. H. (2008) Two roads diverged: the structure of hydroxymandelate synthase from Amycolatopsis orientalis in complex with 4-hydroxymandelate. *Biochemistry* **47**, 2002-2013
54. Fritze, I. M., Linden, L., Freigang, J., Auerbach, G., Huber, R., and Steinbacher, S. (2004) The crystal structures of Zea mays and Arabidopsis 4-hydroxyphenylpyruvate dioxygenase. *Plant Physiol* **134**, 1388-1400
55. Yang, C., Pflugrath, J. W., Camper, D. L., Foster, M. L., Pernich, D. J., and Walsh, T. A. (2004) Structural Basis for Herbicidal Inhibitor Selectivity Revealed by Comparison of Crystal Structures of Plant and Mammalian 4-Hydroxyphenylpyruvate Dioxygenases. *Biochemistry* **43**, 10414-10423
56. He, P., and Moran, G. R. (2011) Structural and mechanistic comparisons of the metal-binding members of the vicinal oxygen chelate (VOC) superfamily. *Journal of inorganic biochemistry* **105**, 1259-1272

57. Armstrong, R. N. (2000) Mechanistic diversity in a metalloenzyme superfamily. *Biochemistry* **39**, 13625-13632

58. Zhang, Z., Ren, J., Harlos, K., McKinnon, C. H., Clifton, I. J., and Schofield, C. J. (2002) Crystal structure of a clavaminate synthase-Fe(II)-2-oxoglutarate-substrate-NO complex: evidence for metal centred rearrangements. *FEBS Lett* **517**, 7-12.

59. Hegg, E. L., and Que, L., Jr. (1997) The 2-His-1-carboxylate facial triad--an emerging structural motif in mononuclear non-heme iron(II) enzymes. *Eur J Biochem* **250**, 625-629

60. Koehntop, K. D., Emerson, J. P., and Que, L., Jr. (2005) The 2-His-1-carboxylate facial triad: a versatile platform for dioxygen activation by mononuclear non-heme iron(II) enzymes. *J Biol Inorg Chem* **10**, 87-93

61. O'Hare, H. M., Huang, F., Holding, A., Choroba, O. W., and Spencer, J. B. (2006) Conversion of hydroxyphenylpyruvate dioxygenases into hydroxymandelate synthases by directed evolution. *FEBS Lett* **580**, 3445-3450

62. Gunsior, M., Ravel, J., Challis, G. L., and Townsend, C. A. (2004) Engineering p-hydroxyphenylpyruvate dioxygenase to a p-hydroxymandelate synthase and evidence for the proposed benzene oxide intermediate in homogentisate formation. *Biochemistry* **43**, 663-674

63. Shah, D. D., Conrad, J. A., Heinz, B., Brownlee, J. M., and Moran, G. R. (2011) Evidence for the mechanism of hydroxylation by 4-hydroxyphenylpyruvate dioxygenase and hydroxymandelate synthase from intermediate partitioning in active site variants. *Biochemistry* **50**, 7694-7704

64. Shah, D. D., Conrad, J. A., and Moran, G. R. (2013) Intermediate partitioning kinetic isotope effects for the NIH shift of 4-hydroxyphenylpyruvate dioxygenase and the hydroxylation reaction of hydroxymandelate synthase reveal mechanistic complexity. *Biochemistry* **52**, 6097-6107

65. Moran, G. R. (2014) 4-Hydroxyphenylpyruvate dioxygenase and hydroxymandelate synthase: exemplars of the alpha-keto acid dependent oxygenases. *Archives of biochemistry and biophysics* **544**, 58-68

66. Pavel, E. G., Zhou, J., Busby, R. W., Gunsior, M., Townsend, C. A., and Solomon, E. I. (1998) Circular Dichroism and Magnetic Circular Dichroism Spectroscopic Studies of the Non-Heme Ferrous Active Site in Clavaminate Synthase and Its Interaction with alpha-Ketoglutarate Cosubstrate. *J. Am. Chem. Soc.* **120**, 743-753

67. Solomon, E. I., Decker, A., and Lehnert, N. (2003) Bioinorganic Chemistry Special Feature: Non-heme iron enzymes: Contrasts to heme catalysis. *Proceedings of the National Academy of Sciences of the United States of America* **100**, 3589-3594

68. Cosper, N. J., Stalhandske, C. M., Saari, R. E., Hausinger, R. P., and Scott, R. A. (1999) X-ray absorption spectroscopic analysis of Fe(II) and Cu(II) forms of a herbicide-degrading alpha-ketoglutarate dioxygenase. *J Biol Inorg Chem* **4**, 122-129

69. Neidig, M. L., Kavana, M., Moran, G. R., and Solomon, E. I. (2004) CD and MCD Studies of the Non-Heme Ferrous Active Site in (4-Hydroxyphenyl)pyruvate Dioxygenase: Correlation Between Oxygen Activation in the Extradiol and alpha-KG Dependent Dioxygenases. *J Am Chem Soc* **126**, 4486-4487

70. Ryle, M. J., Padmakumar, R., and Hausinger, R. P. (1999) Stopped-Flow Kinetic Analysis of Escherichia coli Taurine/alpha- Ketoglutarate Dioxygenase: Interactions with alpha-Ketoglutarate, Taurine, and Oxygen. *Biochemistry* **38**, 15278-15286

71. Elkins, J. M., Ryle, M. J., Clifton, I. J., Dunning Hotopp, J. C., Lloyd, J. S., Burzlaff, N. I., Baldwin, J. E., Hausinger, R. P., and Roach, P. L. (2002) X-ray crystal structure of Escherichia coli taurine/alpha-ketoglutarate dioxygenase complexed to ferrous iron and substrates. *Biochemistry* **41**, 5185-5192.

72. Zhou, J., Kelly, W. L., Bachmann, B. O., Gunsior, M., Townsend, C. A., and Solomon, E. I. (2001) Spectroscopic studies of substrate interactions with clavaminate synthase 2, a multifunctional alpha-KG-dependent non-heme iron enzyme: correlation with mechanisms and reactivities. *J Am Chem Soc* **123**, 7388-7398.

73. He, P., Conrad, J. A., and Moran, G. R. (2010) The rate-limiting catalytic steps of hydroxymandelate synthase from Amycolatopsis orientalis. *Biochemistry* **49**, 1998-2007

74. Johnson-Winters, K., Purpero, V. M., Kavana, M., and Moran, G. R. (2005) Accumulation of Multiple Intermediates in the Catalytic Cycle of (4-Hydroxyphenyl)pyruvate Dioxygenase from Streptomyces avermitilis. *Biochemistry* **44**, 7189-7199

75. Johnson-Winters, K., Purpero, V. M., Kavana, M., Nelson, T., and Moran, G. R. (2003) (4-Hydroxyphenyl)pyruvate Dioxygenase from Streptomyces avermitilis: The Basis for Ordered Substrate Addition. *Biochemistry* **42**, 2072-2080

76. Neidig, M. L., Decker, A., Choroba, O. W., Huang, F., Kavana, M., Moran, G. R., Spencer, J. B., and Solomon, E. I. (2006) Spectroscopic and electronic structure studies of aromatic electrophilic attack and hydrogen-atom abstraction by non-heme iron enzymes. *Proceedings of the National Academy of Sciences of the United States of America* **103**, 12966-12973

77. Neidig, M. L., Brown, C. D., Kavana, M., Choroba, O. W., Spencer, J. B., Moran, G. R., and Solomon, E. I. (2006) Spectroscopic and electronic structure studies of the role of active site interactions in the decarboxylation reaction of alpha-keto acid-dependent dioxygenases. *J Inorg Biochem* **100**, 2108-2116

78. Wojcik, A., Broclawik, E., Siegbahn, P. E., and Borowski, T. (2012) Mechanism of benzylic hydroxylation by 4-hydroxymandelate synthase. A computational study. *Biochemistry* **51**, 9570-9580

79. Freeman, B. A., and Crapo, J. D. (1982) Biology of disease: free radicals and tissue injury. *Laboratory investigation; a journal of technical methods and pathology* **47**, 412-426

80. Zhang, Z., Ren, J., Stammers, D. K., Baldwin, J. E., Harlos, K., and Schofield, C. J. (2000) Structural origins of the selectivity of the trifunctional oxygenase clavaminic acid synthase. *Nat Struct Biol* **7**, 127-133.

81. Clifton, I. J., Hsueh, L. C., Baldwin, J. E., Harlos, K., and Schofield, C. J. (2001) Structure of proline 3-hydroxylase. Evolution of the family of 2-oxoglutarate dependent oxygenases. *Eur J Biochem* **268**, 6625-6636

82. Wilmouth, R. C., Turnbull, J. J., Welford, R. W., Clifton, I. J., Prescott, A. G., and Schofield, C. J. (2002) Structure and mechanism of anthocyanidin synthase from Arabidopsis thaliana. *Structure (Camb)* **10**, 93-103.

83. O'Brien, J. R., Schuller, D. J., Yang, V. S., Dillard, B. D., and Lanzilotta, W. N. (2003) Substrate-induced conformational changes in Escherichia coli taurine/alpha-ketoglutarate dioxygenase and insight into the oligomeric structure. *Biochemistry* **42**, 5547-5554

84. Brownlee, J., Johnson-Winters, K., Harrison, D. H. T., and Moran, G. R. (2004) The Structure of the Ferrous Form of (4–Hydroxyphenyl)pyruvate Dioxygenase from Streptomyces avermitilis in Complex with the Therapeutic Herbicide, NTBC. *Biochemistry* **43**, 6370-6377

85. Muller, I., Kahnert, A., Pape, T., Sheldrick, G. M., Meyer-Klaucke, W., Dierks, T., Kertesz, M., and Uson, I. (2004) Crystal structure of the alkylsulfatase AtsK: Insights into the catalytic mechanism of the Fe(II) alpha-ketoglutarate-dependent dioxygenase superfamily. *Biochemistry* **43**, 3075-3088

86. McDonough, M. A., Kavanagh, K. L., Butler, D., Searls, T., Oppermann, U., and Schofield, C. J. (2005) Structure of human phytanoyl-CoA 2-hydroxylase identifies molecular mechanisms of Refsum disease. *J Biol Chem* **280**, 41101-41110

87. Lin, J. F., Sheih, Y. L., Chang, T. C., Chang, N. Y., Chang, C. W., Shen, C. P., and Lee, H. J. (2013) The interactions in the carboxyl terminus of human 4-hydroxyphenylpyruvate dioxygenase are critical to mediate the conformation of the final helix and the tail to shield the active site for catalysis. *PloS one* **8**, e69733

88. Conrad, J. A., and Moran, G. R. (2008) The Interaction of Hydroxymandelate Synthase with the 4-Hydroxyphenylpyruvate Dioxygenase Inhibitor: NTBC. *Inorganica Chim Acta* **361**, 1197-1201

89. Garcia, I., Job, D., and Matringe, M. (2000) Inhibition of p-hydroxyphenylpyruvate dioxygenase by the diketonitrile of isoxaflutole: a case of half-site reactivity. *Biochemistry* **39**, 7501-7507

90. Krohn, K. A., and Link, J. M. (2003) Interpreting enzyme and receptor kinetics: keeping it simple, but not too simple. *Nuclear medicine and biology* **30**, 819-826

91. Kavana, M., and Moran, G. R. (2003) Interaction of (4-hydroxyphenyl)pyruvate dioxygenase with the specific inhibitor 2-[2-nitro-4-(trifluoromethyl)benzoyl]-1,3-cyclohexanedione. *Biochemistry* **42**, 10238-10245

92. Neidig, M. L., Decker, A., Kavana, M., Moran, G. R., and Solomon, E. I. (2005) Spectroscopic and computational studies of NTBC bound to the non-heme iron enzyme (4-hydroxyphenyl)pyruvate dioxygenase: Active site contributions to drug inhibition. *Biochemical and biophysical research communications* **338**, 206-214

93. Diebold, A. R., Brown-Marshall, C. D., Neidig, M. L., Brownlee, J. M., Moran, G. R., and Solomon, E. I. (2011) Activation of alpha-Keto Acid-Dependent Dioxygenases: Application of an {FeNO}(7)/{FeO(2)}(8) Methodology for Characterizing the Initial Steps of O(2) Activation. *Journal of the American Chemical Society* **133**, 18148-18160

94. Borowski, T., Bassan, A., and Siegbahn, P. E. M. (2004) 4-hydroxyphenylpyruvate dioxygenase: A hybrid density functional study of the catalytic reaction mechanism. *Biochemistry* **43**, 12331-12342

95. Costas, M., Mehn, M. P., Jensen, M. P., and Que, L. (2004) Dioxygen activation at mononuclear nonheme iron active sites: Enzymes, models, and intermediates. *Chemical Reviews* **104**, 939-986

96. Price, J. C., Barr, E. W., Glass, T. E., Krebs, C., and Bollinger, J. M., Jr. (2003) Evidence for hydrogen abstraction from C1 of taurine by the high-spin Fe(IV) intermediate detected during oxygen activation by taurine:alpha-ketoglutarate dioxygenase (TauD). *J Am Chem Soc* **125**, 13008-13009

97. Price, J. C., Barr, E. W., Hoffart, L. M., Krebs, C., and Bollinger, J. M., Jr. (2005) Kinetic Dissection of the Catalytic Mechanism of Taurine:alpha-Ketoglutarate Dioxygenase (TauD) from Escherichia coli. *Biochemistry* **44**, 8138-8147

98. Price, J. C., Barr, E. W., Tirupati, B., Bollinger, J. M., Jr., and Krebs, C. (2003) The first direct characterization of a high-valent iron intermediate in the reaction of an alpha-ketoglutarate-dependent dioxygenase: a high-spin FeIV complex in

taurine/alpha-ketoglutarate dioxygenase (TauD) from Escherichia coli. *Biochemistry* **42**, 7497-7508

99. Riggs-Gelasco, P. J., Price, J. C., Guyer, R. B., Brehm, J. H., Barr, E. W., Bollinger, J. M., Jr., and Krebs, C. (2004) EXAFS spectroscopic evidence for an Fe=O unit in the Fe(IV) intermediate observed during oxygen activation by taurine:alpha-ketoglutarate dioxygenase. *J Am Chem Soc* **126**, 8108-8109
100. Krebs, C., Galonic Fujimori, D., Walsh, C. T., and Bollinger, J. M., Jr. (2007) Non-heme Fe(IV)-oxo intermediates. *Acc Chem Res* **40**, 484-492
101. Hoffart, L. M., Barr, E. W., Guyer, R. B., Bollinger, J. M., Jr., and Krebs, C. (2006) Direct spectroscopic detection of a C-H-cleaving high-spin Fe(IV) complex in a prolyl-4-hydroxylase. *Proceedings of the National Academy of Sciences of the United States of America* **103**, 14738-14743
102. Bradley, F. C., Lindstedt, S., Lipscomb, J. D., Que, L., Jr., Roe, A. L., and Rundgren, M. (1986) 4-Hydroxyphenylpyruvate dioxygenase is an iron-tyrosinate protein. *J Biol Chem* **261**, 11693-11696
103. Liu, A., Ho, R. Y., Que, L., Ryle, M. J., Phinney, B. S., and Hausinger, R. P. (2001) Alternative Reactivity of an alpha-Ketoglutarate-Dependent Iron(II) Oxygenase: Enzyme Self-Hydroxylation. *J Am Chem Soc* **123**, 5126-5127
104. Muller, I., Stuckl, C., Wakeley, J., Kertesz, M., and Uson, I. (2005) Succinate complex crystal structures of the alpha-ketoglutarate-dependent dioxygenase AtsK: steric aspects of enzyme self-hydroxylation. *J Biol Chem* **280**, 5716-5723
105. Purpero, V. M., and Moran, G. R. (2006) Catalytic, noncatalytic, and inhibitory phenomena: kinetic analysis of (4-hydroxyphenyl)pyruvate dioxygenase from Arabidopsis thaliana. *Biochemistry* **45**, 6044-6055
106. Lindblad, B., Lindstedt, G., and Lindstedt, S. (1970) The Mechanism of Enzymic Formation of Homogentisate from p-Hydroxyphenylpyruvate. *J. Am. Chem. Soc.* **92**, 7446-7449
107. Leinberger, R., Hull, W. E., Simon, H., and Retey, J. (1981) Steric course of the NIH shift in the enzymic formation of homogentisic acid. *Eur J Biochem* **117**, 311-318

108. Pascal, R. A., Jr., Oliver, M. A., and Chen, Y. C. (1985) Alternate substrates and inhibitors of bacterial 4- hydroxyphenylpyruvate dioxygenase. *Biochemistry* **24**, 3158-3165

109. Daly, J. W., Jerina, D. M., and Witkop, B. (1972) Arene oxides and the NIH shift: The metabolism, toxicity and carcinogenicity of aromatic compounds. *Experientia* **28**, 1129-1264

110. Jerina, D. M., Daly, J. W., and Witkop, B. (1968) The role of arene oxide-oxepin systems in the metabolism of aromatic substrates. II. Synthesis of 3,4-toluene-4-2H oxide and subsequent "NIH shift" to 4-hydroxytoluene-3-2H. *J.Am.Chem.Soc.* **90**, 6523-6525

111. Kasperek, G. J., Bruice, T. C., Yagi, H., and Jerina, D. M. (1972) Differentiation between the concerted and stepwise mechanisms for aromatization (NIH-shift) of arene epoxides. *J.C.S.Chem.Comm.*, 784-785

112. Moran, G. R., Derecskei-Kovacs, A., Hillas, P. J., and Fitzpatrick, P. F. (2000) On the Catalytic Mechanism of Tryptophan Hydroxylase. *J Am Chem Soc* **122**, 4535-4541

113. Fitzpatrick, P. F. (2006) Isotope Effects from Partitioning of Intermediates in Enzyme-Catalyzed Hydroxylation Reactions. in *Isotope Effects in Chemsitry and Biology* (Kohen, A., and Limbach, H.-H. eds.), CRC Taylor & Francis, Boca Raton. pp 861-873

114. G.R. Moran, P. He, Treatment of microbial infections with compounds that inhibit 4-hydroxyphenylpyruvate dioxygenase, in: U.P. Office (Ed.), US20100227936 A1, USA, 2010.

Chapter 2

Evidence for the Mechanism of Hydroxylation by 4-Hydroxyphenylpyruvate Dioxygenase and Hydroxymandelate Synthase from Intermediate Partitioning in Active Site Variants

2.1 Introduction

Both 4-Hydroxyphenylpyruvate dioxygenase (HPPD) and hydroxymandelate synthase (HMS) catalyze very similar dioxygenation reactions, even to the extent that they require the same substrates, 4-hydroxyphenylpyruvate (HPP) and dioxygen (Scheme 2.1). With respect to the reactions catalyzed, HPPD and HMS principally differ in the placement of one of the atoms of dioxygen. For each, one oxygen atom is committed to an oxidative decarboxylation that converts the pyruvate side chain to an aceto substituent. The other oxygen atom is then added as a hydroxyl with HMS hydroxylating at the benzylic carbon forming hydroxymandelate (HMA) and HPPD at the adjacent C1 of the aromatic ring. Hydroxylation of the ring then induces a fascinating transformation involving a 1,2-shift of the aceto substituent forming 2,5-dihydroxyphenylacetate (homogentisate, HG).

HPPD is common to ostensibly all aerobes and is almost certainly the progenitor of HMS that is found in a relatively small number of bacteria. The HPPD reaction is the second step of tyrosine catabolism, a five-step pathway whose fundamental purpose is to produce the energy-yielding products, fumarate and acetoacetate (1). However, pathway intermediates can be drawn into the biosynthesis of other molecules (2-5). HMS participates in one example of this, as it functions to divert HPP from tyrosine catabolism to form HMA toward the biosynthesis of hydroxyphenylglycine that is incorporated into a variety of non-ribosomal peptides such as vancomycin (6,7). Another example occurs in plants where HG is the precursor to tocopherol and the critical photosynthetic cofactor, plastoquinone. It is this that has, for the last three decades, garnered considerable research interest in HPPD. Molecules that inhibit HPPD have potent herbicidal effects and a number of such molecules are now sold worldwide as broad-leaf herbicides (8-10). An

unexpected additional use for one of the molecules originally developed as a herbicide has been as a therapeutic that can alleviate the symptoms of a number of in-born defects in tyrosine catabolism (11-13). It could be argued that the study of the inhibition of HPPD has eclipsed the study of its reaction mechanism and key details of the reaction mechanism remain unsupported. Similarly, as it has only been described in the literature recently, relatively little is known of the chemistry catalyzed by HMS (7,14).

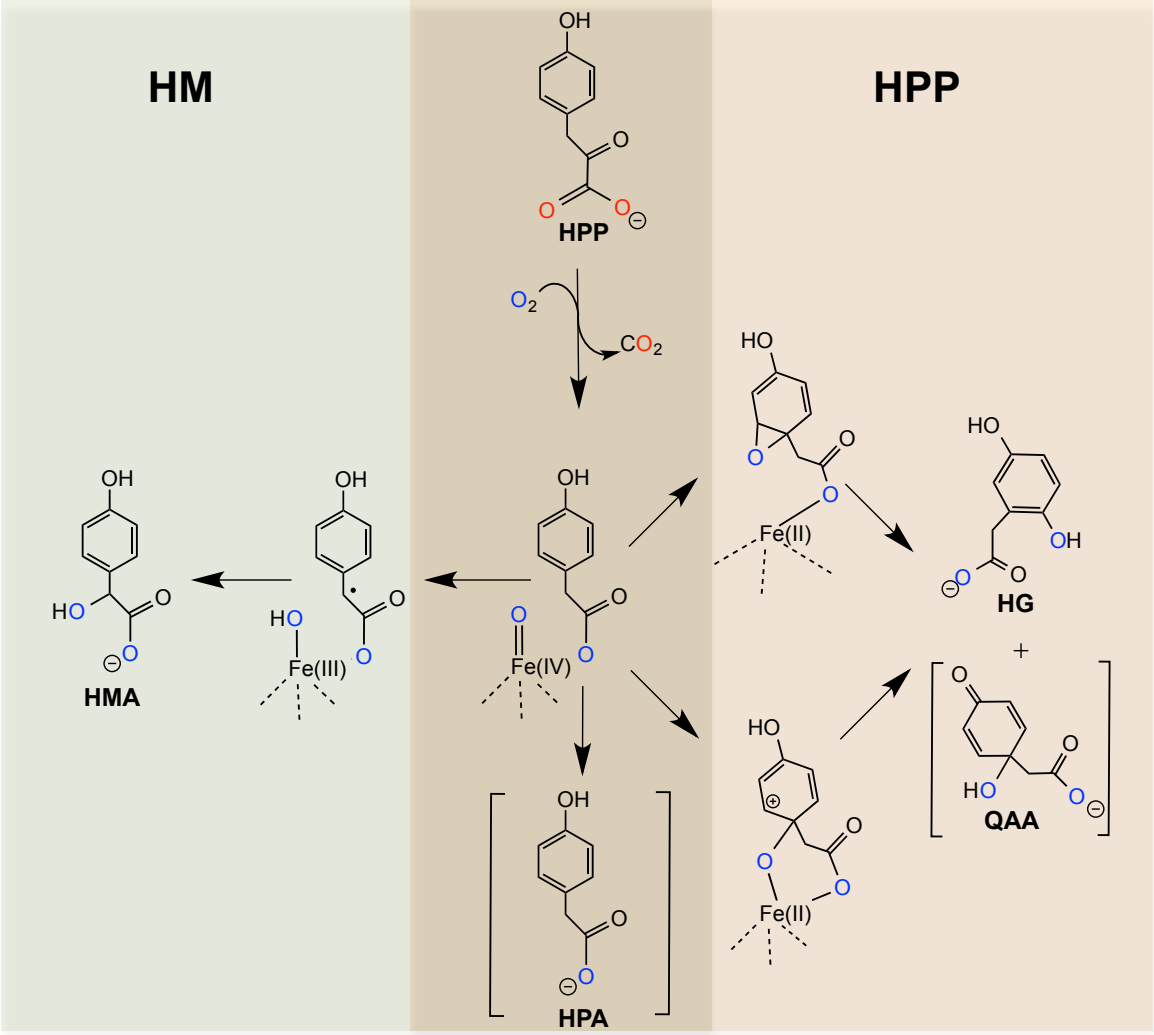

[a] Brackets indicate non-native products

Scheme 2.1 Product partitioning in HPPD and HMS

HPPD and HMS are Fe(II)-dependent dioxygenases that, from a chemical standpoint, are grouped with the α-keto acid dependent oxygenases (α-KAOs) (15). Structurally, however, both enzymes differ from the majority of α-KAOs that have a jellyroll fold. Instead, HPPD and HMS have a topology that is common to the vicinal oxygen chelate superfamily (16). α-KAO enzymes all obtain electrons to activate molecular oxygen from oxidative decarboxylation of an α-keto acid. The most common ensuing reaction of this group of enzymes is hydroxylation. HPPD is somewhat unusual in that it hydroxylates an aromatic ring inducing the 1,2-shift of the aceto substituent (Scheme 2.1). While shifts of this type have been observed in a number of oxygenases, it is more common that only small substituents such as deuteriums, tritiums, halides and methyl groups can be induced to shift in this manner and generally only in a fraction of total catalysis (17-25). The identity of the intermediate that is the immediate product of hydroxylation in such reactions has been the source of conjecture for more than 40 years. The principle division is based around the intermediacy of an epoxide or a benzylic cation. Either species can be readily envisaged to resolve as the final aromatic product and experiments that unambiguously show one mechanism over the other have proven exceedingly difficult to design. One definitive method to distinguish between these two mechanisms is to measure the secondary kinetic isotope effect on the hydroxylation step when a deuterium is substituted ortho to (or if applicable at) the point of hydroxylation (26). However, in terms of direct observation or kinetic resolution, few if any of the systems that exhibit an NIH shift are amenable to this observation. That is to say that the hydroxylation rate constant cannot be measured with sufficient precision or else cannot be observed independently due to the balance of rate constants for steps before and after

(25,27-29). Moreover, this is a recurrent limitation in the study of many metal dependent oxygenases, including for enzymes that carry out less complicated hydroxylation reactions such as hydroxylation at aliphatic carbon atoms, as is the case for HMS. These hydroxylation reactions exhibit primary kinetic isotope effects when deuterium atoms are substituted at the point of hydroxylation (30) but these effects can also be completely shrouded (31). The utility of intermediate partitioning and product analysis has emerged as a robust and accurate method that can be used to unveil otherwise hidden kinetic isotope effects (26,32-35). In this chapter we describe the application of this methodology to variants of HPPD and HMS that exhibit bifurcation and trifurcation during the hydroxylation step and as such yield multiple distinct products in a defined ratio (Scheme 2.1).

2.2 Materials and Methods

Materials. HPP and HG were purchased from Acros Chemicals. HMA and 4-hydroxphenylacetatete (HPA) were obtained from Sigma-Aldrich. Mutagenesis was performed using the materials and protocol of the Stratagene QuikChange Lightning ® kit. Competent BL21(DE3) *Escherichia coli* cells were obtained from New England Biolabs. IPTG was from Gold Biochemicals. D_2O was from Cambridge Isotope Labs. Q-Sepharose was from Bio-Rad. Sephacryl S-200 was obtained from Amersham. Quinolacetate (QAA) was made using the P243T variant described in this manuscript and purified as previously described (13). Per-deutero-HPP and 3'3'-dideutero-HPP were prepared according to our previously published methods (27,31). All other chemicals, buffers, and biological media were obtained from Fisher Scientific or Sigma-Aldrich Chemicals and were of high purity.

Mutagenesis. pET17b-derived (Novagen) plasmids carrying the *Streptomyces avermitilis* HPPD gene (pSAHPPD; (36)) and the *Amycolatopsis orientalis* HMS gene (pAOHMS; (37)) were mutated using the Stratagene QuikChange Lightning ® kit. Mutations were identified in the transformants by either incorporating changes to the plasmid restriction pattern by the addition of silent mutations or by sequencing the plasmid from multiple transformants. In each case, sequencing the entire gene confirmed the desired mutations and the absence of additional spurious mutations (Sequetech, Mountainview CA). The following oligonucleotides and their respective reverse complement oligonucleotide were used to mutate the HPPD gene(s):

HPPD Oligos

SAHPPDN245I: GGTCAAGTTCCCGATCATCGAGCCCGCCCTGGCCAAGAAGAA

SAHPPDN245Q: CAAGTTCCCGATCCAGGAGCCCGCCCTGGCCAAGAAGAA

SAHPPDP243T:

CTCAAGGTCAAGTTCACGATCAACGAGCCCGCCTTGGCCAAGAAGAAGTCC

SAHPPDS230A:

GACATCGCGACCGAGTATTCGGCGCTGATGGCGAAGGTCGTGGC

HMS Oligos

AOHMSI216N: CACCCTCACCCTGAACGAGCCCGACCG

AOHMST214P: GCGGTCACCCTCCCGCTGATCGAGCCC

AOHMSS201A: CAGGCGATGAACGCCACCGTCGTGCAG

Expression and Purification. The apo-forms of WT and variants of HPPD and HMS were expressed and purified using ammonium sulfate fractionation, anion exchange chromatography and size exclusion chromatography according to published methods (36,37).

Standard Assay Conditions and Steady-State Analysis. HPPD/HMS activity was measured using a Hansatech Oxygraph dioxygen electrode. Standard activity assays included 1-2 μM of enzyme, 1 mM β-mercaptoethanol (βME), 20 μM ferrous sulfate, and 400 μM HPP in 20 mM HEPES pH 7.0 at 25 ^{o}C with atmospheric oxygen (250 μM). Reactions were initiated with HPP, and rates were measured between 20 and 50 s of initiation. Apparent kinetic parameters were measured by varying the concentration of

HPP. Data were fit to the Michaelis-Menten Equation (equation 1).

equation 1. $$v = V_{max}\,[S]/(K_m+[S])$$

Kinetic Isotope Effects from HPLC Product Analysis. The ratio of products of each variant enzyme was determined using high-pressure liquid chromatography. Initially enzyme turnover reactions were undertaken at 25 °C and were comprised of 25 μM ferrous sulfate, 6-10 μM HPPD or HMS, 1 mM reductant (either βME or dithiothreitol), 250 μM O_2, and 100 μM HPP in 10 mM potassium phosphate or 20 mM HEPES buffer (pH 7.0). The initial background rate of dioxygen reduction due to Fenton chemistry was observed before the enzymatic reaction was initiated by either the addition of unlabeled or deutero-labeled HPP (ring-deutero for HPPD and 3'3'-dideutero for HMS). After completion of the reaction (i.e, when the observed rate of dioxygen consumption approximated that due to background dioxygen reduction), 400 μL of the reaction mixture was withdrawn added to a 0.5 mL, 10 kDa nominal molecular weight limit ultra centrufugal filter (Amicon) and centrifuged at 14000g for 7 min to remove the enzyme. The resulting filtrate was chromatographed using a Waters 600E HPLC system fitted with a 4.6 mm x 150 mm Waters 5 μm Xterra reverse phase C18 column. The column was run under isocratic conditions at 1 mL/min with a mobile phase consisting of 10 mM potassium phosphate (pH 2.0) and 0.5% acetonitrile. Elution was monitored at 220 and 276 nm using a Waters 2487 dual wavelength detector. Individual products were identified by co-elution with standards for each. Quantitation was accomplished by preparing standard curves from 0–100 μM for each product under the same conditions.

Kinetic isotope effects were calculated using Equation 2 that computes the factor of perturbation of the product ratio in the presence of the deuterated substrate for the case of a trifurcating mechanism (35).

equation 2. $$^{D}k_{obs} = \frac{(P_1/(P_1+P_2+U))^{H}}{(P_1/(P_1+P_2+U))^{D}}$$

In this equation, P_1 is the concentration of product for which the isotope effect is being determined and P_2 is the concentration of an alternate product formed in the same reaction. For both HPPD and HMS, U refers to uncoupling in the hydroxylation step that is isotopically insensitive and results in the production of HPA. For the case of bifurcating reactions where two products are evolved the P_2 term is omitted. To ensure that all of catalysis was considered, the total consumption of molecular oxygen was compared to the total concentration of products formed.

The KIE values for HG would be skewed if QAA were to act as a shunt substrate for HPPD and converted to HG. In order to establish if HPPD can catalyze the conversion of QAA to HG, 60 μM QAA was incubated with 15 μM HPPD in the presence of 25 μM ferrous sulfate, 1 mM ascorbate in 10 mM potassium phosphate buffer pH 7.0. After incubation at 25 ^{o}C for 10 min (approximately twice as the length of time used for the KIE assays), 200 μL of the reaction was withdrawn, filtered and chromatographed as above. The chromatogram obtained from this sample was then compared to the control incubated in an equivalent manner in the absence of HPPD.

2.3 Results

Characterization of the Variant Enzymes. Each of the HPPD and HMS variants described could be expressed and purified using published methods for the wild type enzymes (31,36). Moreover, the yield of purified enzyme was generally comparable to the wild type forms and each could be stored at – 80 ^{o}C without appreciable loss of activity. Apparent steady-state turnover values for each variant are listed in Table 2.1. These values are not directly applicable to the conclusions made here but do indicate that each mutation yields an active and competent enzyme.

Table 2.1 Steady-State Kinetic Values

HPPD Variant	**WT**	**N245I**	**N254Q**	**P243T**	**S230A**
k_{cat} (s^{-1})	6.8 ± 0.6	0.64 ± 0.09	0.03 ± 0.01	2.1 ± 0.1	2.8 ± 0.4
K_{HPP} (μM)	27 ± 6	27 ± 5	15.0 ± 3.3	8.7 ± 2.8	47 ± 16
k_{cat}/K_{HPP} (mM^{-1} s^{-1})	254 ± 70	24 ± 6	2.4 ± 0.4	241 ± 36	60 ± 15
HMS Variant	**WT**	**I216N**		**T214P**	**S201A**
k_{cat} (s^{-1})	3.7 ± 0.1	1.4 ± 0.1		1.18 ± 0.04	3.0 ± 0.6
K_{HPP} (μM)	47.6 ± 5.6	14.3 ± 3.0		20.5 ± 2.8	28.0 ± 13.5
k_{cat}/K_{HPP} (mM^{-1} s^{-1})	77 ± 5	98.5 ± 14.5		57.5 ± 6.5	108 ± 19

Product Analysis. The percentages of products formed by each variant of HPPD and HMS are shown in Table 2.2 and the position of each residue in the active site is shown in Figure 2.1. For each variant all major products were accounted for in that the percentages of all products summed to ~100 % based on the uptake of dioxygen. This indicates that for both HPPD and HMS, hydroxylation is tightly coupled to dioxygen

reduction and that all reducing equivalents committed to catalysis result in substrate decarboxylation.

Table 2.2 Percentage of Products Formed

HPPD Variant	**WT**	**N245I**	**N245Q**	**P243T**	**S230A**
HG (%)	84.5	13	44.5	13	11.6
QAA (%)	0	0	4	78	57.8
HPA (%)	15.4	86.6	52	8.7	30.6
HMA (%)	0	0	0	0	0
Total	99.9	99.6	100.5	99.7	100
HMS Variant	**WT**	**I216N**		**T214P**	**S201A**
HG (%)	0	0		0	0
QAA (%)	0	0		0	0
HPA (%)	0	10		0	12
HMA (%)	100	90		100	88
Total	100	100		100	100

None of the variants presented made any fraction of the product of the other enzyme. In other words, HPPD variants were observed to make only HG, HPA and QAA, while HMS variants made only HMA and HPA, indicating that the preference for hydroxylation regiospecificity was not altered by these mutations. Under the conditions used in this investigation wild type HPPD is prone to uncoupling to form HPA. This suggests that the hydroxylation of the aromatic ring is less optimized than the hydroxylation of the benzylic position by HMS, that is fully coupled to the formation of HMA. For respective HPPD/HMS variants, alteration of the 245/216 position and the 230/201 position increases uncoupling in the hydroxylation reaction yielding more HPA than is observed in the wild type of either enzyme (Figure 2.1).

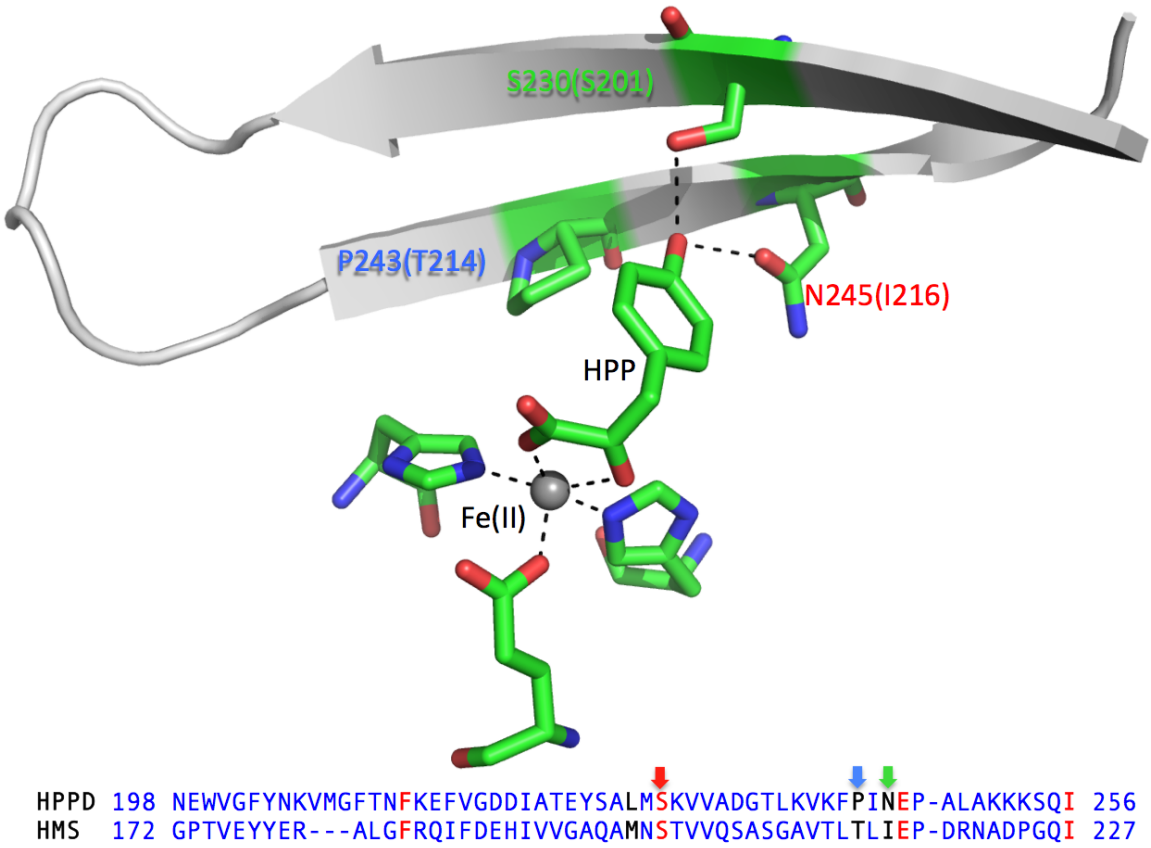

Figure 2.1 Positions of the residues targeted for mutagenesis. The positions are shown for HPPD with residues and numbers in parentheses indicating the corresponding residue in HMS. All three positions are clustered on the third and fourth β strands of the β-barrel that is common to the vicinal oxygen chelate superfamily of enzymes. The putative 4-hydroxyphenylpyuvate binding site was modeled in earlier work using molecular dynamics and was based the observed binding position for hydroxymandelate in hydroxymandelate synthase (37). In this position the 4-hydroxyl of the substrate phenol is within hydrogen bonding distance to the conserved serine residue. The sections of amino acid sequence shown compare the primary sequences of HPPD from *Strepomyces avermitilis* and HMS from *Amycolatopsis orientalis* local to the residues altered by mutation.

Interestingly, mutating to counterpart residues at the 243/214 positions resulted in improved or equivalent hydroxylation efficiency. For HMS, this result is contrary to what would be predicted from structure as threonine 214 is observed to hydrogen bond to the newly added side chain hydroxyl in the HMS•HMA product complex, prompting the proposal that this threonine may participate in the delivery of the oxygen to the benzylic

carbon (37). P243 in HPPD clearly contributes an important steric component to the execution of the NIH shift. Mutating this residue to threonine results in the majority (~80%) of the hydroxylation reaction terminating with the formation of QAA; where the hydroxyl has been delivered to the ring C1 without displacement of the aceto substituent bonded in this position. The N245 position is also critically important in the NIH shift. In previous work we have shown that mutation of this position to a serine residue results in a predominance of QAA (13). Here, mutation to an isoleucine results in ~90% uncoupling in the hydroxylation step and the formation of HPA. Curiously, the N245Q and N245I variants were able to complete the shift for most instances in which they hydroxylate the ring (~50%, ~10% respectively) and uncouple to make HPA for the remaining fraction of total turnover. Together these results suggest that a hydrogen-bonding residue in the 245 position aids the initial ring hydroxylation reaction and that only in the presence of a large and/or amide side chain can the NIH shift occur.

The serine at position 230/201 is fully conserved in all HPPD and HMS primary structures implying that it is vital in the mechanisms of both enzymes. This would appear to be correct for HPPD that either uncouples or predominantly fails to execute the shift when this residue is mutated to an alanine. However, S201A in HMS has a very modest effect on the product distribution, causing the enzyme to uncouple in only ~10% of turnovers, prompting the question as to why this residue is fully conserved in HMS primary structure.

Kinetic Isotope Effects from Hydroxylation Partitioning. The kinetic isotope effects as measured from hydroxylation partitioning for both HPPD and HMS are listed in Table 2.3.

Table 2.3 KIEs from Isotopic Perturbation of Hydroxylation Partitioning

HPPD Variant	**WT**	**N245I**	**N245Q**	**P243T**	**S230A**
$^{D}k_{obs}$ HG	0.84 ± 0.01	1.02 ± 0.06	0.99 ± 0.01	1.05 ± 0.08	1.07 ± 0.10
replicates	3	2	2	3	2
$^{D}k_{obs}$ QAA	n.m.[a]	n.m.	1.09 ± 0.08	0.76 ± 0.04	1.02 ± 0.04
replicates	3	2	2	3	2
HMS Variant	**WT**	**I216N**		**T214P**	**S201A**
$^{D}k_{obs}$ HMA	n.m. [a]	2.19 ± 0.01		n.m.	2.56 ± 0.24
replicates	1	3		1	3

[a]not measureable.

In prior research we have shown using the isotopic substitutions of HPP used here, that neither HPPD nor HMS accumulates the hydroxylating intermediate to any measureable extent. The decay of this species is not limiting for any of the observed catalytic events and as such simple isotopic substitution and kinetic investigation has not elucidated any part of the early hydroxylation mechanism for either enzyme. This has limited our ability to apply rapid mixing quench studies to characterize this step (27,31). As such, it is assumed that the hydroxylating intermediate is an oxo-ferryl species as has been observed in a number of mononuclear Fe(II) dependent hydroxylases (38-42). In Figures 2.2 & 2.3, example HPLC chromatograms in the presence and absence of the isotopic label are included to illustrate how these otherwise shrouded kinetic isotope effects were measured.

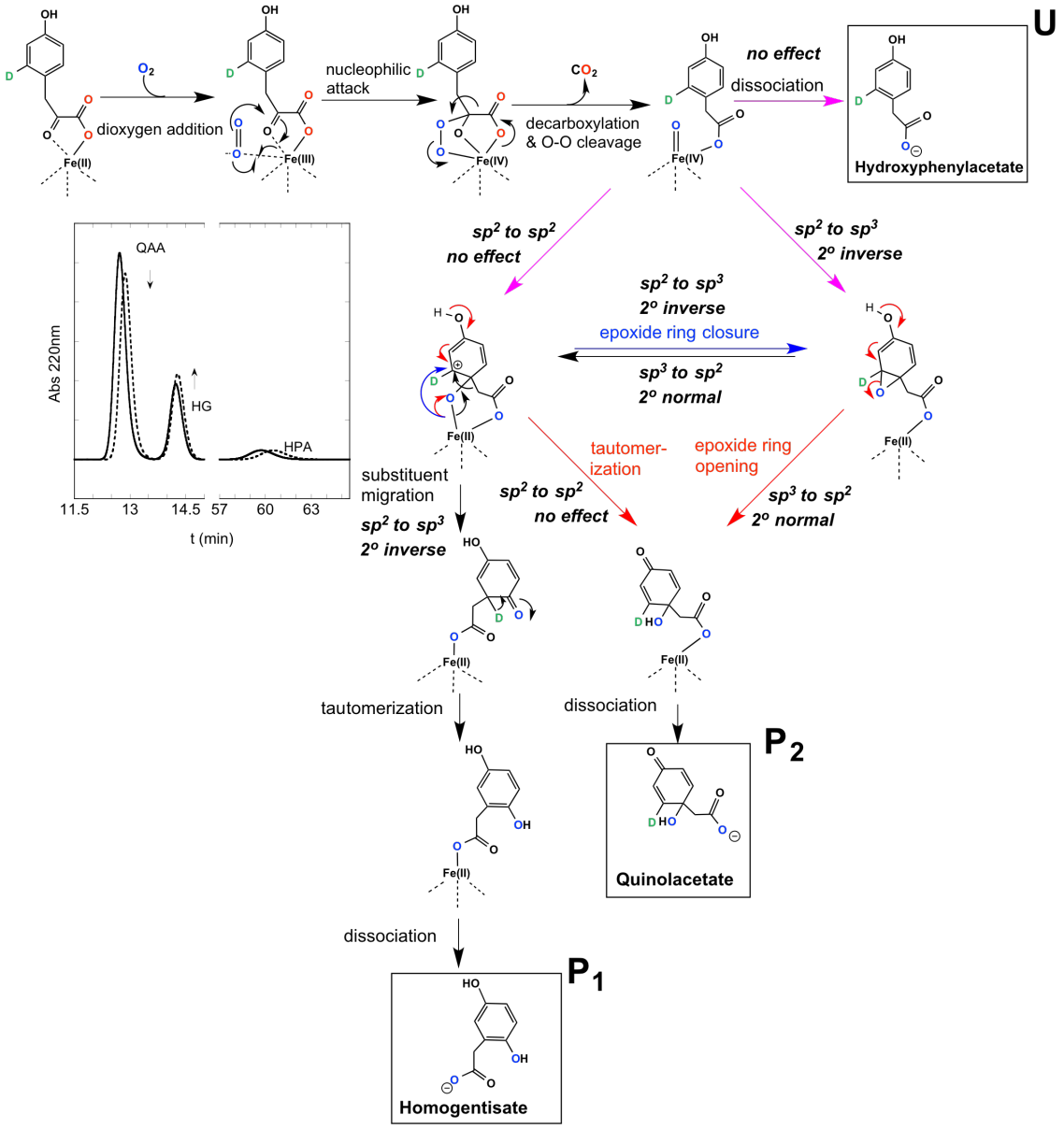

Figure 2.2 Hydroxylation mechanism of HPPD as deduced from intermediate partitioning. The proposed chemical mechanism of HPPD is shown. Molecules shown boxed are detected as products. The origin of the kinetic isotope effects is shown as italicized notations. Notations, $\mathbf{P_1}$, $\mathbf{P_2}$, and **U** refer to the variables of equation 2. The inset depicts two chromatograms for P243T variant in the absence (solid line) and presence (dashed line) of the ring-deuterium label of HPP.

The kinetic isotope effects for HPPD indicate that multiple saddle points are possible and that a variant enzyme may bias one of multiple pathways (Figure 2.2). As stated, one of the unexpected observations was that the native form of HPPD exhibits uncoupling to form HPA in a fraction of total turnover. The advantage of this is that it affords the measurement of the secondary isotope effect associated with hydroxylation to form HG for the native form of the enzyme. This value was 0.84 and strongly suggests that an *sp2* to *sp3* hybridization change is occurring with the hydroxylation event. Such a value is entirely consistent with the formation of a 1,2 ring epoxide during the hydroxylation step and is the first direct evidence for the native mechanism of hydroxylation by HPPD. Each of the variant enzymes investigated, however, show kinetic isotope effects of 1 within error for the formation of HG which indicates either no change in hybridization during hydroxylation, more consistent with the formation of a benzylic cation or that multiple simultaneous pathways contribute to the effect. Similarly, the KIE for the formation of QAA by the variants can be either inverse or unity indicating that it is possible to yield this product via either of the proposed branches in Figure 2.2.

The native form of HMS is fully coupled in hydroxylation and forms only HMA. As such the KIE for hydroxylation cannot be measured using partition analysis. This is also true for the T214P mutation. Therefore we cannot observe the native function of the enzyme by these methods. However, the kinetic isotope effect for hydroxylation by HMS as it relates to mechanism is less disputed than is that for HPPD (Figure 2.3).

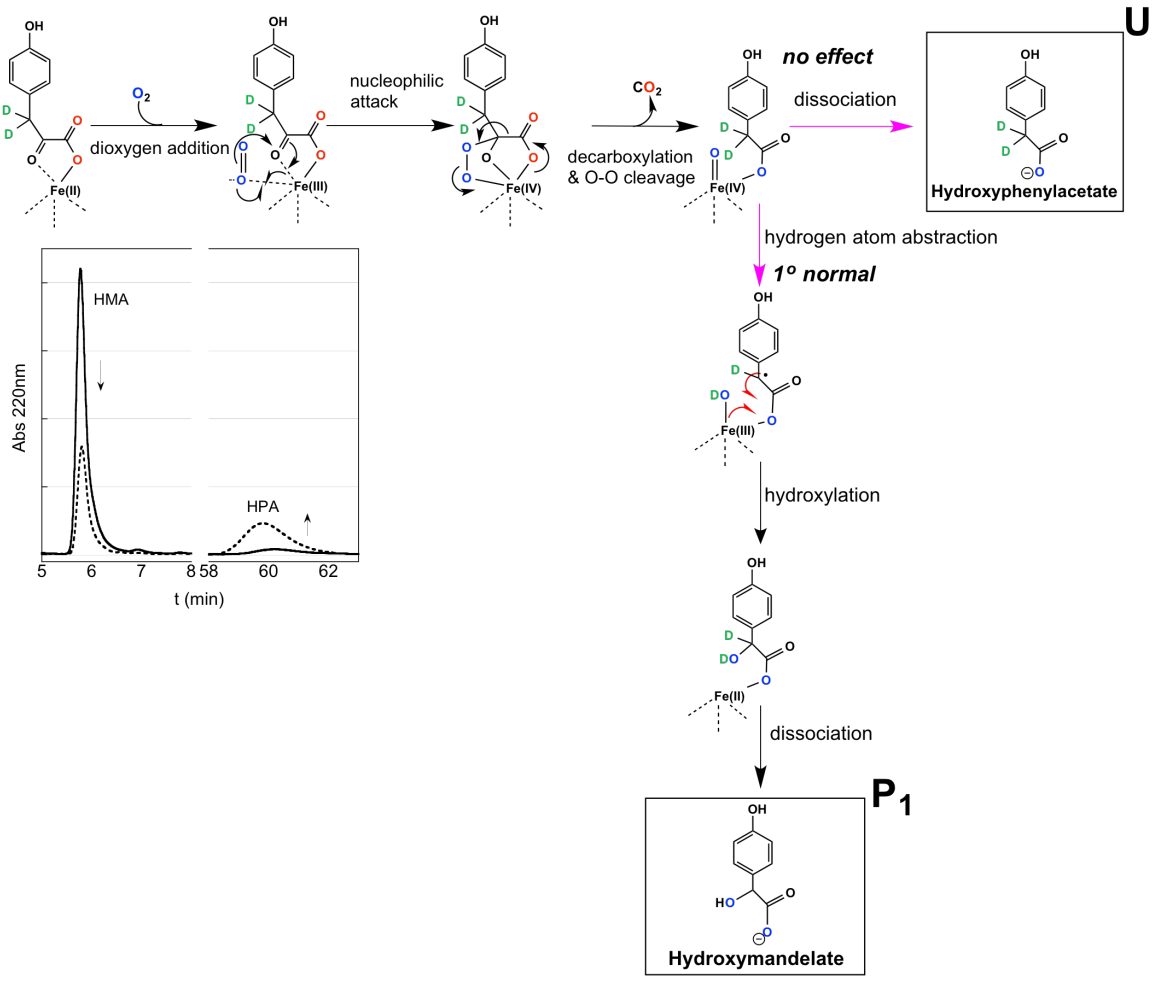

Figure 2.3 Hydroxylation mechanism of HMS as deduced from intermediate partitioning. The proposed chemical mechanism of HMS is shown. Molecules shown boxed are detected as products. The origin of the kinetic isotope effects is shown as italicized notations. Notations, $\mathbf{P_1}$ and **U** refer to the variables of equation 2. The inset depicts two chromatograms for I216N variant in the absence (solid line) and presence (dashed line) of the benzylic dideuterium label of HPP.

The mechanism must include displacement of a hydrogen from the benzylic carbon and as such is expected to show a primary KIE when this atom is replaced with a deuterium atom. Two of the HMS variants studied do show uncoupling and the formation of HPA and the measured KIEs for these are modest normal effects around 2.2-2.6. These values confirm the displacement of the hydrogen in the hydroxylation step but do not

delineate between hydrogen atom abstraction or hydride transfer mechanisms. The former of these has been adopted by consensus, fundamentally due to the propensity of the iron cofactor to carry out one-electron chemistry but either mechanism can account for the observed product, HMA. The labeled HPP substrate in this case is dideutero at the benzylic position. As such, the effect is multiplicative with the KIE on the concomitant formation of the benzylic radical (in the case of H-atom abstraction) or cation (in the event of hydride transfer). The cation would be predominantly sp^2 in character while the radical could be sp^2 or sp^3. Although, the extent of these contributions cannot be established from the data presented, the relatively small KIE observed may argue for a single contribution altering the rate constant. This would occur with H-atom abstraction that yields a largely sp^3 hybridized benzylic radical. This is the first evidence for the nature of the hydroxylation mechanism of HMS and indicates that the hydrogen at the point of substitution is displaced during the hydroxylation step. The effect is considerably smaller than that measured in other α-KAO enzymes that typically show KIEs for aliphatic hydroxylation as high as 40 suggesting greater hydrogen transfer optimization and tunneling in these enzymes (30,39,40,42,43).

2.4 Discussion

Understanding the role each residue plays in the reaction mechanism is the common objective of site directed mutagenesis. The purpose of this chapter, however, is not to assign functions to the residues that were mutated. The principal objective was instead to determine the kinetic isotope effects for the hydroxylation step and thereby further define the chemical mechanism of the sister enzymes, HPPD and HMS. The mutations selected for this study target specific residues implicated to be important in the mechanisms of HMS and HPPD (13,37,44-46). These form part of a broader effort to understand the basis of hydroxylation regiospecificity and the enzymatic machinery required to carryout the NIH shift. Each of the residues mutated is hypothesized to cluster about the phenol of HPP in both enzymes (Figure 2.1). Two of the residues are distinct in HPPD (N245, P243) and HMS (I216, T214) and these were mutated to their counterpart residues (N245I, P243T, I216N and T214P). The conserved serine residue (S230/201) was shown to form a hydrogen bond with the HMA phenol hydroxyl in the product complex of HMS (37) and this residue was mutated to an alanine in each enzyme. The HPPD variant N245Q was included also as it was one of the only variants to yield a large fraction of the native product, HG.

A number of qualitative mechanistic conclusions based on the ratio of products are possible. The first is that all enzymes investigated are fully coupled to formation of products, ie each molecule of dioxygen that is consumed results in the formation of a product that has, at a minimum, undergone decarboxylation. This is evidence that the oxidative decarboxylation reaction is tightly coupled to dioxygen reduction. Moreover, it also to some extent confirms the accepted order of events, in that the hydroxylation

reaction is contingent on the decarboxylation reaction and thus must occur later in the catalytic cycle.

The variant forms of HPPD and HMS used in this investigation were selected for their capacity to form multiple products and most particularly HPA. HPA is an abortive singly oxygenated and decarboxylated product that is released when a form of either enzyme fails to hydroxylate the ligand (Figures 2.2 & 2.3). It is thus very likely that HPA is an intermediate in the catalytic cycle that is common to both enzymes. However, measurement of the fractional yield of HPA also allows us both to account for the total products formed and provides a necessary internal reference for a step in the bi- or trifurcation (depicted as magenta arrows in Figures 2.2 & 2.3) that, in terms of formation rate constant, is independent of the isotopic substitutions. However, for each instance in which HPA is made an equal number of oxygen atoms is unaccounted for. These atoms may result in self-hydroxylation of the enzyme as has been reported for a number of α-KAO enzymes (47-49).

For cases that show kinetic isotope effects close to 1, the complexity of the hydroxylation mechanism of HPPD and the potential for simultaneous compensatory secondary isotope effects, undermines a direct intuitive explanation. The predicted mechanistic possibilities depicted in Figure 2.2 are summarized (minus the substrate binding and product release steps) in Figure 2.4. B to G parts of Figure 2.4 show the unique linear pathways for the production of HG and QAA and in each case the competing branch point that forms HPA. Any one path has a unique predicted isotope effect that reflects only the first intermediate formed during ring oxygenation and this

outcome is independent of isotope effects in subsequent steps including the interconversion of the epoxide and cationic species.

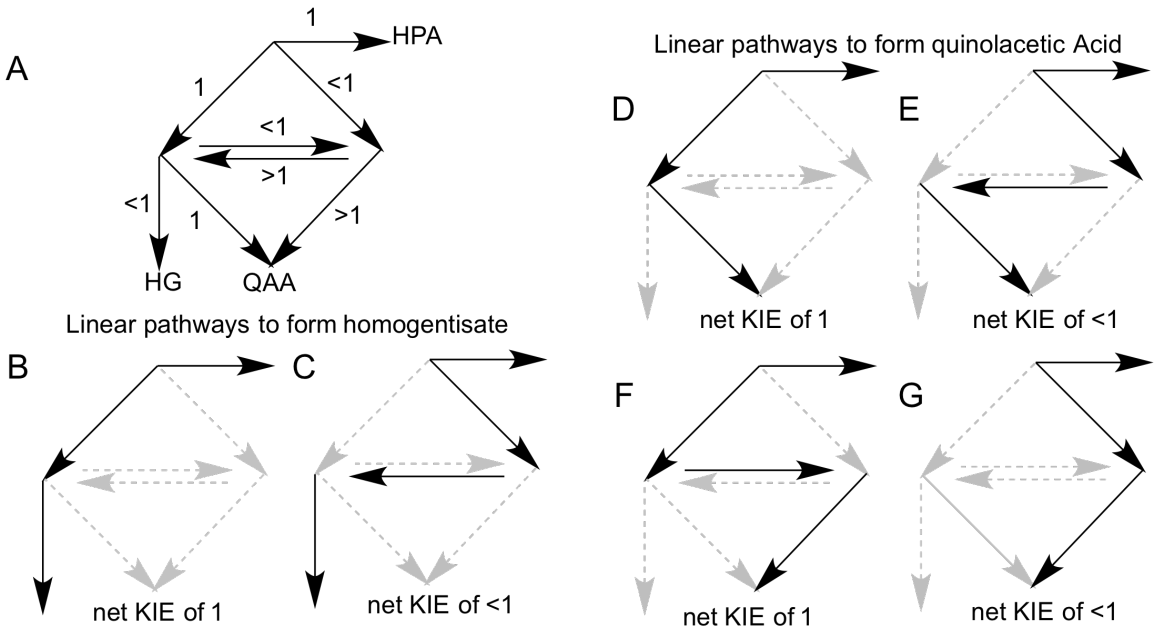

Figure 2.4 Summary of the unique linear pathways that yield HG and QAA based on the mechanism depicted in figure 2.2. Part A shows the predicted kinetic isotope effects relative to 1 for each of the relevant isotopically sensitive steps in Figure 2.2. Parts B and C show the two unique pathways for the formation of HG and parts D-G show the four unique pathways that yield QAA. Gray arrows are included for references only and are considered as non-operative steps when depicting any one pathway.

If individual linear pathways were exclusively operative for any one product the interpretation of the kinetic isotope effects would be simple and definitive. That is, an inverse effect would indicate the intermediacy of the epoxide and an isotope effect of 1 would indicate the benzylic cation intermediate. However, generally we cannot know which or how many or to what extent any of these possible pathways are biased for any form of the enzyme nor the value of the intrinsic kinetic isotope effect for any one step.

Simulation of the interconnected mechanism depicted in Figure 2.2 including all possible steps shows that the result of multiple pathways occurring and interconverting for any one product is that the observed net kinetic isotope effect will be ~1 and this is what we see for most observations (Table 2.3). However, we observe two cases that show substantially inverse kinetic isotope effects. These are, for the production of HG for the wild type enzyme and for the production of QAA in the P243T variant enzyme (Table 2.3). These values strongly suggest that for these two cases the epoxide pathway is dominant (pathways C E and G, Figure 3). This can be concluded for two reasons. Firstly, these effects are observed for the major fractional product in both instances, negating the influence of competing pathways for the alternate product, QAA. Secondly, the effects are significantly inverse and the contribution of other pathways would be to make the observed value less so. This suggests that for any one pathway the intrinsic oxygenation isotope effect arises only in this initial pathway selection (between HPA, the epoxide and the benzylic cation intermediates) and that it is only in the epoxide path that the possibility for significantly inverse isotope effects is established.

The conclusion is that once the hydroxylation pathway is selected from the three possibilities branching from the hydroxylating intermediate, the pathway to form either HG or QAA is linear and as such the isotope effect is defined by only by the relative probability of one of the first three steps in the absence and presence of the deuteron. This conclusion is aided by the assumption that no species other than the epoxide and cationic forms can interconvert. This lack reversibility toward products is consistent generally as we expect the reduction of dioxygen to be significantly exothermic overall. However it is also consistent with the mechanism presented in that we would predict high

forward reactivity for the hydroxylating intermediate, and the relative instability of the benzylic cation and epoxide species compared to QAA or the dienone intermediate that precedes rearomatization to HG.

The data obtained suggest that the native HPPD hydroxylation reaction results in the formation of a ring epoxide as the first intermediate. Inverse KIE values arising from deuterons placed ortho to the site of hydroxylation are reasonably explicit in this regard. The observation of a KIE of ~1 in the variant enzymes for the hydroxylation step that ultimately results in the liberation of HG differs from the wild type observation and suggests either no change in hybridization at ring C2, in keeping with a benzylic cation or that we are observing the net effect of multiple simultaneous pathways. Together these data suggest that the hydroxylation reaction can proceed through either intermediate and that changes in the active site promote to some extent the benzylic cation pathway for HG production. KIEs for the formation of QAA can only be measured for three of the variant enzymes. Again, two show KIEs close to unity and one is significantly inverse, bolstering the multiple similar pathway theory from above.

The concept of multiple pathways yielding a given product where the overall reaction traverses an energy landscape involving multiple saddle points has been suggested for a number of systems (50,51). Such phenomena account for the multiple conformational states that an enzyme population adopts at any point in time and yet remains catalytic. It cannot be gleaned if the observations made here are a consequence of biasing one conformational state and/or a different dynamic population of states in the variant enzymes. However, it does seem to be a fascinating example of built in

malleability in the reaction coordinate as a consequence of multiple energetically similar pathways being available.

The KIEs measured for variants of HMS each show small normal values consistent with abstraction of the hydrogen during hydroxylation (Figure 2.3). This narrows the mechanistic possibilities and shows that HMS, in all likelihood, functions much the same as other aliphatic hydroxylating α-KAO enzymes. The magnitude of the KIE (~2) suggests that the abstraction of the hydrogen is less optimized than in other αKAO enzymes and unlikely to be aided by tunneling effects in the hydrogen abstraction step.

Prior to this investigation, the only available studies to suggest the hydroxylation reaction intermediate in the NIH shift by HPPD was the work of Gunsior et al., who observed the liberation of an oxepinone from the P243T variant (46) and Raspail et al., who later perpetuated this notion without identifying the actual product formed from an S246A mutant (equivalent to the S230A mutant in this study) (52). In both studies, the conclusion was that the oxepinone was a rearrangement product derived from the abortive release of an epoxide intermediate following the second oxygenation. Our data show that the P243T and S230A variants make predominantly QAA and not the oxepinone. The observations of Gunsior et al., who correctly identified the oxepinone, are accounted for by the conversion of QAA to the oxepinone under the conditions used to purify the product for identification. Specifically, the use of triflouroacetic acid in the chromatography buffer, a molecule known to catalyze conversion of quinol derivatives to oxepinones (53,54). We therefore respectfully propose that the earlier observation was an artifact. However, the irony of this assertion is that QAA formed by the P243T variant

clearly suggests the intermediacy of the epoxide in that the KIE for QAA production by this variant is 0.76 (Table 2.3).

The remaining oddity is that QAA is known to convert quantitatively to HG in solution at pH 12.0 (55), suggesting that the NIH shift does not require elaborate enzymatic machinery. QAA however is not a substrate for HPPD as no amount of HG is observed when QAA is incubated with the enzyme (data not shown). With the delivery of the second oxygen atom, an accounting of electrons would indicate that the enzyme has returned to the ferrous state (Figure 2.2). As such the resting enzyme should be in the correct form to carry out the NIH shift from QAA to yield HG. The tentative conclusion is that QAA is thus an off-pathway product and not an intermediate that occurs in normal catalysis.

Acknowledgments

John A. Conrad collected the data for HMS variants. Brian Heinz and June M. Brownlee created variants of HPPD. Graham R. Moran helped with experimental design and preparation of this document.

2.5 References

1. Kavana, M., and Moran, G. R. (2003) Interaction of (4-hydroxyphenyl)pyruvate dioxygenase with the specific inhibitor 2-[2-nitro-4-(trifluoromethyl)benzoyl]-1,3-cyclohexanedione. *Biochemistry* **42**, 10238-10245
2. Kotob, S. I., Coon, S. L., Quintero, E. J., and Weiner, R. M. (1995) Homogentisic acid is the primary precursor of melanin synthesis in Vibrio cholerae, a Hyphomonas strain, and Shewanella colwelliana. *Applied and environmental microbiology* **61**, 1620-1622
3. Chatfield, C. H., and Cianciotto, N. P. (2007) The secreted pyomelanin pigment of Legionella pneumophila confers ferric reductase activity. *Infection and immunity* **75**, 4062-4070
4. Turick, C. E., Caccavo, F., Jr., and Tisa, L. S. (2008) Pyomelanin is produced by Shewanella algae BrY and affected by exogenous iron. *Can J Microbiol* **54**, 334-339
5. Eirich, L. D., Vogels, G. D., and Wolfe, R. S. (1979) Distribution of coenzyme F420 and properties of its hydrolytic fragments. *J Bacteriol* **140**, 20-27
6. Hubbard, B. K., Thomas, M. G., and Walsh, C. T. (2000) Biosynthesis of L-p-hydroxyphenylglycine, a non-proteinogenic amino acid constituent of peptide antibiotics. *Chemistry & Biology* **7**, 931-942
7. Li, T. L., Choroba, O. W., Charles, E. H., Sandercock, A. M., Williams, D. H., and Spencer, J. B. (2001) Characterisation of a hydroxymandelate oxidase involved in the biosynthesis of two unusual amino acids occurring in the vancomycin group of antibiotics. *Chem Commun (Camb)*, 1752-1753
8. Mitchell, G., Bartlett, D. W., Fraser, T. E., Hawkes, T. R., Holt, D. C., Townson, J. K., and Wichert, R. A. (2001) Mesotrione: a new selective herbicide for use in maize. *Pest Manag Sci* **57**, 120-128.
9. Pallett, K. E., Cramp, S. M., Little, J. P., Veerasekaran, P., Crudace, A. J., and Slater, A. E. (2001) Isoxaflutole: the background to its discovery and the basis of its herbicidal properties. *Pest Manag Sci* **57**, 133-142.

10. Kim, J.-S., Kim, T.-J., Kwon, O. K., and Cho, K. Y. (2002) Mechanism of Action of Sulcotrione, a 4-Hydroxyphenylpruvate Dioxygenase Inhibitor, in Developed Plant Tissues. *Photosynthetica* **40**, 541-545
11. Lindstedt, S., Holme, E., Lock, E. A., Hjalmarson, O., and Strandvik, B. (1992) Treatment of hereditary tyrosinaemia type I by inhibition of 4-hydroxyphenylpyruvate dioxygenase. *Lancet* **340**, 813-817
12. Suwannarat, P., O'Brien, K., Perry, M. B., Sebring, N., Bernardini, I., Kaiser-Kupfer, M. I., Rubin, B. I., Tsilou, E., Gerber, L. H., and Gahl, W. A. (2005) Use of nitisinone in patients with alkaptonuria. *Metabolism* **54**, 719-728
13. Brownlee, J. M., Heinz, B., Bates, J., and Moran, G. R. (2010) Product analysis and inhibition studies of a causative Asn to Ser variant of 4-hydroxyphenylpyruvate dioxygenase suggest a simple route to the treatment of Hawkinsinuria. *Biochemistry* **49**, 7218-7226
14. Walsh, C. (2000) Molecular mechanisms that confer antibacterial drug resistance. *Nature* **406**, 775-781
15. Purpero, V., and Moran, G. R. (2007) The diverse and pervasive chemistries of the alpha-keto acid dependent enzymes. *J Biol Inorg Chem* **12**, 587-601
16. Armstrong, R. N. (2000) Mechanistic diversity in a metalloenzyme superfamily. *Biochemistry* **39**, 13625-13632
17. Guroff, G., Daly, J. W., Jerina, D. M., Renson, J., Witkop, B., and Udenfriend, S. (1967) Hydroxylation-induced migration: The NIH shift. *Science* **157**, 1524-1530
18. Jerina, D. M., Daly, J. W., and Witkop, B. (1968) The role of arene oxide-oxepin systems in the metabolism of aromatic substrates. II. Synthesis of 3,4-toluene-4-2H oxide and subsequent "NIH shift" to 4-hydroxytoluene-3-2H. *J.Am.Chem.Soc.* **90**, 6523-6525
19. Jerina, D. M., Daly, J. W., and Witkop, B. (1971) Migration of Substituents during Hydroxylation of Aromatic Substrates (NIH Shift). Oxidations with Peroxytrifluoroacetic Acid. *Biochemistry* **10**, 366-372
20. Daly, J. W., Jerina, D. M., and Witkop, B. (1972) Arene oxides and the NIH shift: The metabolism, toxicity and carcinogenicity of aromatic compounds. *Experientia* **28**, 1129-1264

21. Bowman, W. R., Gretton, W. R., and Kirby, G. W. (1980) Hydroxylation of phenylalanine by Pseudomonas sp.: Measurement of an isotope effect following the NIH shift. *J.C.S.Perkin I* **3**, 218-220

22. Leinberger, R., Hull, W. E., Simon, H., and Retey, J. (1981) Steric course of the NIH shift in the enzymic formation of homogentisic acid. *Eur J Biochem* **117**, 311-318

23. Moran, G. R., Phillips, R. S., and Fitzpatrick, P. F. (1999) Influence of steric bulk and electrostatics on the hydroxylation regiospecificity of tryptophan hydroxylase: characterization of methyltryptophans and azatryptophans as substrates. *Biochemistry* **38**, 16283-16289

24. Hillas, P. J., and Fitzpatrick, P. F. (1996) A mechanism for hydroxylation by tyrosine hydroxylase based on partitioning of substituted phenylalanines. *Biochemistry* **35**, 6969-6975

25. Moran, G. R., Derecskei-Kovacs, A., Hillas, P. J., and Fitzpatrick, P. F. (2000) On the Catalytic Mechanism of Tryptophan Hydroxylase. *J Am Chem Soc* **122**, 4535-4541

26. Frantom, P. A., and Fitzpatrick, P. F. (2003) Uncoupled forms of tyrosine hydroxylase unmask kinetic isotope effects on chemical steps. *Journal of the American Chemical Society* **125**, 16190-16191

27. Johnson-Winters, K., Purpero, V. M., Kavana, M., and Moran, G. R. (2005) Accumulation of Multiple Intermediates in the Catalytic Cycle of (4-Hydroxyphenyl)pyruvate Dioxygenase from Streptomyces avermitilis. *Biochemistry* **44**, 7189-7199

28. Pavon, J. A., and Fitzpatrick, P. F. (2005) Intrinsic isotope effects on benzylic hydroxylation by the aromatic amino acid hydroxylases: evidence for hydrogen tunneling, coupled motion, and similar reactivities. *J Am Chem Soc* **127**, 16414-16415

29. Panay, A. J., and Fitzpatrick, P. F. (2008) Kinetic isotope effects on aromatic and benzylic hydroxylation by Chromobacterium violaceum phenylalanine hydroxylase as probes of chemical mechanism and reactivity. *Biochemistry* **47**, 11118-11124

30. Price, J. C., Barr, E. W., Glass, T. E., Krebs, C., and Bollinger, J. M., Jr. (2003) Evidence for hydrogen abstraction from C1 of taurine by the high-spin Fe(IV) intermediate detected during oxygen activation by taurine:alpha-ketoglutarate dioxygenase (TauD). *J Am Chem Soc* **125**, 13008-13009

31. He, P., Conrad, J. A., and Moran, G. R. (2010) The rate-limiting catalytic steps of hydroxymandelate synthase from Amycolatopsis orientalis. *Biochemistry* **49**, 1998-2007

32. Korzekwa, K. R., Trager, W. F., and Gillette, J. R. (1989) Theory for the observed isotope effects from enzymatic systems that form multiple products via branched reaction patyways: Cytochrome P-450. *Biochemistry* **28**, 9012-9018

33. Darbyshire, J. F., Iyer, K. R., Grogan, J., Korzekwa, K. R., and Trager, W. F. (1996) Substrate probe for the mechanism of aromatic hydroxylation catalyzed by cytochrome P450. *Drug metabolism and disposition: the biological fate of chemicals* **24**, 1038-1045

34. Mitchell, K. H., Rogge, C. E., Gierahn, T., and Fox, B. G. (2003) Insight into the mechanism of aromatic hydroxylation by toluene 4-monooxygenase by use of specifically deuterated toluene and p-xylene. *Proceedings of the National Academy of Sciences of the United States of America* **100**, 3784-3789

35. Fitzpatrick, P. F. (2006) Isotope Effects from Partitioning of Intermediates in Enzyme-Catalyzed Hydroxylation Reactions. in *Isotope Effects in Chemsitry and Biology* (Kohen, A., and Limbach, H.-H. eds.), CRC Taylor & Francis, Boca Raton. pp 861-873

36. Johnson-Winters, K., Purpero, V. M., Kavana, M., Nelson, T., and Moran, G. R. (2003) (4-Hydroxyphenyl)pyruvate Dioxygenase from Streptomyces avermitilis: The Basis for Ordered Substrate Addition. *Biochemistry* **42**, 2072-2080

37. Brownlee, J., He, P., Moran, G. R., and Harrison, D. H. (2008) Two roads diverged: the structure of hydroxymandelate synthase from Amycolatopsis orientalis in complex with 4-hydroxymandelate. *Biochemistry* **47**, 2002-2013

38. Riggs-Gelasco, P. J., Price, J. C., Guyer, R. B., Brehm, J. H., Barr, E. W., Bollinger, J. M., Jr., and Krebs, C. (2004) EXAFS spectroscopic evidence for an

Fe=O unit in the Fe(IV) intermediate observed during oxygen activation by taurine:alpha-ketoglutarate dioxygenase. *J Am Chem Soc* **126**, 8108-8109

39. Price, J. C., Barr, E. W., Hoffart, L. M., Krebs, C., and Bollinger, J. M., Jr. (2005) Kinetic Dissection of the Catalytic Mechanism of Taurine:alpha-Ketoglutarate Dioxygenase (TauD) from Escherichia coli. *Biochemistry* **44**, 8138-8147
40. Bollinger, J. M., Jr., and Krebs, C. (2006) Stalking intermediates in oxygen activation by iron enzymes: motivation and method. *J Inorg Biochem* **100**, 586-605
41. Price, J. C., Barr, E. W., Tirupati, B., Bollinger, J. M., Jr., and Krebs, C. (2003) The first direct characterization of a high-valent iron intermediate in the reaction of an alpha-ketoglutarate-dependent dioxygenase: a high-spin FeIV complex in taurine/alpha-ketoglutarate dioxygenase (TauD) from Escherichia coli. *Biochemistry* **42**, 7497-7508
42. Hoffart, L. M., Barr, E. W., Guyer, R. B., Bollinger, J. M., Jr., and Krebs, C. (2006) Direct spectroscopic detection of a C-H-cleaving high-spin Fe(IV) complex in a prolyl-4-hydroxylase. *Proceedings of the National Academy of Sciences of the United States of America* **103**, 14738-14743
43. Galonic, D. P., Barr, E. W., Walsh, C. T., Bollinger, J. M., Jr., and Krebs, C. (2007) Two interconverting Fe(IV) intermediates in aliphatic chlorination by the halogenase CytC3. *Nat Chem Biol* **3**, 113-116
44. Serre, L., Sailland, A., Sy, D., Boudec, P., Rolland, A., Pebay-Peyroula, E., and Cohen-Addad, C. (1999) Crystal structure of Pseudomonas fluorescens 4-hydroxyphenylpyruvate dioxygenase: an enzyme involved in the tyrosine degradation pathway. *Structure Fold Des* **7**, 977-988
45. O'Hare, H. M., Huang, F., Holding, A., Choroba, O. W., and Spencer, J. B. (2006) Conversion of hydroxyphenylpyruvate dioxygenases into hydroxymandelate synthases by directed evolution. *FEBS Lett* **580**, 3445-3450
46. Gunsior, M., Ravel, J., Challis, G. L., and Townsend, C. A. (2004) Engineering p-hydroxyphenylpyruvate dioxygenase to a p-hydroxymandelate synthase and evidence for the proposed benzene oxide intermediate in homogentisate formation. *Biochemistry* **43**, 663-674

47. Muller, I., Stuckl, C., Wakeley, J., Kertesz, M., and Uson, I. (2005) Succinate complex crystal structures of the alpha-ketoglutarate-dependent dioxygenase AtsK: steric aspects of enzyme self-hydroxylation. *J Biol Chem* **280**, 5716-5723

48. Liu, A., Ho, R. Y., Que, L., Ryle, M. J., Phinney, B. S., and Hausinger, R. P. (2001) Alternative Reactivity of an alpha-Ketoglutarate-Dependent Iron(II) Oxygenase: Enzyme Self-Hydroxylation. *J Am Chem Soc* **123**, 5126-5127

49. Bradley, F. C., Lindstedt, S., Lipscomb, J. D., Que, L., Jr., Roe, A. L., and Rundgren, M. (1986) 4-Hydroxyphenylpyruvate dioxygenase is an iron-tyrosinate protein. *J Biol Chem* **261**, 11693-11696

50. Hammes, G. G. (2008) How do enzymes really work? *The Journal of biological chemistry* **283**, 22337-22346

51. Nashine, V. C., Hammes-Schiffer, S., and Benkovic, S. J. (2010) Coupled motions in enzyme catalysis. *Current opinion in chemical biology* **14**, 644-651

52. Raspail, C., Graindorge, M., Moreau, Y., Crouzy, S., Lefebvre, B., Robin, A. Y., Dumas, R., and Matringe, M. (2011) 4-Hydroxyphenylpyruvate Dioxygenase Catalysis: Identification Of Catalytic Residues And Production Of A Hydroxylated Intermediate Shared With A Structurally Unrelated Enzyme. *The Journal of biological chemistry* **286**, 26061-26070

53. Nishinaga, A., Nakamura, K., and Matsuura, T. (1980) Reaction of Peroxy-p-quinol Acetates with Trifluoroacetic acid Anhydride Formation of New Oxepinone Derivatives. *Tetrahedron letters* **21**, 1269-1272

54. Nishinaga, A., Nakamura, K., and Matsuura, T. (1979) Acid-Catalyzed Reaction of 4-Hydroperoxy-2,5-cyclohexadienones and their Derivatives. *Tetrahedron* **35**, 2493-2499

55. Saito, I., Yamane, M., Shimazu, H., Matsuura, T., and Cahnmann, H. J. (1975) Biogenetic Type Conversion of p-Hydroxyphenylpyruvic Acid into Homogentisic Acid. *Tetrahedron letters* **9**, 641-644

Chapter 3

Intermediate Partitioning Kinetic Isotope Effects for the NIH shift of 4-Hydroxyphenylpyruvate Dioxygenase and the Hydroxylation Reaction of Hydroxymandelate Synthase Reveal Mechanistic Complexity

3.1 Introduction

4-hydroxyphenylpyruvate dioxygenase (HPPD) and hydroxymandelate synthase (HMS) catalyze similar reactions, using the same substrates, 4-hydroxyphenylpyruvate (HPP) and dioxygen. Initially both enzymes reduce and activate dioxygen in order to decarboxylate HPP yielding 4-hydroxyphenylacetate (HPA), CO_2 and an activated oxo intermediate (1). Both enzymes then hydroxylate HPA but do so in different positions. HPPD catalyzes aromatic hydroxylation at the ring C1 resulting in a migration of the aceto group of HPA to yield 2,5-dihydroxyphenylacetate (homogentisate, HG), whereas HMS catalyzes hydroxylation of the HPA benzylic methylene to form S-hydroxymandelate (HMA) (Scheme 3.1).

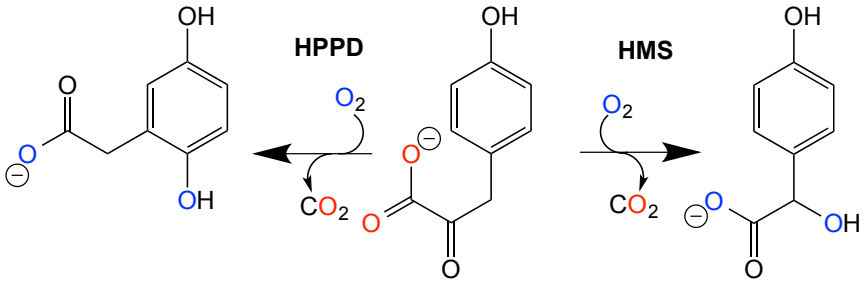

Scheme 3.1 Reactions catalyzed by HPPD and HMS

Despite modest sequence identity and similarity, the two enzymes clearly have a common ancestry in that they share numerous active site residues and adopt a highly similar fold (2). HPPD is in all likelihood the progenitor as it is ostensibly ubiquitous in aerobes where it catalyzes the second step of tyrosine catabolism while HMS catalyzes the first step in the biosynthesis of hydroxyphenylglycine, an uncommon tailoring reaction in a relatively small number of bacteria (3,4).

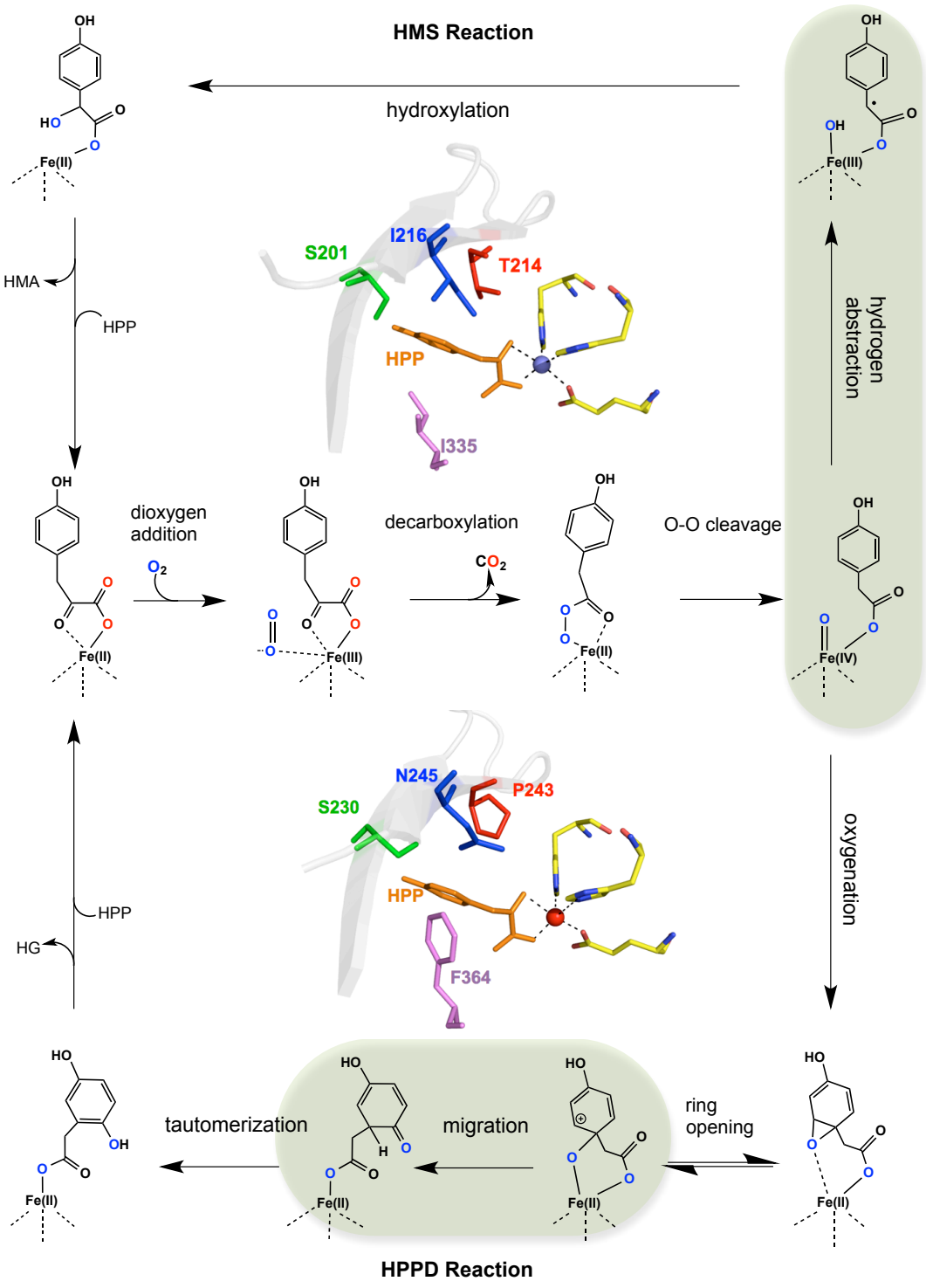

Figure 3.1 Proposed reaction mechanisms for HPPD and HMS

Both HPPD and HMS are Fe(II)-dependent dioxygenases, and on the basis of the reactions they catalyze can be grouped with the α-keto acid dependent oxygenases (*α*-KAOs)(5,6). Structurally HPPD and HMS have no resemblance to other *α*-KAOs so this classification is based solely on their chemical reactions (7-9). *α*-KAOs catalyze an extraordinary range of chemistries, however, each member begins catalysis with the cleavage of dioxygen and the oxidative decarboxylation of an alpha-keto acid (almost universally α-ketoglutarate). These steps are thought to result in the formation of a common reactive intermediate (Fe(IV)=O) that is then directed to unique purposes by individual enzymes (10-12). While these purposes include an impressive array of oxidation reactions, halogenation and even epimerization, this reactive oxo species is most often used to hydroxylate (6). HPPD and HMS offer respective examples of aromatic and aliphatic hydroxylation chemistry in which the requisite α-keto acid is supplied by the pyruvate substituent of HPP rather than from α-ketoglutarate (Figure 3.1).

Aromatic hydroxylation by HPPD induces substituent migration. Guroff et al. in 1960s discovered that aromatic hydroxylation by pterin-dependent hydroxylases can induce an intramolecular migration or shift of the substituent from the site of hydroxylation (13). Coined the *NIH shift*, this phenomenon has since been documented for a variety of metal-dependent oxygenases (14-17). For essentially all, the shift is observed with compact substituents such as halides, deuteriums, tritiums, (presumably protons,) and methyl groups. It has also been observed that, for substituents larger than a proton, the shift occurs in only a fraction of total catalysis (13,15,18-24). The aromatic hydroxylation reaction catalyzed by HPPD induces the migration of the comparatively

large aceto substituent with high efficiency (25) and so, from an experimental standpoint, is an important example of this chemistry.

Initial attempts to define the mechanism of the HPPD shift used single enantiomer chiral mono-deutero HPP labeled at the benzylic carbon and subsequent configurational analysis of the product. It was contended that if a two-electron or carbanion mechanism was at work, sp^3 geometry at the benzylic carbon would predominate in the cleaved intermediate and therefore a chiral substrate would retain the configuration in the product. Conversely, if the one-electron mechanism were operative, a symmetrical sp^2 in-flight radical could rotate before recombining with the ring resulting in racemization at a chiral benzylic carbon. From these experiments Leinberger et al. concluded that the NIH-shift of HPPD occurred via two-electron mechanism with retention of configuration at the benzylic methylene C atom (22). More recently, using density functional approaches to compute the more probable of a comprehensive set of reaction coordinate possibilities, Borowski et al. concluded that the NIH shift of HPPD was likely to occur via a homolytic mechanism and that retention of configuration at the benzylic position was simply a consequence of a low barrier to the transition state (TS) for the displaced group to recombine with the ring relative to the barrier for bond rotation (26). As such, there is some incongruity in the literature that is open to be settled by experimental observation that reports discriminating evidence for the mechanism of the NIH-shift in HPPD.

The hydroxylation reaction catalyzed by HMS is less complex than that of HPPD and is thought to involve only an initial hydrogen abstraction by the Fe(IV)=O species from the benzylic position to form a benzylic radical followed by hydroxyl addition from the resulting Fe(III)-OH species (25). Computational methods have provided a

comprehensive description of the basis for hydroxylation regiospecificity in HMS and have suggested that H-atom abstraction forming a benzylic radical followed by oxygen rebound is the dominant mechanism (27,28). Experimental evidence for the mechanism has come from kinetic isotope effect (KIE) values for the hydroxylation reaction from intermediate partitioning (*vide infra*) and were consistent with H-atom abstraction as the first step (12,25,29).

The fundamental objectives of this study were to obtain experimental evidence that discriminates between the heterolytic and homolytic NIH-shift mechanisms with HPPD and to define the geometry of the benzylic radical that forms with H-atom abstraction in HMS (highlighted steps in Figure 3.1). The measurement of KIEs for the relevant catalytic steps would provide data evidence for the mechanism(s), but for both HPPD and HMS this observation cannot be made directly as the hydroxylation and NIH shift steps are kinetically shrouded in single turnover reactions (30-32). We have recently shown that HPPD wild-type and also HPPD and HMS variants exhibit bifurcations that produce multiple products (25). For HPPD, bifurcation at the NIH-shift step yields either quinolacetic acid (QAA), a molecule that is hydroxylated but has not undergone the shift, or the native shift product, HG (25,33), whereas bifurcation for H-atom abstraction step that forms HMA yields HPA, an intermediate that has undergone decarboxylation but is not hydroxylated (25) (Scheme 3.2). Thus these systems are amenable to the measurement of intermediate partitioning based KIE values. The basis for this method is that the ratio of products is a direct result of a probability-based selection that is defined by the decay rate constant for individual paths bifurcating from some reactive state of the enzyme (34). As such, substitutions of heavy isotopes for atoms

that are involved in the chemistry of these diverging steps can alter the balance of the rate constants and thus the product ratio.

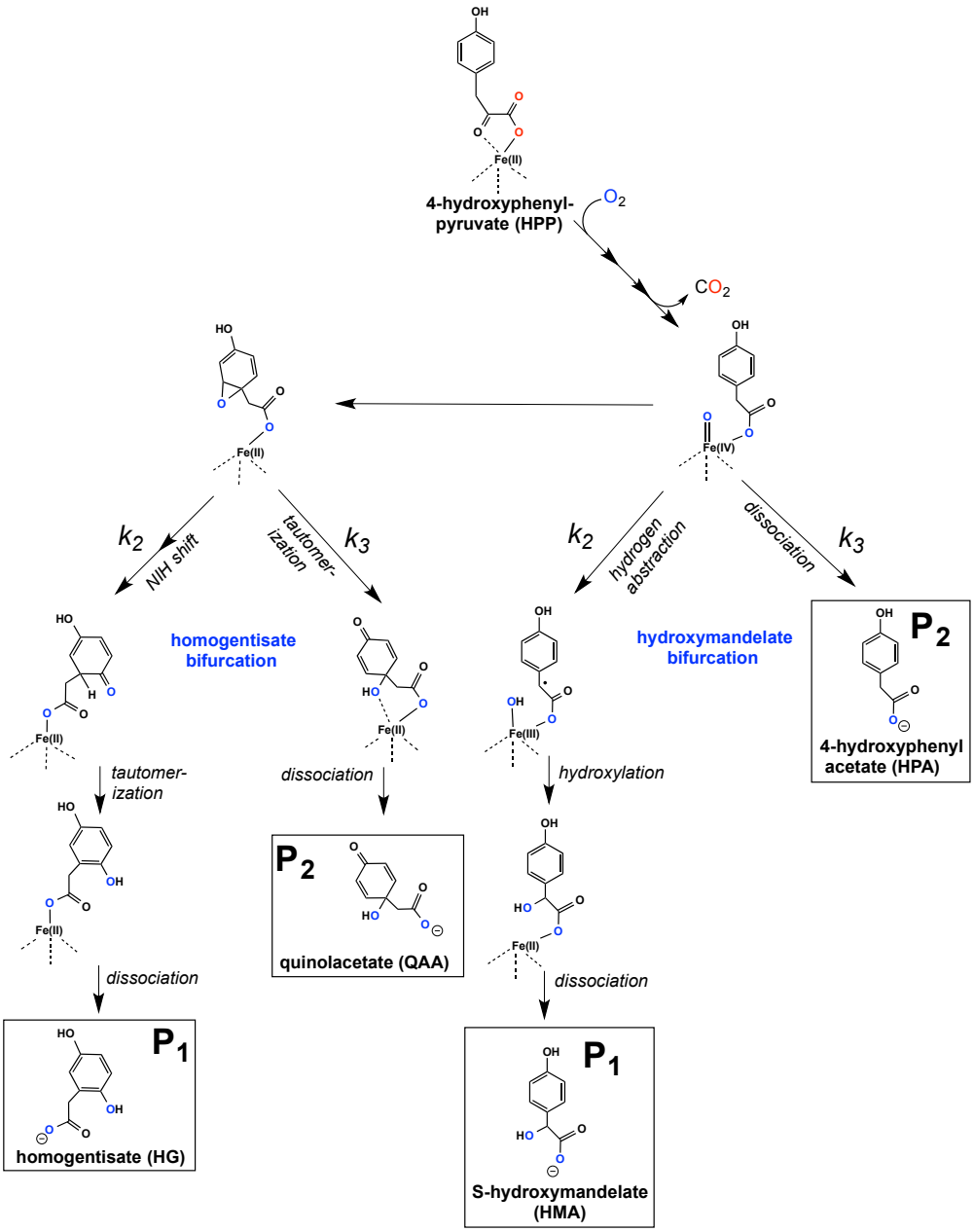

Scheme 3.2 Proposed Bifurcations at the NIH-shift in HPPD and H-atom abstraction steps in HMS

Thus an intrinsic kinetic isotope effect for a specific reaction step can be calculated simply. This accurate and highly robust method was originally applied to the P450 hydroxylases and more recently to mono- and dinuclear Fe(II) dependent oxygenases (16,35-37). The data we have obtained via these methods give KIE values that are consistent with the mechanisms proposed for each of the catalytic steps, at least narrow the mechanistic possibilities and suggest that alternate pathways can be induced that yield the same product in variant forms of the enzymes.

3.2 Materials and Methods

Materials. HPP and HG were purchased from Acros Chemicals. HMA and 4-hydroxyphenylacetate (HPA) were obtained from Sigma-Aldrich. Phusion® High-Fiedility PCR Master Mix and Competent BL21(DE3) *Escherichia coli* cells were obtained from New England Biolabs. IPTG was from Gold Biochemicals. D_2O and $CDCl_3$ were obtained from Cambridge Isotope Laboratories. DMSO-d_6 was from Acros Chemicals. The gene for mouse phenylpyruvate tautomerase (PPT) optimized for expression in *Escherichia coli* and including codons for a His-Tag was purchased from EnzymaX and subcloned into the Nde I and Xho I restriction sites of pET17b for expression. Q-Sepharose was from Bio-Rad. Sephacryl S-200 was obtained from Amersham. Quinolacetate (QAA) was made using the HPPD P243T variant and purified as previously described (33). 3',3'-Diduetero-HPP was prepared according to our previously published method (32). Solutions of the enol form of HPP were prepared by dissolving crystalline enol-HPP (as purchased) in the aprotic water miscible solvent, methanol to prevent ketonization. Chiral shift reagent, rhombamine macrocycle, was a kind gift from Dr. Koichi Tanaka (38). All other chemicals, buffers, and biological media were obtained from Fisher Scientific or Sigma-Aldrich Chemicals and were of high purity.

Mutagenesis. pET17b-derived (Novagen) plasmids carrying the *Streptomyces avermitilis* HPPD gene (pSAHPPD;(39)) and the *Amycolatopsis orientalis* HMS gene (pAOHMS; (2)) were mutated as previously described to obtain the N245Q, P243T, S230A, N245S variants of HPPD and the S201A variant of HMS (25,33). An additional HPPD variant

for this study, F364I, was obtained using the Stratagene QuickChange protocol using Phusion® High-Fidelity PCR Master mix and the following oligonucleotide: TCGGCAAGGGCAAC**A**TCAAGGCCCTGTTC, paired with an oligonucleotide that was its reverse complement. All variants were screened for spurious mutations by sequencing the entire dioxygenase genes (Sequetech, Mountain View CA).

Expression and Purification. The apo-forms of wild-type and variants of HPPD and HMS were expressed and purified using ammonium sulfate fractionation, anion exchange chromatography and size exclusion chromatography according to published methods (2,39).

His-tagged PPT was purified using the following protocol. Aliquots from frozen cell stocks were plated (200 µL/L of culture) on LB agar, 100 µg/mL ampicillin. After incubation for 9–12 h at 37 °C, the cells from two plates were suspended in ~20 mL of LB broth and used to inoculate 1 L of LB broth with 100 µg/mL ampicillin. The culture was grown with vigorous shaking (225 rpm) at 37 °C until the cell density had reached on OD_{600} of 1.0. At this time, IPTG was added to a final concentration of 0.1 mM and incubation was continued for 2.5 h. The cells were harvested by centrifugation at 4665 g for 30 min and used immediately for protein purification. Unless otherwise stated, all subsequent purification procedures were undertaken at 4 °C. Cells were resuspended using 20 mL of 20 mM HEPES, pH 7.0, per L of culture and lysed with sonication (2 x 6 min at 45 W) using a Branson sonicator fitted with a blunt tungsten tip. The temperature of the solution was monitored to ensure that it did not exceed 10 °C. The lysed cells were then centrifuged at 15600 g for 30 min, and the pellet was discarded. Streptomycin

sulfate in water was then added to the supernatant to a final concentration of 1.5% w/v. The mixture was stirred for 10 min and centrifuged at 12,900 g for 15 min. The supernatant was then loaded directly onto a Talon® metal affinity column pre-equilibrated in the 20 mM HEPES, pH 7.0 at a flow rate of 1 mL/min. The column was washed with 20 mM HEPES, 10 mM imidazole, pH 7.0 to elute nonspecifically bound proteins. The PPT was eluted with a linear 600 mL gradient from 10 to 250 mM imidazole in 20 mM HEPES, pH 7.0 at a flow rate of 1 mL/min. The fractions containing PPT were pooled and stored at –80 °C.

KIE Values from HPLC Product Analysis. The ratio of products for wild-type and each variant enzyme were determined using high-pressure liquid chromatography. Enzyme turnover reactions were undertaken at 25 °C and were comprised of 25-30 μM ferrous sulfate, 10-20 μM enzyme (wild-type or variant HPPD or HMS), 1 mM reductant (either βME or ascorbic acid), 250 μM O_2, and 100-250 μM HPP (either 3',3'-dideutero or diprotio) in 10 mM potassium phosphate, pH 7.0. Isotope effects were based on peak areas for products measured by HPLC as previously published (25).

KIE values measured with R-3'-monodeutero HPP were obtained from coupled turnover reactions in which the stereospecifically labeled monodeutero substrate was formed and consumed *in situ.* R-3'-monodeutero HPP was prepared using phenylpyruvate tautomerase (PPT) in deuterium oxide solvent. PPT catalyzes a stereospecific reaction where it interconverts the enol and keto forms of HPP by incorporating or abstracting a proton at the *pro-R* position (40). The ratio of products observed for HPPD or HMS when R-3'-monodeutero HPP was used as a substrate was

determined by adding the enol form of HPP to a reaction that had both PPT and HMS or HPPD activities. The reaction was designed such that the combined PPT and non-enzymatic conversion of enol-HPP to R-3'monodeutero-keto-HPP was 7-fold faster than the non-enzymatic conversion of the enol-HPP to the S-3'monodeutero-keto-HPP and the HMS or HPPD activity was 4-fold greater than that of PPT, accounting for both the solvent kinetic isotope effect (SKIE) on the product release step of HPPD and HMS and the SKIE for PPT (30,32,40,41). Enzyme turnover reactions were undertaken at 25 °C and were comprised of ferrous sulfate equivalent to the concentration of HMS or HPPD that gave 1.06 U activity (12.5 μM S201A HMS or 106 μM F364I HPPD), 0.28 U of PPT, 1 mM ascorbate in 5 mM sodium phosphate buffer prepared in deuterium oxide, pD 7.0 (U is a unit of enzyme activity and is equal to 1 μMole of substrate consumed or product evolved per min). The low concentration of buffer used in these reactions suppresses the observed rate-constant for the non-enzymatic conversion of the enolic HPP to ketoic HPP. The reaction was initiated by the addition of 50 μM enol HPP in 100% methanol. After completion of the reaction all other steps required to determine the product concentrations were as previously published (25).

Calculation of KIEs. Kinetic isotope effects were calculated using equation 1 that computes the factor of perturbation of the product ratio in the presence of the deuterated substrate for the case of a bifurcating mechanism and incorporates a correction accounting for the fractional extent by which $^{D}k_{obs}$ is reduced from the intrinsic value ($^{D}k_{2}$) by the bifurcation (34).

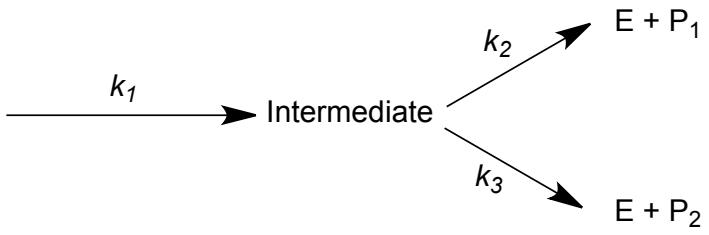

equation 1. $^{D}k_{obs} = \frac{(P_1/(P_1+P_2))^{H}}{(P_1/(P_1+P_2))^{D}} = \frac{^{D}k_2 + (k_2/k_3)}{1 + (k_2/k_3)}$

In this equation, $^{D}k_{obs}$ is determined by measuring P_1, the concentration of product for which the isotope effect is being determined (HG or HMA for HPPD and HMA for HMS) and P_2, the concentration of the product that results from bifurcation in a step that is insensitive to the isotopic insertion (QAA or HPA for HPPD and HPA for HMS). In each measurement the total consumption of molecular oxygen was compared to the total concentration of products formed, to ensure that all catalysis was considered.

Preparation of Monodeuterated HG from Wild-type HPPD. For the production of HG in sufficient quantity for NMR analysis a large-scale turnover reaction (40 mL) was undertaken in D_2O with wild-type HPPD. Reaction mixture was comprised of 420 U of wild-type HPPD, 112 U of PPT, 60 μM ferrous sulfate and 1 mM ascorbate in 5 mM sodium phosphate buffer, pD 7.0 and was initiated with the addition of 1.5 mM enol HPP in methanol. The reaction was run at 25°C and was equilibrated with 100% O_2 by stirring in a vessel with two small ports so that 100% dioxygen gas could continuously flush the headspace of the container. Complete conversion of the available HPP to HG was achieved within ~40 minutes, as determined by analytical reverse phase HPLC using published methods (25). The reaction was then brought down to pD 2.0 by the addition of H_2SO_4 to stabilize the HG hydroquinone and the precipitated protein was removed by

centrifugation at 12,900 g for 20 min. Supernatant was then passed through 10 kDa nominal molecular weight limit centrifugal filter (Vivaspin15) by centrifuging at 3,000 g to remove residual soluble peptide. The filtrate was then lyophilized overnight to a volume of ~5 mL and the sample was loaded on to Sep-Pak® Vac 35 cc C18 column pre-equilibrated with 40 mM sodium phosphate buffer, pH 7.0. The column was washed with 60 mL of H_2O and the HG was then eluted with 10% acetonitrile in water. Each eluted fraction was examined spectrophotometrically for the characteristic λ_{max} absorbance of HG at 290nm. Fractions showing significant absorbance at 290nm were combined together and lyophilized to obtain dry (powdered) HG.

Chiral Shift Analysis of Monodeuterated HG. Lyophilized HG was dissolved in $CDCl_3$ containing 10% DMSO-d_6, out of which 5 mg of HG was taken for NMR analysis. As a standard, a comparable amount of unlabeled HG solution in $CDCl_3$ containing 10% DMSO-d_6 was also prepared. Monodeuterated HG and unlabeled HG solutions were titrated with 0 to 0.05 eq rhombamine macrocycle (chiral shift reagent) by small additions (38). ^{1}H NMR spectra were recorded on a 500 MHz Bruker NMR instrument.

3.3 Results

Product Analysis and Characterization of Variant Enzymes. All the HPPD and HMS variants except F364I HPPD and N245D HPPD have been characterized in prior work (25). The product ratios for wild-type, N245Q, N245S, P243T and S230A vary slightly from those previously published. However, the KIE values obtained by partitioning methods are calculated from a ratio of ratios and so are largely immune from such variation (equation 1). F364I HPPD and N245D HPPD could be expressed and purified using the same methods as wild-type HPPD (39). Interestingly F364I HPPD showed four different products from product analysis (Table 3.4). Of which the most interesting was HMA, the product of the HMS reaction. This was consistent with the work of O'Hare et al. and Gunsior et al. who also observed HMA production with this variant (42,43). While rationalizing the function of individual residues is secondary to the purpose of this study, it is interesting to note that the position occupied by F364 in the structure of HPPD is filled by I335 in the structure of HMS (44). As such this mutation yields one of the only single positional-switching variants for these two enzymes that has resulted in the alternate activity to any significant extent. N245D was a largely competent HPPD, successfully completing NIH shift to form HG in 50% of total turnovers with the remaining fractions of turnover yielding QAA (20%) and HPA (30%).

Table 3.1 Product Ratios from which KIE Values for the Formation of HG were Derived

Product%	HG%		QAA%		HPA%	
	3'3'H	3'3'D	3'3'H	3'3'D	3'3'H	3'3'D
WT HPPD	90.37	95.6	0.98	0.66	8.65	3.75
N245Q	51.83	58.72	3.00	2.98	45.08	38.10
N245D	51.91	58.57	21.24	26.80	26.86	14.64
N245S	3.36	2.45	90.10	91.45	6.60	5.40
P243T	8.4	7.39	45.05	43.45	46.50	49.15
S230A	6.7	6.75	36.48	40.15	56.82	53.20

3'3'H – diprotio HPP, 3'3'D – dideutero HPP

KIEs for the NIH-shift from Intermediate Partitioning in Wild-type and Variant HPPDs. Despite that HPPD catalysis represents one of the more compelling examples of shift chemistry, the NIH shift step neither contributes to the limiting rate of turnover nor is it resolved kinetically in single turnover reactions and so is difficult to study by conventional methods (30,31). Intermediate partitioning is one of the few experimental methods capable of providing direct evidence for the chemistry occurring in this step. Moreover, the precision obtained with this method is sufficient to discern between mechanisms based on KIEs of small magnitude as are often obtained for secondary deuterium isotope effects arising from subtle hybridization changes at specific carbon atoms. Table 3.2 shows the utility of the product partitioning in differentiating between possible pathways for the NIH shift. For HPPD, QAA acts as an internal reference product for the shift step, having undergone hydroxylation but not the shift and thus its formation rate constant would not be sensitive to deuterons placed at the benzylic carbon (C3'). To form HG, however, the enzyme must transiently severe the bond to this carbon and so the rate constant for the formation of HG will reflect an extent of influence of benzylic deuterons (Scheme 3.2). Wild-type HPPD and variant N245Q show KIE of 1 for the formation of the native product HG, which indicates that no significant geometric change at C3' occurs in the formation of the (first) TS for the shift, or more precisely that sp^3 geometry predominates. The interpretation of this number does not converge on single mechanism. A trigonal C3' in the shift TS is consistent with and early TS that has retained much of the initial hybridization of the pre-shift benzylic methylene. It does not however, indicate explicitly that the mechanism is hetero- or homolytic, as the TS could readily progress to either an in-flight radical or carbanion intermediate.

Table 3.2 The NIH Shift KIEs from Wild-type HPPD and Variants[a]

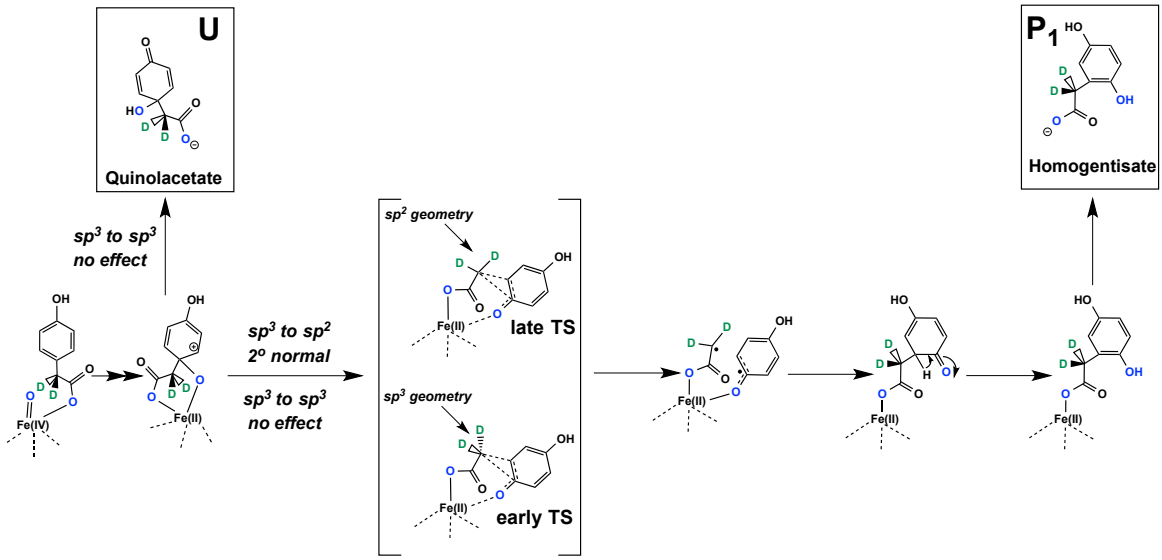

Variant	Wild-type	N245Q	N245D	N245S	P243T	S230A
HG%	90	52	52	3.4	8.4	7
QAA%	1	3	21.2	90	45	36
HPA%	9	45	26.8	6.6	46.5	57
$^{D}k_{obs}$ HG	0.990±0.001	0.99±0.03	1.03±0.01	1.39±0.02	1.08±0.05	1.08±0.01
Replicates	2	2	2	2	2	2

[a]N.B. All product percentages are those obtained with the protio substrates.

In contrast, N245S HPPD showed distinctly normal KIE of 1.39. This indicates that the (net) rate constant leading the formation of HG for this variant is slowed by deuterons in the benzylic position and that a transient geometry change at C3' must accompany the formation of the shift TS. An sp^3 to sp^2 hybridization change resulting from homolytic severing of the C1-C3' bond would account for the observed effect with this variant suggesting a later TS in which the unrestrained in-flight radical character (sp^2) is developed in the TS.

Taken together, and assuming that the reaction traverses the same barrier for both wild-type and variants, these data support homolytic cleavage of the bond to the methylene attending the NIH-shift. This conclusion is consistent with what has been proposed by Borowski et al. who, from calculation, also propose a highly unstable biradical intermediate resulting from the severed bond that collapses to form the new bond to the ring (26). All other HPPD variants tested in this manner, N245D, P243T and S230A, show small secondary normal KIEs (1.03-1.08) for the formation of HG. Within error, these values suggest shift TS geometry similar to the wild-type (C3' -sp^3).

NMR Chiral Shift Analysis of 3'-Monodeutero-HG. To further add to our evidence for the nature of the NIH shift chemistry we examined the native product, HG, for evidence of deuterium scrambling when derived from stereospecifically labeled HPP (R-3'-monodeutero). This experiment was undertaken to simply to reaffirm the observations of Leinberger et al. who conceded that derivatization of the product may have influenced the degree of scrambling observed (22). The hypothesis for this experiment is that heterolytic cleavage of the C1-C3' bond would dis-favor racemization of the label at C3' due to the polar trigonal shape of the in-flight carbanion, while the inherently planar and symmetrical sp^2 radical in this position could permit scrambling. Figure 3.2 shows NMR spectra that depict a titration of HPPD-derived monodeuterated HG with rhombamine macrocycle chiral shift reagent (38). In this figure, inset spectra in blue are for unlabeled HG. The lower of these standard spectra is without shift reagent and shows a single shift for the equivalent benzylic protons. The upper standard spectrum shows splitting of these two benzylic protons in AB spin system with the addition of the shift reagent.

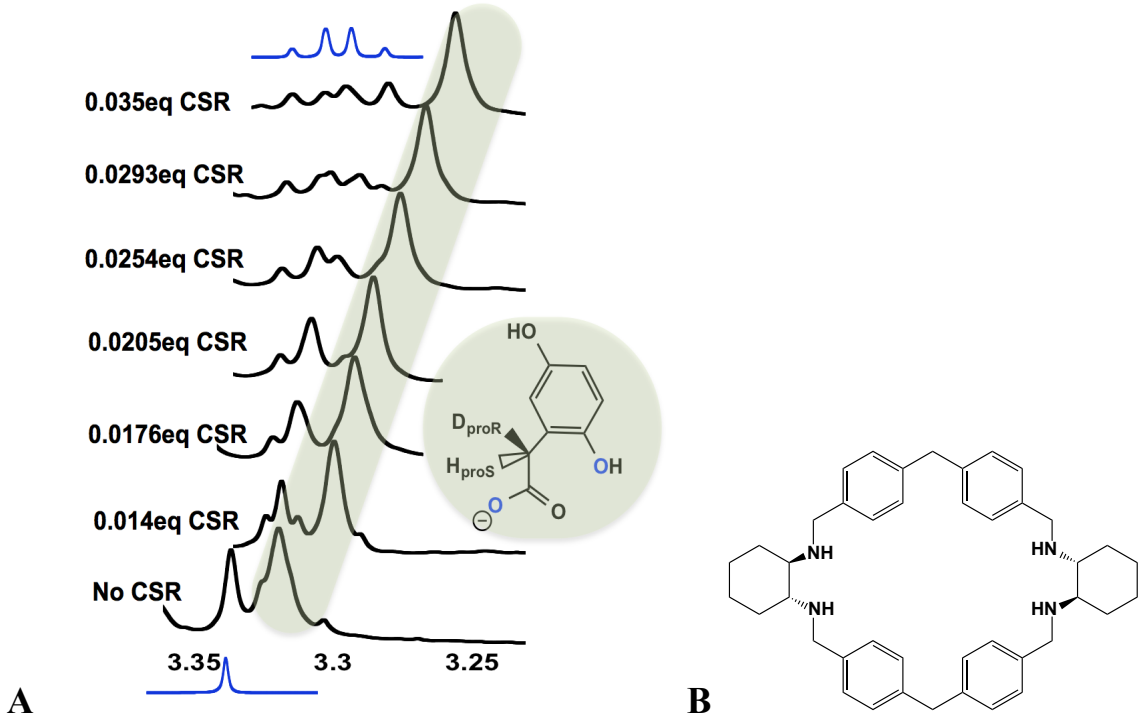

Figure 3.2 Evidence for a single enantiomer of homogentisate derived from R-3'-deutero 4-Hydroxyphenylpyruvate. **A.** 5 mg of HG derived from HPPD reacting with R-3'-monodeutero-HPP was dissolved in $CDCl_3$, 10% DMSO-d_6. A comparable amount of unlabeled HG solution in $CDCl_3$ containing 10% DMSO-d_6 was also prepared. Monodeuterated HG and unlabeled HG solutions were titrated with 0 to 0.05 eq rhombamine macrocycle (chiral shift reagent) by small additions. ^{1}H NMR spectra were recorded on a 500 MHz Bruker NMR instrument. Blue spectra show the spectra of 3'-diprotic HG in the presence and absence of the chiral shift reagent. **B.** rhombamine macrocycle (chiral shift reagent)

The spectra in black include the titration of the HPPD-derived HG with the shift reagent. In the absence of the shift reagent two HG populations are observed, one resonates at 3.34 ppm and corresponds to the benzylic protons of unlabeled HG. The second resonance at 3.32 ppm is for R- or S- and/or RS 3'-monodeutero HG. The greatest extent of splitting for unlabeled HG was observed for 0.035 equivalents of the shift reagent, however HPPD derived monodeutero-HG does not show evidence of splitting indicating a single enantiomer of monoduterated HG. It can now be stated that this lack

of label scrambling is indeed *characteristic* to the reaction. However, as noted by Borowski et al. this evidence by itself is not discriminating for the chemistry of the shift. Such a result would be predicted for the heterolytic pathway but also equally consistent with a homolytic pathway in which the collapse of a biradical intermediate occurs orders of magnitude more rapidly than the time taken for C2'-C3' bond rotation (26).

Table 3.3 Product Ratios from which KIE Values for the Formation of HMA were Derived

Product%	HMA%			HPA%		
	3'3'H	3'3'D	3'-R-D	3'3'H	3'3'D	3'-R-D
F364I HPPD	20.48	5.82	10.70	15.00	13.84	14.40
S201A HMS	97	47.93	91.27	3.00	52.07	8.73

3'3'H – diprotio HPP, 3'3'D – dideutero HPP, 3'-R-D – R-monodeutero HPP

Deconstruction of Net KIE values for the Production of HMA Using Stereospecifically Deuterated HPP. In prior work, we have measured the primary deuterium KIE on the initial hydrogen abstraction step of the hydroxylation reaction for HMS using 3',3'-dideutero-HPP (25). While the value measured was modest (2.2-2.6 dependent on the enzyme variant) it includes a multiplicative component from the geometry at the benzylic carbon for the deuteron not in-flight (Table 3.4). Two variants were selected to measure KIEs for the production of HMA with R-3'-monodeutero-HPP. The first was S201A HMS and the second was F364I HPPD (that makes 20% HMA). Table 3.4 includes the percentage of each product produced by these variants and KIEs measured for the formation of HMA with 3',3'-dideutero-HPP as well as 3'-R-monodeuterated HPP. With 3',3'-dideutero HPP as a substrate, S201A HMS and F364I HPPD show combined primary/secondary KIEs of 2.02 and 3.52 respectively. For KIEs measured with 3'-R-

Table 3.4 Delineation of KIE for the Formation of HMA to Identify Hybridization Geometry of the Radical[a]

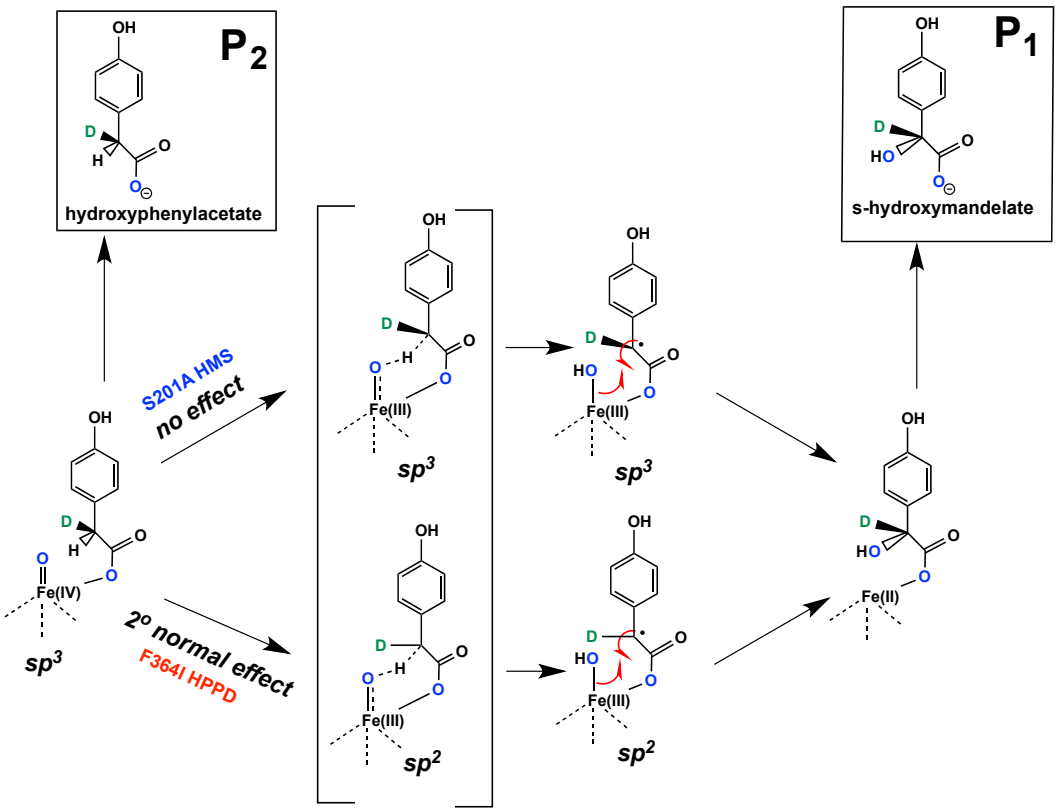

Variant	F364I HPPD	S201A HMS
HG (%)	47	0
QAA (%)	19	0
HPA (%)	15	3
HMA (%)	20	97
Total (%)	100	100
$^{D}k_{obs}$, 3',3'-dideutero HPP	3.52 ± 0.1	2.020 ± 0.004
Replicates	2	3
$^{D}k_{obs}$ R-3'-monodeutero HPP	1.92 ± 0.16	1.06 ± 0.04
Replicates	2	3

[a]N.B. All product percentages are those obtained with the protio substrates.

monodeuterated HPP as a substrate, S201A HMS showed a value of 1.06 ± 0.04 for the production of HMA indicating the benzylic carbon retains predominant sp^3 character in

the TS for the initial hydrogen abstraction. Conversely for F364I HPPD, the secondary KIE measured with 3'-R-monodeuterated HPP for the formation of HMA was 1.92 ± 0.16 indicating that a geometry change accompanies benzylic hydrogen abstraction for this HPPD variant. This would be consistent with a change from sp^3 to sp^2 geometry in the TS for this step.

3.4 Discussion

Both HPPD and HMS have been studied in single turnover reactions in some detail (30-32). While both enzymes accumulate multiple transients, none of the steps observed show sensitivity to isotopic substitutions at positions of the substrate that are involved in hydroxylation (30). As such it was concluded that the hydroxylation steps of the catalytic cycle were fast relative to other steps and so the reactive species involved could not be observed directly by kinetic methods. Recently we have shown that active site variants of both enzymes can form alternate products in some fraction of total turnover (25,33). While it may be tempting to rationalize the meaning of the ratios of products observed with regard to the function of specific residues, the ratios are dependent on the prevailing conditions of the reaction (data not shown) and so offer limited opportunities for meaningful conclusions. However, multiple products indicate that bifurcations (and trifurcations) are occurring at identifiable stages of catalysis. Specific heavy isotope substitutions have therefore the potential to alter the rate constant associated with one arm of the bifurcation and as such the KIE for that step can be calculated if the other arm(s) of the branch is unaffected by the substitution (equation 1, Scheme 3.2). While the data obtained by such methods can be exceedingly precise, they

are also easily over-intrepreted. The inherent kinetic complexity of a multiproduct system dictates that rationalization of results will likely offer explanations that are narrow relative to all possible mechanistic and kinetic possibilities. Herein, we have attempted to explain our data primarily on the basis of geometric changes in the transition state of the step affected by the isotope substitution. This approach assumes that the individual steps are largely irreversible or that they are commitment forward is such that any reversibility can be ignored. This is broadly reasonable as oxygenases catalyze highly exothermic reactions for which most steps will be irreversible and/or committed forward. Reversibility is only relevant for those steps that define the ratio of products of interest. That is, the initial steps that lead from the branch point to the products that define the KIE value. Reversibility in either of the steps leading away from bifurcating intermediate will increase the proportion of the other product independent of the TS geometry. Thus it should be noted that the assumptions on which conclusions are based in this study cannot, in the absence of additional data, be validated and so what follows is a confined set of conclusions that attempt to form a reasoned explanation for the observations but cannot account exhaustively for the nuanced nature of the interpretation of individual KIE values for complex systems.

In our earlier work using similar methods we measured KIE values on the ring-oxygen insertion step for HPPD using ring-per-deutero HPP and on the hydrogen abstraction step of HMS using 3',3'-dideutero HPP. We observed an inverse secondary isotope effect for ring hydroxylation in HPPD consistent with the formation of an epoxide as the initial product of oxygen addition to the aromatic ring. For HMS, abstraction of the S-deuteron from HPP dideuterated at the benzylic position gave a

normal primary effect consistent with H-atom abstraction before hydroxylation (25) (Figure 3.1). In the present study we have again investigated one branch-point for each enzyme (Scheme 3.2). For HPPD we have studied a branch point beyond ring-oxygen insertion from which either the native product HG or QAA is formed. This branch was probed using 3',3'-dideutero HPP to examine if the formation rate constant for HG is influenced by geometric changes at the benzylic carbon during the NIH shift. The shift reaction was further studied using R-3'-monodeutero HPP to detect evidence of racemization at the benzylic carbon during the aceto group migration. For HMS we have expanded our prior investigation of the hydroxylation step with the use of R-3'-monodeutero HPP. The single enantiomer of the substrate permitted the measurement of the contribution from the non-abstracted deuteron to the KIE value measured for HMS variants in prior work and so has provided evidence for the hybridization state at the benzylic carbon atom in the TS for the step that precedes hydroxylation.

The hydroxylation/shift reaction of HPPD has long been a biochemical curiosity and has been investigated using experimental and computational methods. The earliest direct evidence for the chemistry of the shift in HPPD came from Leinberger, et al. who were able to show that the configuration of the benzylic carbon was retained during the shift and proposed that a two-electron process (heterolytic pathway) was at work (22). The conclusions made here differ from those of Leinberger. Our KIE data show that no isotope effect is observed for the formation of HG when 3',3'-dideutero HPP is used as a substrate (Table 3.2). While this alone could be said to be consistent with a TS leading to a benzylic carbanion (sp^3) intermediate it is also consistent with an sp^3 hybridized TS that exhibits little of the character of an ensuing sp^2 hybridized intermediate (i.e. an early TS).

The more definitive observation is the KIE value measured for this branch with the N245S variant, which is distinctly normal (1.4). If we accept that the mechanism is conserved between the wild-type and variant, this value represents a more mature TS in which the benzylic methylene is largely departed from the ring C1 and has adopted the geometry of an untethered radical (sp^2) (Scheme in Table 3.2).

Leinberger, et al. showed both that configuration at the benzylic position was retained and that the product HG was not racemized to any measurable extent (22). This important work established a fundamental facet of HPPD chemistry. However, the methods chosen required derivatization of HG in order to compare chirality with synthesized chirality standards, undermining to some extent the certainty of the observation. In order to solidify the conclusions regarding racemization during the NIH-shift, we repeated the scrambling experiments of Leinberger et al. using a chiral shift reagent to induce chirality, a method that has the advantage of not chemically altering the product. Our data confirm the earlier observations that the monodeuterated HG formed in the reaction of HPPD with R-3'-monodeutero HPP is a single enantiomer and so conclude simply that bond rotation does not occur during the migration step (Figure 3.2). Borowski et al. have proposed that the NIH shift occurs through a homolytic pathway that does not induce racemization due to a relative high barrier for bond rotation compared to that for radical collapse that forms the new substituent bond (26). The integrated conclusion is thus in agreement with that of Borowski and suggest homolytic cleavage in the first shift TS followed by facile collapse of a biradical intermediate.

Partitioning KIEs measured with deuteriums substituted at the benzylic carbon of HPP for S201A HMS and F364I HPPD for the product HMA report the geometry of the

H-atom abstraction TS. Our data indicate that these variants undergo different geometry changes at the benzylic carbon during the initial H-atom abstraction. KIE values measured using 3',3'-dideutero HPP are multiplicative for the hydrogen abstracted and the hydrogen retained and thus are expected to be greater than KIE values measured with R-3'-monodeuterated HPP (given that inverse effects are not predicted). Wojcik et al. and Neidig et al. both concluded from density functional approaches that the HMS hydroxylation chemistry involves H-atom abstraction leading to formation of a largely planar (predominately sp^2) benzylic radical (27,28). Our conclusions regarding this step deviate only slightly from these prior determinations. The measured KIEs for HMA formation with both HPPD (F364I) and HMS (S201A) are internally consistent in that each value determined with the monodeuterated substrate is smaller than the value recorded with the 3',3'-dideutero substrate. For S201A HMS, KIE values with 3',3'-dideutero HPP are higher than with R-3'-monodeutero HPP by a factor of two indicating a primary KIE for abstraction, suggesting a more optimized benzylic hydroxylation process in HMS compared to the HPPD F364I variant. However, the KIE obtained with R-3'-monodeutero HPP is, within error, unity indicating that the benzylic carbon does not change geometry significantly to reach the hydrogen abstraction TS. The conclusion in this case is that the TS for this step has sp^3 character at C3'. Interestingly, Wojcik et al. proposed that the S201 residue is vital for hydroxylation regiospecificity by tethering the phenol of HPA at unique angles in HPPD and HMS and so mutation of this residue may have resulted in a change in geometry in the abstraction TS (27). For F364I HPPD the KIE values for H-atom abstraction TS are, 1.83 for hydrogen abstraction and 1.92 for geometry changes at the benzylic carbon in this step, suggesting that the benzylic carbon

develops predominant sp^2 character with relatively little lengthening of the bond to the abstracted hydrogen in the TS. These values are inline with the prior modeling studies and raises the possibility for redundancy in the chemistry, where the dominant chemistry is to form a TS that is largely sp^2 hybridized at C3' but a HMS variant can be made to exhibit sp^3 character at this position for the TS of this step and yet yield the same product.

Acknowledgments

John A. Conrad expressed and purified phenylpyruvate tautomerase. Graham R. Moran helped with experimental design and preparation of this document.

3.5 References

1. Diebold, A. R., Brown-Marshall, C. D., Neidig, M. L., Brownlee, J. M., Moran, G. R., and Solomon, E. I. (2011) Activation of alpha-Keto Acid-Dependent Dioxygenases: Application of an {FeNO}(7)/{FeO(2)}(8) Methodology for Characterizing the Initial Steps of O(2) Activation. *Journal of the American Chemical Society* **133**, 18148-18160
2. Brownlee, J., He, P., Moran, G. R., and Harrison, D. H. (2008) Two roads diverged: the structure of hydroxymandelate synthase from Amycolatopsis orientalis in complex with 4-hydroxymandelate. *Biochemistry* **47**, 2002-2013
3. Hubbard, B. K., Thomas, M. G., and Walsh, C. T. (2000) Biosynthesis of L-p-hydroxyphenylglycine, a non-proteinogenic amino acid constituent of peptide antibiotics. *Chem Biol* **7**, 931-942
4. Li, T. L., Choroba, O. W., Charles, E. H., Sandercock, A. M., Williams, D. H., and Spencer, J. B. (2001) Characterisation of a hydroxymandelate oxidase involved in the biosynthesis of two unusual amino acids occurring in the vancomycin group of antibiotics. *Chem Commun (Camb)*, 1752-1753
5. Hausinger, R. P. (2004) FeII/alpha-ketoglutarate-dependent hydroxylases and related enzymes. *Crit Rev Biochem Mol Biol* **39**, 21-68
6. Purpero, V., and Moran, G. R. (2007) The diverse and pervasive chemistries of the alpha-keto acid dependent enzymes. *J Biol Inorg Chem* **12**, 587-601
7. Armstrong, R. N. (2000) Mechanistic diversity in a metalloenzyme superfamily. *Biochemistry* **39**, 13625-13632
8. He, P., and Moran, G. R. (2011) Structural and mechanistic comparisons of the metal-binding members of the vicinal oxygen chelate (VOC) superfamily. *Journal of inorganic biochemistry* **105**, 1259-1272
9. Zhang, Z., Ren, J., Harlos, K., McKinnon, C. H., Clifton, I. J., and Schofield, C. J. (2002) Crystal structure of a clavaminate synthase-Fe(II)-2-oxoglutarate-substrate-NO complex: evidence for metal centred rearrangements. *FEBS Lett* **517**, 7-12.
10. Price, J. C., Barr, E. W., Glass, T. E., Krebs, C., and Bollinger, J. M., Jr. (2003) Evidence for hydrogen abstraction from C1 of taurine by the high-spin Fe(IV)

intermediate detected during oxygen activation by taurine:alpha-ketoglutarate dioxygenase (TauD). *J Am Chem Soc* **125**, 13008-13009

11. Galonic, D. P., Barr, E. W., Walsh, C. T., Bollinger, J. M., Jr., and Krebs, C. (2007) Two interconverting Fe(IV) intermediates in aliphatic chlorination by the halogenase CytC3. *Nat Chem Biol* **3**, 113-116
12. Hoffart, L. M., Barr, E. W., Guyer, R. B., Bollinger, J. M., Jr., and Krebs, C. (2006) Direct spectroscopic detection of a C-H-cleaving high-spin Fe(IV) complex in a prolyl-4-hydroxylase. *Proceedings of the National Academy of Sciences of the United States of America* **103**, 14738-14743
13. Guroff, G., Daly, J. W., Jerina, D. M., Renson, J., Witkop, B., and Udenfriend, S. (1967) Hydroxylation-induced migration: The NIH shift. *Science* **157**, 1524-1530
14. Hillas, P. J., and Fitzpatrick, P. F. (1996) A mechanism for hydroxylation by tyrosine hydroxylase based on partitioning of substituted phenylalanines. *Biochemistry* **35**, 6969-6975
15. Moran, G. R., Derecskei-Kovacs, A., Hillas, P. J., and Fitzpatrick, P. F. (2000) On the Catalytic Mechanism of Tryptophan Hydroxylase. *J Am Chem Soc* **122**, 4535-4541
16. Mitchell, K. H., Rogge, C. E., Gierahn, T., and Fox, B. G. (2003) Insight into the mechanism of aromatic hydroxylation by toluene 4-monooxygenase by use of specifically deuterated toluene and p-xylene. *Proceedings of the National Academy of Sciences of the United States of America* **100**, 3784-3789
17. Sono, M., Roach, M. P., Coulter, E. D., and Dawson, J. H. (1996) Heme-containing oxygenases. *Chem.Rev.* **96**, 2841-2888
18. Jerina, D. M., Daly, J. W., and Witkop, B. (1968) The role of arene oxide-oxepin systems in the metabolism of aromatic substrates. II. Synthesis of 3,4-toluene-4-2H oxide and subsequent "NIH shift" to 4-hydroxytoluene-3-2H. *J.Am.Chem.Soc.* **90**, 6523-6525
19. Jerina, D. M., Daly, J. W., and Witkop, B. (1971) Migration of Substituents during Hydroxylation of Aromatic Substrates (NIH Shift). Oxidations with Peroxytrifluoroacetic Acid. *Biochemistry* **10**, 366-372

20. Daly, J. W., Jerina, D. M., and Witkop, B. (1972) Arene oxides and the NIH shift: The metabolism, toxicity and carcinogenicity of aromatic compounds. *Experientia* **28**, 1129-1264

21. Bowman, W. R., Gretton, W. R., and Kirby, G. W. (1980) Hydroxylation of phenylalanine by Pseudomonas sp.: Measurement of an isotope effect following the NIH shift. *J.C.S.Perkin I* **3**, 218-220

22. Leinberger, R., Hull, W. E., Simon, H., and Retey, J. (1981) Steric course of the NIH shift in the enzymic formation of homogentisic acid. *Eur J Biochem* **117**, 311-318

23. Moran, G. R., Phillips, R. S., and Fitzpatrick, P. F. (1999) Influence of steric bulk and electrostatics on the hydroxylation regiospecificity of tryptophan hydroxylase: characterization of methyltryptophans and azatryptophans as substrates. *Biochemistry* **38**, 16283-16289

24. Hillas, P. J., and Fitzpatrick, P. F. (1996) A mechanism for hydroxylation by tyrosine hydroxylase based on partitioning of substituted phenylalanines. *Biochemistry* **35**, 6969-6975

25. Shah, D. D., Conrad, J. A., Heinz, B., Brownlee, J. M., and Moran, G. R. (2011) Evidence for the mechanism of hydroxylation by 4-hydroxyphenylpyruvate dioxygenase and hydroxymandelate synthase from intermediate partitioning in active site variants. *Biochemistry* **50**, 7694-7704

26. Borowski, T., Bassan, A., and Siegbahn, P. E. M. (2004) 4-hydroxyphenylpyruvate dioxygenase: A hybrid density functional study of the catalytic reaction mechanism. *Biochemistry* **43**, 12331-12342

27. Wojcik, A., Broclawik, E., Siegbahn, P. E., and Borowski, T. (2012) Mechanism of benzylic hydroxylation by 4-hydroxymandelate synthase. A computational study. *Biochemistry* **51**, 9570-9580

28. Neidig, M. L., Decker, A., Choroba, O. W., Huang, F., Kavana, M., Moran, G. R., Spencer, J. B., and Solomon, E. I. (2006) Spectroscopic and electronic structure studies of aromatic electrophilic attack and hydrogen-atom abstraction by non-heme iron enzymes. *Proceedings of the National Academy of Sciences of the United States of America* **103**, 12966-12973

29. Price, J. C., Barr, E. W., Hoffart, L. M., Krebs, C., and Bollinger, J. M., Jr. (2005) Kinetic Dissection of the Catalytic Mechanism of Taurine:alpha-Ketoglutarate Dioxygenase (TauD) from Escherichia coli. *Biochemistry* **44**, 8138-8147

30. Johnson-Winters, K., Purpero, V. M., Kavana, M., and Moran, G. R. (2005) Accumulation of Multiple Intermediates in the Catalytic Cycle of (4-Hydroxyphenyl)pyruvate Dioxygenase from Streptomyces avermitilis. *Biochemistry* **44**, 7189-7199

31. Purpero, V. M., and Moran, G. R. (2006) Catalytic, noncatalytic, and inhibitory phenomena: kinetic analysis of (4-hydroxyphenyl)pyruvate dioxygenase from Arabidopsis thaliana. *Biochemistry* **45**, 6044-6055

32. He, P., Conrad, J. A., and Moran, G. R. (2010) The rate-limiting catalytic steps of hydroxymandelate synthase from Amycolatopsis orientalis. *Biochemistry* **49**, 1998-2007

33. Brownlee, J. M., Heinz, B., Bates, J., and Moran, G. R. (2010) Product analysis and inhibition studies of a causative Asn to Ser variant of 4-hydroxyphenylpyruvate dioxygenase suggest a simple route to the treatment of Hawkinsinuria. *Biochemistry* **49**, 7218-7226

34. Fitzpatrick, P. F. (2006) Isotope Effects from Partitioning of Intermediates in Enzyme-Catalyzed Hydroxylation Reactions. in *Isotope Effects in Chemsitry and Biology* (Kohen, A., and Limbach, H.-H. eds.), CRC Taylor & Francis, Boca Raton. pp 861-873

35. Korzekwa, K. R., Trager, W. F., and Gillette, J. R. (1989) Theory for the observed isotope effects from enzymatic systems that form multiple products via branched reaction patyways: Cytochrome P-450. *Biochemistry* **28**, 9012-9018

36. Darbyshire, J. F., Iyer, K. R., Grogan, J., Korzekwa, K. R., and Trager, W. F. (1996) Substrate probe for the mechanism of aromatic hydroxylation catalyzed by cytochrome P450. *Drug metabolism and disposition: the biological fate of chemicals* **24**, 1038-1045

37. Frantom, P. A., and Fitzpatrick, P. F. (2003) Uncoupled forms of tyrosine hydroxylase unmask kinetic isotope effects on chemical steps. *Journal of the American Chemical Society* **125**, 16190-16191

38. Tanaka, K., Nakai, Y., and Takahashi, H. (2011) Efficient NMR chiral discrimination of carboxylic acids using rhombamine macrocycles as chiral shift reagent. *Tetrahedron-Asymmetr* **22**, 178-184

39. Johnson-Winters, K., Purpero, V. M., Kavana, M., Nelson, T., and Moran, G. R. (2003) (4-Hydroxyphenyl)pyruvate Dioxygenase from Streptomyces avermitilis: The Basis for Ordered Substrate Addition. *Biochemistry* **42**, 2072-2080

40. Retey, J., Bartl, K., Ripp, E., and Hull, W. E. (1977) Stereospecificity of phenylpyruvate tautomerase. A convenient method for the preparation of chirally labelled phenylpyruvates. *European journal of biochemistry / FEBS* **72**, 251-257

41. Johnson, W. H., Jr., Czerwinski, R. M., Stamps, S. L., and Whitman, C. P. (1999) A kinetic and stereochemical investigation of the role of lysine-32 in the phenylpyruvate tautomerase activity catalyzed by macrophage migration inhibitory factor. *Biochemistry* **38**, 16024-16033

42. O'Hare, H. M., Huang, F., Holding, A., Choroba, O. W., and Spencer, J. B. (2006) Conversion of hydroxyphenylpyruvate dioxygenases into hydroxymandelate synthases by directed evolution. *FEBS Lett* **580**, 3445-3450

43. Gunsior, M., Ravel, J., Challis, G. L., and Townsend, C. A. (2004) Engineering p-hydroxyphenylpyruvate dioxygenase to a p-hydroxymandelate synthase and evidence for the proposed benzene oxide intermediate in homogentisate formation. *Biochemistry* **43**, 663-674

44. Brownlee, J., Johnson-Winters, K., Harrison, D. H. T., and Moran, G. R. (2004) The Structure of the Ferrous Form of (4–Hydroxyphenyl)pyruvate Dioxygenase from Streptomyces avermitilis in Complex with the Therapeutic Herbicide, NTBC. *Biochemistry* **43**, 6370-6377

Chapter 4

Characterization of Active Site Variants of 4-Hydroxyphenylpyruvate Dioxygenase from *Streptomyces avermitilis*

4.1 Introduction

4-Hydroxyphenylpyruvate dioxygenase (HPPD) is a non-heme Fe(II)-dependent oxygenase that catalyzes the second step of the tyrosine catabolism pathway, the conversion of 4-hydroxyphenylpyruvate to homogentisate (Scheme 4.1) (1). Based on the reaction catalyzed, HPPD is an α-keto acid dependent oxygenase (2,3). However, HPPD is an exception in this class of enzymes as it does not use α-ketoglutarate as the source of electrons for the reduction of dioxygen. HPPD has a requirement for just two substrates, 4-hydroxyphenylpyruvate (HPP) and molecular oxygen (4,5). Collectively, HPPD catalyzes decarboxylation, aromatic hydroxylation and substituent migration in a one catalytic cycle to form homogentisate. The reaction involves two separate half-reactions, a decarboxylation half reaction and a hydroxylation half-reaction.

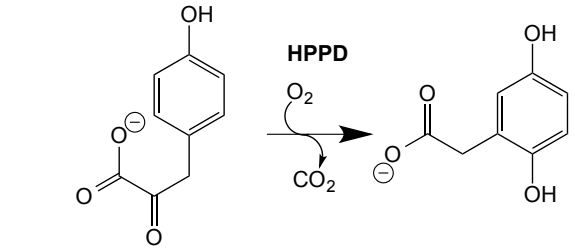

Scheme 4.1 Reaction catalyzed by HPPD

The majority of the α-keto acid dependent oxygenases incorporate one atom of dioxygen at the α-keto carbon displacing the carboxylic acid as carbon dioxide and then incorporate the second oxygen atom as a hydroxyl. There are a number of plausible chemical mechanisms available in literature for this chemistry (6-9), however, for the majority of the three-substrate α-keto acid dependent oxygenases, there is no direct

evidence of the accumulation of catalytic intermediates. As such much of what is proposed for mechanism in this family of enzymes is derived from chemical intuition, computer modeling and consensus rather than experimental evidence. One clear exception is the work of Bollinger et al. who have identified a ferryl species that accumulates prior to hydroxylation in the enzymes taurine:α-ketoglutarate dioxygenase (TauD), prolyl-4-hydroxylase, and the halogenase CytC3 (7,10,11). The two-substrate enzymes, such as HPPD, have entirely different kinetics and evidence for the accumulation of multiple intermediates was first offered in 2005 when Johnson-Winters et al. obtained data for the accumulation of three intermediates in a single catalytic cycle of HPPD (Scheme 4.2) using spectrophotometric pre-steady-state methods (Figure 4.1) (5,12).

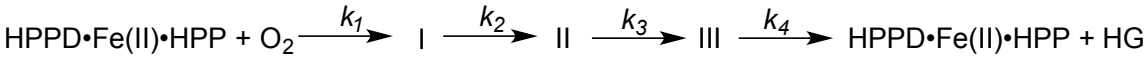

Scheme 4.2 The kinetic model for a single catalytic cycle of HPPD (12)

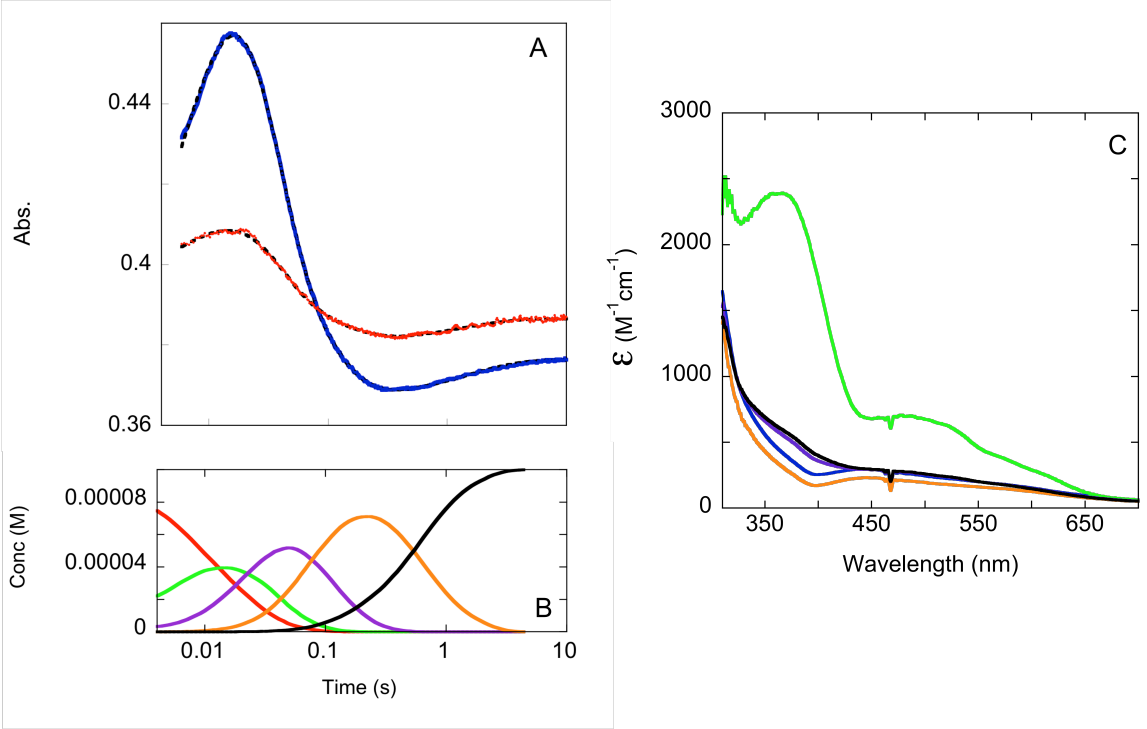

Figure 4.1 Single-turnover kinetics for Wild-type HPPD. (A) Stopped-flow traces and their fits (---) at two different wavelengths, 380 nm (blue) and 490 nm (red) (B) Concentration profiles of species observed in a single-turnover reaction, where intermediate I is depicted in green, intermediate II in violet, intermediate III in orange and HPPD•Fe(II)•HPP + HG in black. (Enzyme-substrate complex was excluded from this figure because of its higher concentration.) (C) Deconvoluted intermediate spectra from the fit to the model depicted in Scheme 4.2. HPPD•Fe(II)•HPP (blue), intermediate I (green), intermediate II (violet), intermediate III (orange), and HPPD•Fe(II)•HPP + HG + CO_2 (black). This figure has been taken from (12).

Figure 4.1 B depicts a concentration profile of all accumulating species in a single turnover of HPPD from *Streptomyces avermitilis*. The kinetics indicate relative high fractional accumulation of each species, the first intermediate accumulating to 40% of total species at 14 ms, the second intermediate accumulating to ~50% at 47 ms and the third intermediate to 70% at 220 ms. (12).

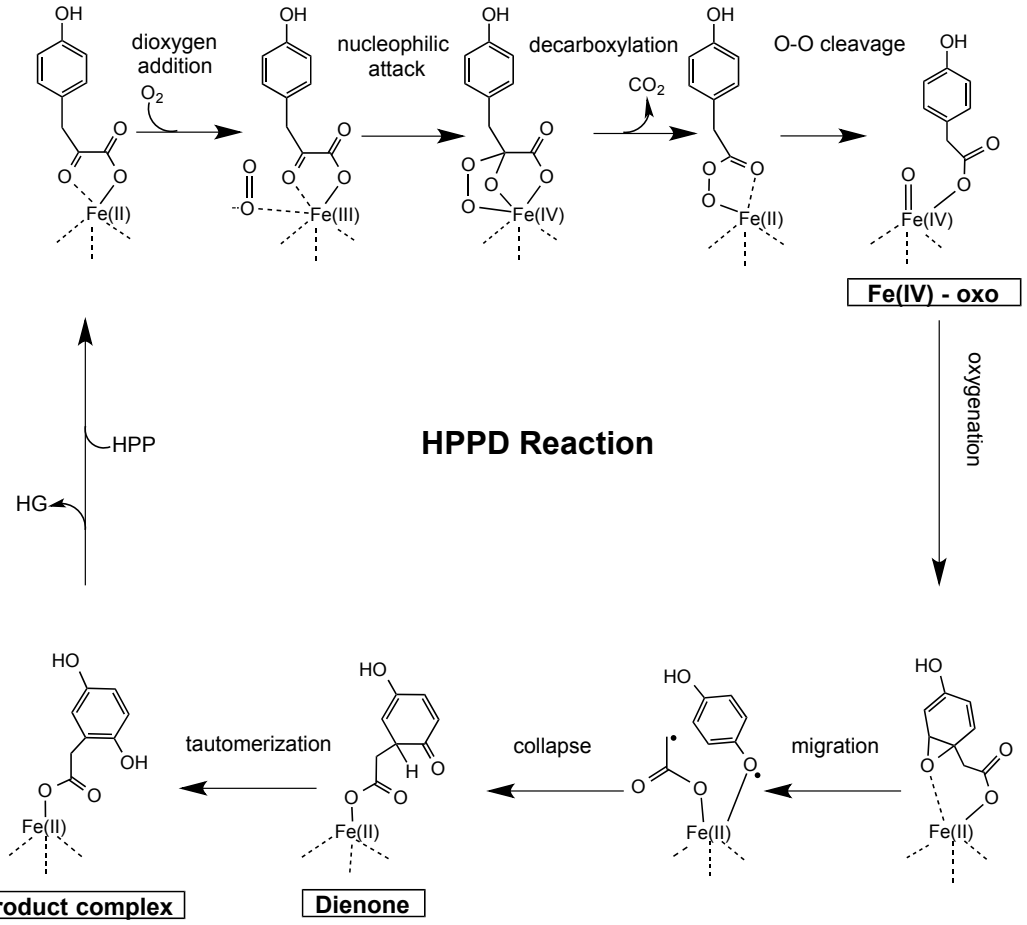

Scheme 4.3 Catalytic cycle of HPPD. Intermediates discussed in this study are depicted with their identity.

Of the three transient species observed, intermediate III has been identified as the HPPD•Fe(II)•HG product complex. This identification was made from a combination of rapid chemical quench and rapid-mixing fluorescence spectroscopy (12). The identity of the other two intermediates could not be established directly, however, select observations permitted some speculative assignments for these intermediates. The formation rate constant of the first intermediate exhibited a first-order dependence on the

concentration of dioxygen. This dependence permitted the calculation of a second-order rate constant for the addition of dioxygen to the HPPD•Fe(II)•HPP complex (10^5 M^{-1} s^{-1}), a value several thousand fold faster than the rate of reaction of the holoenzyme alone with dioxygen. In addition, decay of the first intermediate was not influenced by the deuterons placed on an aromatic ring of HPP, suggesting that intermediate I occurs prior to ring hydroxylation. Consistent with this conclusion, though not definitive in terms of timing, was that this species did not have absorption transitions in the far-visible to near-IR region which are thought to be characteristic of the Fe(IV)-oxo intermediate (Scheme 4.3) (3).

Data pertaining to the second intermediate suggest that it arrives after the ring oxygenation reaction but before the formation of HG. A small normal kinetic isotope effect was observed for the decay of the second intermediate (k_3) in the presence of ring-deuterated substrate, indicating that this process is part of the aromatic oxygenation chemistry. Interestingly, the decay of intermediate II occurred concomitantly with an increase in the fluorescence that was correlated with the appearance of the product, HG. This prompted the proposal that intermediate II was a dienone tautomer of the product (Scheme 4.3). Intermediate III decays slowly and limits the turnover number (k_4). The decay of III occurs concomitantly with re-formation of the HPPD•Fe(II)•HPP charge transfer complex (Scheme 4.3). The rate constant for this step is slowed further by solvent deuterons suggesting that protonation of the product is required for dissociation (12). The evidence obtained suggests that the intermediates observed are not part of a successive linear sequence, but are instead separated by other transient species that form and decay rapidly and therefore do not accumulate. Here, we present spectrophotometric

pre-steady-state analyses for a variant of HPPD in which the catalytic steps that contribute to the turnover number are chemically and kinetically altered. Identification of this variant was part of a broad mutagenesis effort to alter hydroxylation regiospecicity and unveil parts of the catalytic cycle kinetically obscured in the WT enzyme. Conserved residues predicted from structure to be mechanistically important were targeted for this study (4,13-16). This included alterations at positions N245, S230 and P243 that are known specificity and mechanistic determinants. (See chapters 2 & 3)

4.2 Materials and Methods

Materials. HPP and HG were purchased from Acros Chemicals. Competent BL21(DE3) *Escherichia coli* cells were obtained from New England Biolabs. IPTG was from Gold Biochemicals. Q-Sepharose was from Bio-Rad. Sephacryl S-200 was obtained from Amersham. Quinolacetate (QAA) was made using the P243T variant described in this manuscript and purified as previously described (14). All other chemicals, buffers, and biological media were obtained from Fisher Scientific or Sigma-Aldrich Chemicals and were of high purity.

Mutagenesis. Mutagenesis was performed using the materials and protocol of the Stratagene QuikChange Lightning ® kit. pET17b-derived (Novagen) plasmid carrying the *Streptomyces avermitilis* HPPD gene (pSAHPPD;(5)) was mutated as previously described to obtain variant HPPD enzymes in this study (14,17). All variants were screened for spurious mutations by sequencing the entire dioxygenase genes (Sequetech, Mountain View CA). Oligonucleotides (including respective reverse complements) used for mutagenesis are detailed as below:

SAHPPDN245S: GTCAAGTTCCCGATCA**G**CGAGCCCGCCCT**G**GCCAAGAAGAAGTCCC

SAHPPDN245A: AAGGTCAAGTTCCCGATC**GCT**GAGCCCGCCCTCGCCAAG

SAHPPDN245Q: CAAGTTCCCGATC**C**A**G**GAGCCCGCCCT**G**GCCAAGAAGAA

SAHPPDP243T: CTCAAGGTCAAGTTC**A**CGATCAACGAGCCCGCC**T**TGGCCAAGAAGAAGTCC

SAHPPDS230A: GACATCGCGACCGAGTA**T**TCGGCGCTGATGGCGAAGGTCGTGGC

Expression and Purification. The apo-forms of wild-type and variants of HPPD were expressed and purified using ammonium sulfate fractionation, anion exchange

chromatography and size exclusion chromatography according to previously published methods (5).

Measurement of the Dissociation Constants for the Variant HPPD•Fe(II)•HPP Complexes. The binding constant for the HPPD•Fe(II)•HPP complex of each variant was measured according to the methods of Johnson-Winters et al. (5). Each apo-HPPD variant (180-220 μM) in 20 mM HEPES buffer, pH 7.0 was made anaerobic at 4 °C by subjecting them to 45 alternating vacuum and argon cycles (a 2 min period was given to the sample to exchange dissolved gases after each set of three cycles) in a tonometer. A equivalent concentration of ferrous ammonium sulfate was added from a side arm to the enzyme solution after anaerobiosis was obtained. Anaerobic HPP solutions of various concentrations were prepared by sparging argon through each for 10 min just prior mixing them with holo-enzyme solution. Both, the enzyme containing tonometer and substrate syringe were mounted on a Hitech model-SF61-DX2 stopped-flow spectrophotometer. For each HPP concentrations, the enzyme spectrum was monitored until no further change was observed. This absorbance spectrum (300-700 nm) provided a measure of the fractional enzyme-substrate complex concentration ([HPPD•HPP]) obtained for each HPP concentration, which was plotted against total HPP concentration. These data were fit to equation 1 to calculate $K_{d\,HPP}$ and the concentration of the available binding sites.

equation 1. $$[HPPD\bullet HPP] = \{K_{d\,HPP} + [HPP] + [HPPD] - ((K_{d\,HPP} + [HPP] + [HPPD])^2 - 4\,[HPP][HPPD])^{1/2}\}/2$$

Stopped-Flow Measurements. The HPPD•Fe(II)•HPP complex was prepared using the previously described methods of Johnson-Winters et al. (5). A solution of each HPPD variant (N245Q and P243T) (400-450 μM) was added to a tonometer and saturating concentrations of HPP (calculated from a previously measured HPPD•Fe(II)•HPP complex dissociation constant for each variant) were added to a side arm and concentrations of ferrous sulfate sufficient to ensure 1:1 concentration equivalency with the apo-HPPD was placed in a second side arm. This vessel was then used to obtain anaerobiosis using the methods described above. After anaerobiosis was achieved, the apoenzyme was mixed initially with Fe(II) from one sidearm and then with HPP from the other sidearm. The complex formed in this way exhibited a characteristic color (unique to each variant) due to a metal to α-keto acid ligand charge transfer band at around 500 nm.

a) Single Turnover Reactions. An anaerobic N245Q•Fe(II)•HPP complex was made as described above (5). 800 μM apoN245Q HPPD was combined with 850 μM Fe(II), and 2640 μM HPP. The reaction of this complex with limiting dioxygen concentration was observed spectrophotometrically using a HiTech Scientific (now TGK) stopped-flow spectrophotomter using both photomultiplier and photodiode array detection. Data were collected with logarithmic time spacing and were analyzed using Kinetic Studio (TgK Scientific) the Specfit/32 Global Analysis System (SpecSoft Inc) and fit to the four-step model depicted in Scheme 4.2 to determine rate constants for individual steps.

b) Oxygen Dependence of N245Q•Fe(II)•HPP Complex. The reaction of N245Q variant HPPD•Fe(II)•HPP complex (40 μM final) with molecular oxygen was observed at 380 nm. The ternary complex was made anaerobic as described above and then titrated against a range of dioxygen concentrations (200 – 1000 μM final).

4.3 Results

Expression and Purification of the HPPD Variants. All HPPD variants mentioned in this study were expressed and purified using published methods for the wild type enzymes (5,17,18). All the variants studied yielded active enzymes and the yield was comparable to the wild-type enzyme.

Dissociation Constant for the Variant HPPD•Fe(II)•HPP Complexes. Each HPPD variant was titrated against HPP under anaerobic conditions to determine the dissociation constant. The physical signal for the association of HPP was the accumulation of weak metal-to-ligand charge transfer absorption bands that arise in the HPPD•Fe(II)•HPP complex (~500 nm). The absorption maximum of these transitions varied for each variant. Figure 4.2A depicts a difference spectra from the titration of S230A•Fe(II) against varied HPP concentrations. Figure 4.2B and C depict binding isotherms for N245Q, S230A, and N245A, P243T respectively. The $K_{d\ HPP}$ for each variant from binding isotherms were determined by fitting the data to equation 1 (Table 4.1).

Table 4.1 Substrate (HPP) Binding in Wild-type and Variants of HPPD

Variant	$K_{d\ HPP}$ (μM)
Wild-type HPPD	90 ± 3[a]
N245Q	78 ± 23
N245A	172 ± 56
N245S	118 ± 22
S230A	107 ± 41
P243T	269 ± 39

[a]Dissociation constant for wild-type was taken from reference 5.

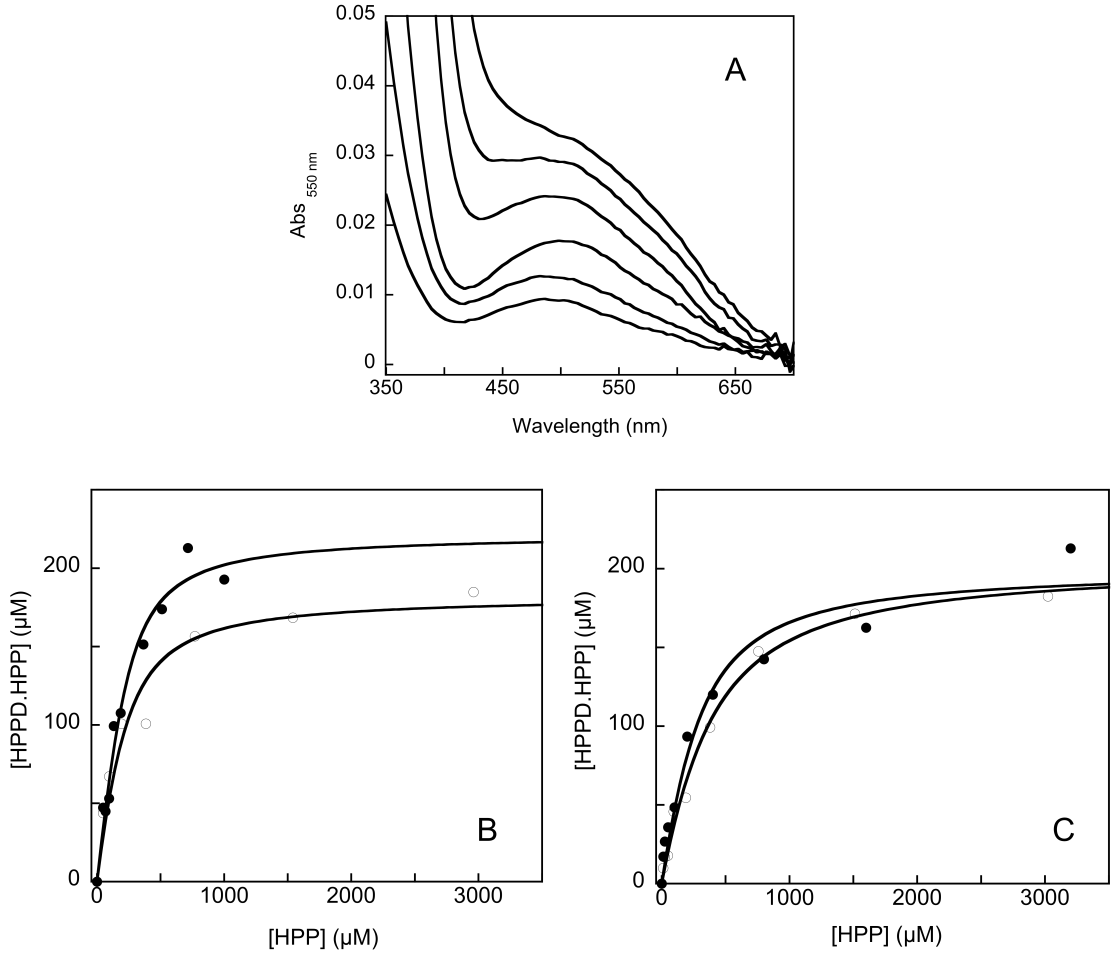

Figure 4.2 Binding isotherms for HPPD Variants at 4 °C. (A) An example difference spectra from the titration of 107 μM holo-S230A with HPP (48 – 2960 μM). (B) 220 μM N245Q•Fe(II) (●) titrated against HPP (12.5 – 1000 μM) and 180 μM S230A•Fe(II) (○) titrated against HPP (48 – 2960 μM) in 20mM HEPES, pH 7.0. The data were fit to equation 1. (C) 200 μM N245A•Fe(II) (●) titrated against HPP (12.5 – 3200 μM) and 180 μM P243T•Fe(II) (○) titrated against HPP (12.5 – 1000 μM) in 20mM HEPES, pH 7.0. The data were fit to equation 1.

The dissociation constant for wild-type HPPD•Fe(II)•HPP complex is 90 ± 3 μM (5). All the variants studied had a dissociation constant very similar to the wild-type HPPD with even the most pronounced difference, that for P243T, exhibiting only a three-fold decrease in affinity. This suggests that the residues altered have little direct energetic contribution to the HPPD•Fe(II)•HPP complex.

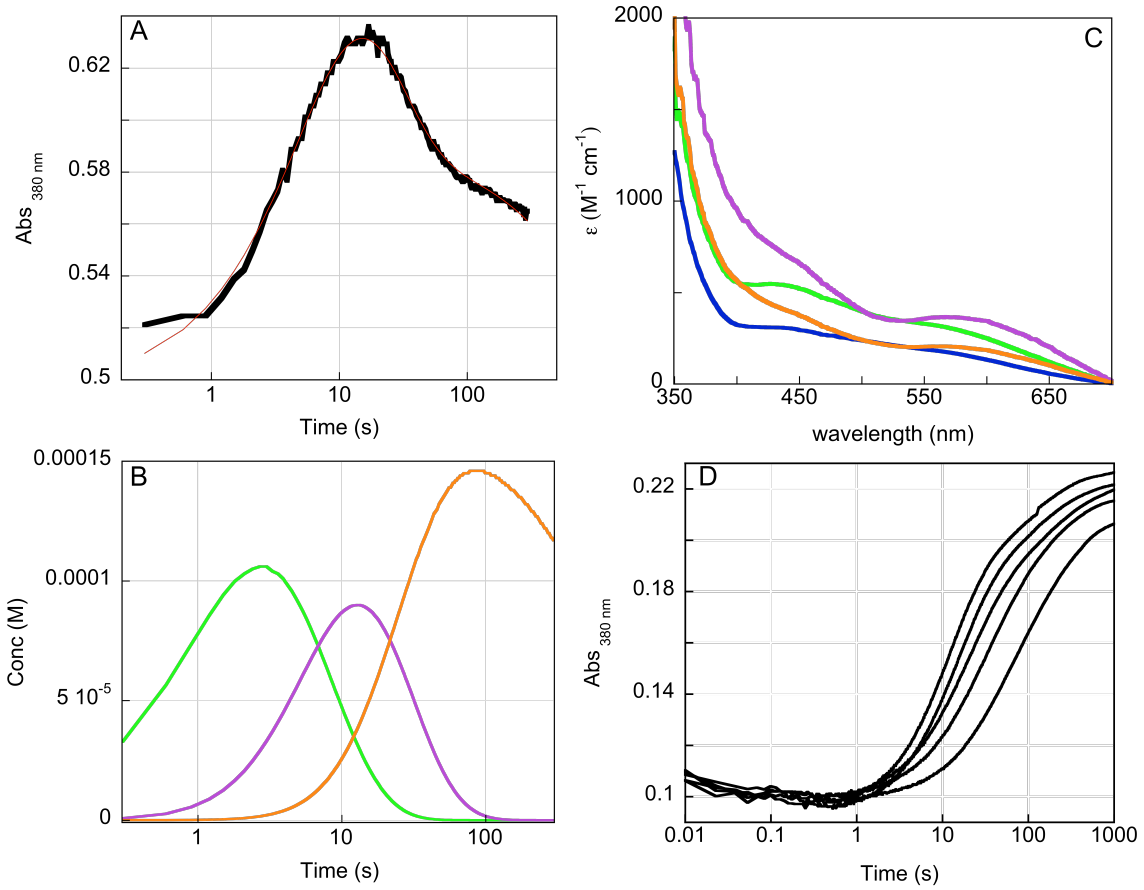

Figure 4.3 Kinetic data and fit for N245Q using pseudo-first-order reactant stoicheometry in the presence of saturating HPP (12). The reaction of the N245Q•Fe(II)•HPP complex (800 μM N245Q, 850 μM Fe(II) and 2.64 mM HPP) with 160 μM molecular oxygen at pH 7.0 and 4 °C can be seen in the figure. (A) 380 nm (black) stopped-flow trace observed with the fit (red) to the model described in Scheme 4.2. (B) Concentration profiles of species observed in a single turnover, where intermediate I is depicted in green, intermediate II in violet, intermediate III in orange. (Enzyme-substrate complex has been omitted due to its higher concentration.) (C) Deconvoluted intermediate spectra: N245Q•Fe(II)•HPP (blue), intermediate I (green), intermediate II (violet), intermediate III (orange). (D) N245Q•Fe(II)•HPP complex (40 μM final) titrated against various oxygen concentrations (200 – 1000 μM) increasing from right to left and observed at 380 nm, in 20 mM HEPES, pH 7.0 at 4 °C.

Single Turnover Reactions. Single turnover reaction kinetics indicated that only the N245Q variant exhibited intermediate accumulation. Limiting oxygen with respect to enzyme-substrate complex concentration allowed the establishment of approximate

pseudo-first-order conditions and confined the number of turnovers to one (for a 20% fraction of the enzyme sample). Figure 4.1 and Figure 4.3 show the deconvoluted intermediate spectra, intermediate concentration profiles and absorbance traces of wild-type HPPD and N245Q variant.

From the fit of the trace depicted in Figure 4.3A, the rate constants derived are; $k_1 = 1 \times 10^3\ M^{-1}\ s^{-1}$, $k_2 = 0.14\ s^{-1}$, $k_3 = 0.05\ s^{-1}$, and $k_4 = 0.002\ s^{-1}$ indicating three accumulating intermediates and assuming that the first event has a first order dioxygen dependence. However, the trace depicted in Figure 4.3A did not include the end of turnover that, based on the half-life of the slowest rate constant, would have occurred at approximately 2,500 seconds. The last rate constant (k_4) is significantly slower than the measured turnover number for this variant, which is 0.01 s^{-1} at 4 °C. This phenomenon will be discussed later in this chapter. Figure 4.1B shows the accumulation of three catalytic intermediates in wild-type HPPD. Both the rate constants and the spectra derived from the accumulation of the three intermediates in N245Q variant differ from those observed with WT HPPD. The comparison of the intermediate I (green) spectra from wild-type HPPD (Figure 4.1C) (12) and N245Q variant (Figure 4.3C), suggests a unique first transient in each enzyme. While in wild-type HPPD, intermediate I absorbs maximum at 370 and 480 nm with extinction coefficients of 2400 and 700 $M^{-1}\ cm^{-1}$ respectively (12), for the N245Q variant, intermediate I has absorption maxima of ~440 nm and ~550 nm with extinction coefficients of 550 and 330 $M^{-1}\ cm^{-1}$ respectively. Qualitatively, intermediate I has features similar to N245Q•Fe(II)•HPP complex (t_{zero} spectrum) but with more intense extinction coefficients. Intermediate II is the most strongly absorbing species with shoulders at 435 and 580 nm and respective extinction

coefficients of 670 and 370 M^{-1} cm^{-1}. This intermediate does not show absorption transitions that resemble any of the transients that are observed to accumulate in wild-type HPPD (Figure 4.1C). Intermediate III is the least intense of all species observed. This intermediate has shoulders at 445 and 560 nm with extinction coefficients of 400 and 200 M^{-1} cm^{-1} respectively. Intermediate III exhibits features very similar to intermediate II (Figure 4.1C), however, because we failed to observe an end of turnover for this variant, we only observed a fraction of the re-formation of the HPPD•Fe(II)•HPP charge-transfer transitions that arise with the dissociation of the product. The lack of data describing the latter stages of catalysis undermines the singular value decomposition algorithm's capacity to deconvolute the dataset. However, it is immediately apparent that the N245Q variant is dramatically slowed in turnover suggesting that the N245 position has critical participation at multiple stages of catalysis.

Figure 4.3D depicts oxygen dependence of the approach to the steady state for the reaction of N245Q. It is apparent that for WT HPPD and HMS the addition of dioxygen has been shown to be a second order reaction that does not include complexation (5,19). Figure 4.3D depicts traces for the reaction of N245Q with various dioxygen concentrations. It is visible that there is dioxygen dependence but the amplitude of the phase associated with dioxygen addition is very small relative to signals from turnoversuch that the dioxygen dependence cannot be determined definitively . The rate constants derived from single turnover reactions of N245Q are all dramatically slower than WT HPPD. The initial rate constant in which the enzyme reacts with dioxygen is at least two orders of magnitude slower than that observed in WT HPPD. This value is now only one order faster than autooxidation observed in the holoenzyme (*Streptomyces*

avermitilis HPPD (39 M^{-1} s^{-1}) (5), *Arabidopsis thaliana* HPPD (46 M^{-1} s^{-1}) (20) and *Amycolatopsis orientalis* HMS (34 M^{-1} s^{-1}) (19)). This indicates that for this variant k_1 is much less catalytically enhanced and is evidence that N245 plays an important role in substrate recognition and substrate as an effector for the dioxygen reaction.

4.4 Discussion

For wild-type HPPD, three intermediates were observed in pseudo-first order single turnover reactions (12). Johnson-winters et al, with the aid of kinetic isotope effects and fluorescence techniques were able to deduce the identity of the product complex and make reasonable speculation of the identity of the second intermediate as the dienone product tautomer complex. The primary objective of this study was to prepare and examine HPPD variants in the hope of unveiling new mechanistic details from single turnover studies and possibly identify variants more amenable to rapid freeze quench for the spectroscopic identification of transients. Residues implicated as key to hydroxylation regiospecificity were targeted. P243, N245 and S230 have been implicated as important positions for HPPD catalysis and hydroxylation regiospecificity. The latter two of these residues are thought to make unique hydrogen bonding arrangements with the substrate/intermediate phenolic hydroxyl group throughout catalysis (13). Interestingly, the dissociation constants measured for variants at these positions exhibited no pronounced difference from that measured for the wild-type HPPD. The primary observation was that for N245Q high accumulation of a first and second intermediate could be observed at greatly prolonged times suggesting that this variant is a candidate for intermediate trapping studies.

The N245Q variant was the only variant that exhibited significant intermediate accumulation. This variant accumulated three intermediates in single turnover reactions. All three intermediates have unique absorption transitions with respect to the intermediates observed with the wild-type HPPD (Figure 4.1C and 4.3C). This plausibly suggests that new intermediates accumulate in single turnover reactions of this variant. Intermediate I depicts a maximum accumulation of 67% at 2.8 s, intermediate II accumulated maximum to 56% at 13 s, while intermediate III had maximum accumulation of 92% at 85 s. These prolonged time points and high fractional accumulations make this variant an excellent candidate for a rapid freeze quench for the spectroscopic identification of new intermediates for the HPPD reaction coordinate. However, this may not allow us to observe the native chemistry as the, N245Q variant shows a different product profile relative to the wild-type HPPD. This variant makes three different products, 52 % homogentisate (HG, native product), 45 % 4-hydroxyphenylacetate (HPA, singly oxygenated and decarboxylated product) and 3 % quinolacetate (QAA, doubly oxygenated anddecarboxylated but without substituent migration). As such the steps that occur after the formation of the hydroxylating intermediate bifurcate (roughly evenly) along unique paths diminishing the actual accumulation of catalytic species involved in the native chemistry that forms HG. With the production of 45% of HPA, ~100% of the enzyme is able to accomplish the decarboxylation half-reaction that yields the putative ferryl-oxo species. The reactive ferry-oxo species can potentially hydroxylate any proximal active site residue. This self-hydroxylation phenomenon has been observed earlier with other α-KAOs (21-24). In

order to establish true fractional accumulations the fate of ~25% of the oxygen atoms must be accounted for.

The dramatically slowed rate constant for the addition of dioxygen indirectly hints at the plausible function of this residue in orienting the substrate HPP in the active site. In prior work it has been shown that flattening of the α-keto acid of HPP in the HPPD•Fe(II)•HPP complex is critical for heightened dioxygen reactivity (24-26). The ~100-fold slower rate constant for dioxygen addition observed with this variant may be a consequence of an inability to define this reactive conformation at the α-keto acid moiety in the substrate complex. However, this assertion needs to be studied in depth using CD and MCD spectroscopies. The observation that the last rate constant observed in single turnover experiments is significantly slower than the measured turnover number, suggests that in the pre-steady state we observed the slower of two linked catalytic cycles that both regenerate active enzyme(Scheme 4.4). One cycle forms HG and is slow while the other forms HPA from a abortive process associated with more rapid steps that occurs in one half of turnovers. This phenomenon would yield a turnover number based solely on dioxygen consumption that is roughly equivalent to one half of the rate constant observed for the step that bifurcates. In this case approximately equal to one half of k_2 (0.14 s^{-1}).

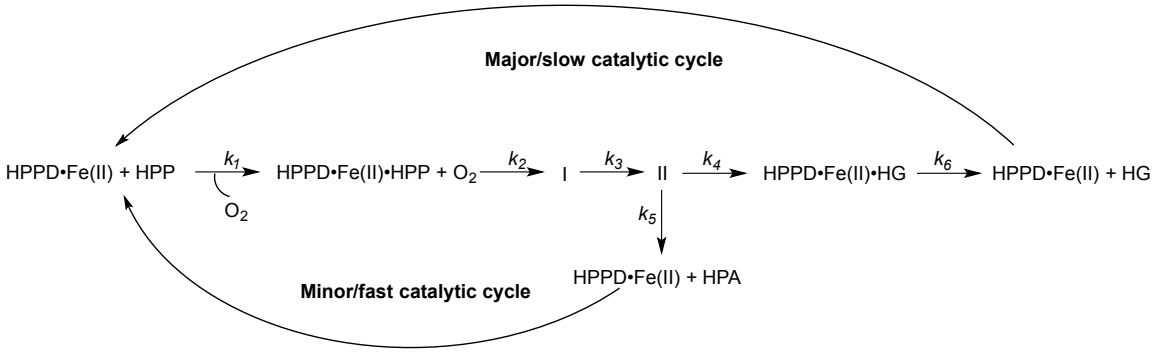

Scheme 4.4 The kinetic model for a single catalytic cycle of N245Q

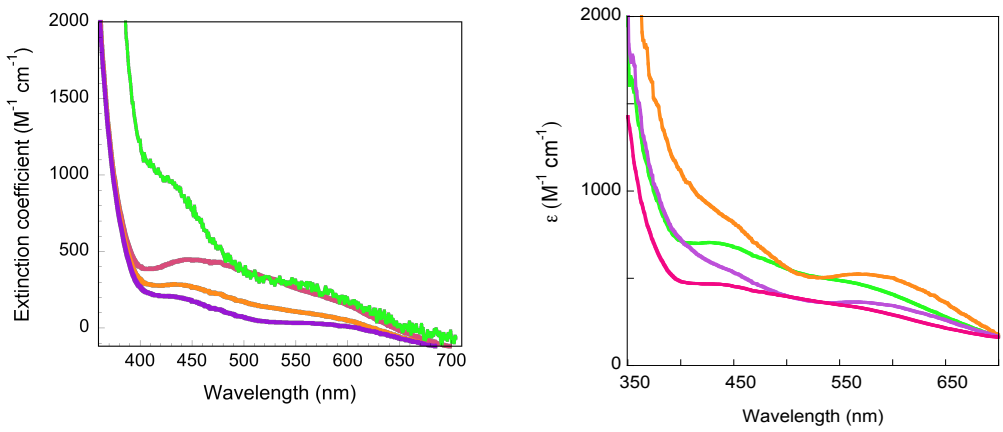

Figure 4.4 Deconvoluted intermediate spectra for HMS and N245Q HPPD. On the left, the intermediate spectra from the single turnover reaction of HMS are demonstrated (This figure is taken from reference (19)). For HMS, intermediate I is depicted in green, intermediate II is orange, intermediate III is violet and HMS•Fe(II)•HPP complex is pink. On the right, the intermediate spectra from the single turnover reaction of N245Q HPPD are demonstrated. For N245Q, intermediate I is depicted in green, intermediate II is orange, intermediate III is violet and HMS•Fe(II)•HPP complex is pink.

The deconvoluted intermediate spectra from N245Q HPPD were also compared to those obtained from the single-turover reactions of hydroxymandelate synthase (HMS) (19), the sister enzyme of HPPD (see chapters 1,2 &3). This comparison exhibited one striking similarity among the deconvoluted spectra observed (Figure 4.4). The spectral

comparison between the intermediate I from HMS and intermediate II from N245Q, suggested a common intermediate that occurs in the catalytic cycle of both enzymes. However, intermediates I and III for N245Q did not show any similarities to the first and third intermediate in HMS. Interestingly, N245Q HPPD does not form HMA (hydroxymandelate-product of HMS reaction), and intermediate II for N245Q is similar to the intermediate I in HMS. This qualitatively suggests that intermediate II arises prior to or is the ferryl-oxo species that is common to both enzymes. For N245Q, the decay of intermediate III is concomitant with the re-formation of the fraction of the charge-transfer complex.

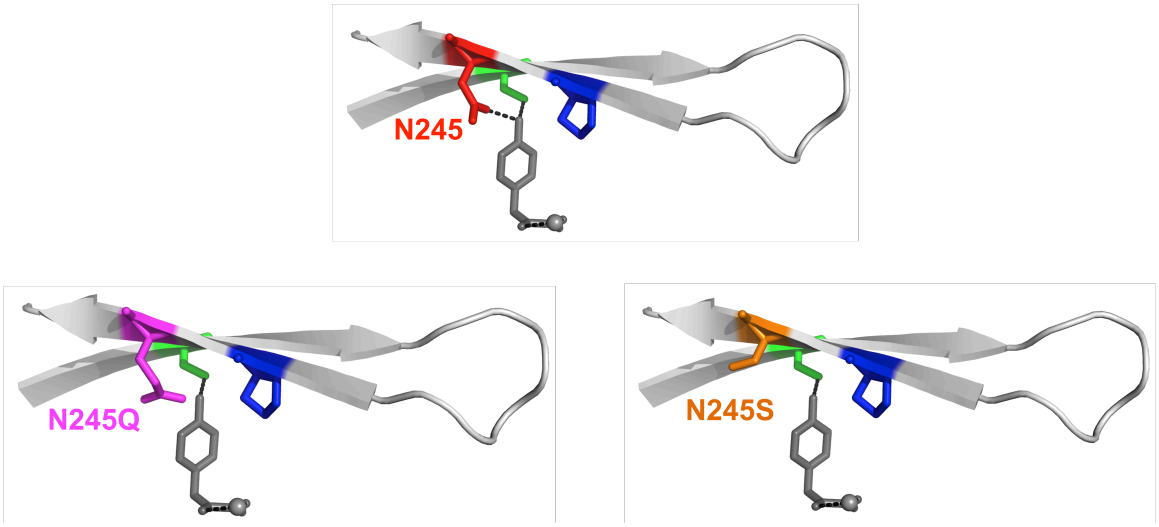

Figure 4.5 N245 position in HPPD wild-type and variants. N245 position in the wild-type has been taken from (13). N245 variants, N245Q and N245S have been generated with PyMOL using wild-type structure with substrate modeled into the active site (13).

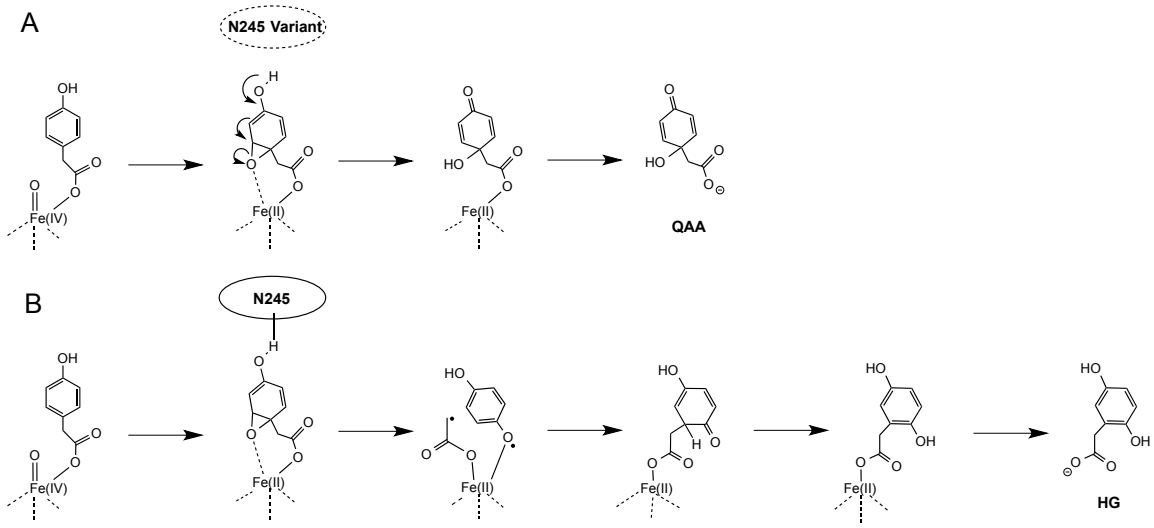

Scheme 4.5 Alternative products in the variants of N245 position in HPPD. (A) The available trajectory for the electron movement in the substrate aromatic ring for N245 variants in the absence of native hydrogen bond. (B) Native reaction in the presence of the hydrogen bond between the substrate hydroxyl group and N245 position in HPPD.

As predicted from the structure of wild-type HPPD, N245 is thought to make a hydrogen-bond with the substrate hydroxyl group. We have observed alternate products in N245 variants, N245S (14) and N245Q (Chapter 2) (17) (Figure 4.5). N245S forms ~80% QAA, whereas N245Q forms ~3% QAA in a mixture of total products. One hypothesis for the formation of these alternative products is that, the native hydrogen bond with N245 residue abolishes the movement of the electrons back into the substrate aromatic ring from the phenol hydroxyl group (Scheme 4.5B) and thus prevents the formation of QAA. In N245 variants, the absence of or an improperly formed hydrogen-bond would permit electrons from the Ph-O-H bond to delocalize into the aromatic ring for a fraction of total turnover forming QAA. This fraction would be higher in the complete absence of a hydrogen-bond as seen in N245S, whereas it would be lower in the presence of an improperly formed hydrogen-bond which could be the case with N245Q.

Collectively these data suggests that N245 plays unique important roles at multiple stages of catalysis; initially promoting dioxygen reactivity in the HPPD•Fe(II)•HPP complex and then limiting the chemical outcomes by localizing the phenol hydroxyl electrons prior to the NIH shift step.

Acknowledgments

Graham R. Moran helped with experimental design and preparation of this document.

4.5 References

1. Lindstedt, S., Holme, E., Lock, E. A., Hjalmarson, O., and Strandvik, B. (1992) Treatment of hereditary tyrosinaemia type I by inhibition of 4-hydroxyphenylpyruvate dioxygenase. *Lancet* **340**, 813-817
2. Hausinger, R. P. (2004) FeII/alpha-ketoglutarate-dependent hydroxylases and related enzymes. *Crit Rev Biochem Mol Biol* **39**, 21-68
3. Costas, M., Mehn, M. P., Jensen, M. P., and Que, L. (2004) Dioxygen activation at mononuclear nonheme iron active sites: Enzymes, models, and intermediates. *Chemical Reviews* **104**, 939-986
4. Gunsior, M., Ravel, J., Challis, G. L., and Townsend, C. A. (2004) Engineering p-hydroxyphenylpyruvate dioxygenase to a p-hydroxymandelate synthase and evidence for the proposed benzene oxide intermediate in homogentisate formation. *Biochemistry* **43**, 663-674
5. Johnson-Winters, K., Purpero, V. M., Kavana, M., Nelson, T., and Moran, G. R. (2003) (4-Hydroxyphenyl)pyruvate Dioxygenase from Streptomyces avermitilis: The Basis for Ordered Substrate Addition. *Biochemistry* **42**, 2072-2080
6. Elkins, J. M., Ryle, M. J., Clifton, I. J., Dunning Hotopp, J. C., Lloyd, J. S., Burzlaff, N. I., Baldwin, J. E., Hausinger, R. P., and Roach, P. L. (2002) X-ray

crystal structure of Escherichia coli taurine/alpha-ketoglutarate dioxygenase complexed to ferrous iron and substrates. *Biochemistry* **41**, 5185-5192.

7. Price, J. C., Barr, E. W., Tirupati, B., Bollinger, J. M., Jr., and Krebs, C. (2003) The first direct characterization of a high-valent iron intermediate in the reaction of an alpha-ketoglutarate-dependent dioxygenase: a high-spin FeIV complex in taurine/alpha-ketoglutarate dioxygenase (TauD) from Escherichia coli. *Biochemistry* **42**, 7497-7508
8. Ryle, M. J., Padmakumar, R., and Hausinger, R. P. (1999) Stopped-Flow Kinetic Analysis of Escherichia coli Taurine/alpha- Ketoglutarate Dioxygenase: Interactions with alpha-Ketoglutarate, Taurine, and Oxygen. *Biochemistry* **38**, 15278-15286
9. Borowski, T., Bassan, A., and Siegbahn, P. E. M. (2004) 4-hydroxyphenylpyruvate dioxygenase: A hybrid density functional study of the catalytic reaction mechanism. *Biochemistry* **43**, 12331-12342
10. Hoffart, L. M., Barr, E. W., Guyer, R. B., Bollinger, J. M., Jr., and Krebs, C. (2006) Direct spectroscopic detection of a C-H-cleaving high-spin Fe(IV) complex in a prolyl-4-hydroxylase. *Proceedings of the National Academy of Sciences of the United States of America* **103**, 14738-14743
11. Galonic, D. P., Barr, E. W., Walsh, C. T., Bollinger, J. M., Jr., and Krebs, C. (2007) Two interconverting Fe(IV) intermediates in aliphatic chlorination by the halogenase CytC3. *Nat Chem Biol* **3**, 113-116
12. Johnson-Winters, K., Purpero, V. M., Kavana, M., and Moran, G. R. (2005) Accumulation of Multiple Intermediates in the Catalytic Cycle of (4-Hydroxyphenyl)pyruvate Dioxygenase from Streptomyces avermitilis. *Biochemistry* **44**, 7189-7199
13. Brownlee, J., He, P., Moran, G. R., and Harrison, D. H. (2008) Two roads diverged: the structure of hydroxymandelate synthase from Amycolatopsis orientalis in complex with 4-hydroxymandelate. *Biochemistry* **47**, 2002-2013
14. Brownlee, J. M., Heinz, B., Bates, J., and Moran, G. R. (2010) Product analysis and inhibition studies of a causative Asn to Ser variant of 4-

hydroxyphenylpyruvate dioxygenase suggest a simple route to the treatment of Hawkinsinuria. *Biochemistry* **49**, 7218-7226

15. Serre, L., Sailland, A., Sy, D., Boudec, P., Rolland, A., Pebay-Peyroula, E., and Cohen-Addad, C. (1999) Crystal structure of Pseudomonas fluorescens 4-hydroxyphenylpyruvate dioxygenase: an enzyme involved in the tyrosine degradation pathway. *Structure Fold Des* **7**, 977-988
16. O'Hare, H. M., Huang, F., Holding, A., Choroba, O. W., and Spencer, J. B. (2006) Conversion of hydroxyphenylpyruvate dioxygenases into hydroxymandelate synthases by directed evolution. *FEBS Lett* **580**, 3445-3450
17. Shah, D. D., Conrad, J. A., Heinz, B., Brownlee, J. M., and Moran, G. R. (2011) Evidence for the mechanism of hydroxylation by 4-hydroxyphenylpyruvate dioxygenase and hydroxymandelate synthase from intermediate partitioning in active site variants. *Biochemistry* **50**, 7694-7704
18. Shah, D. D., Conrad, J. A., and Moran, G. R. (2013) Intermediate partitioning kinetic isotope effects for the NIH shift of 4-hydroxyphenylpyruvate dioxygenase and the hydroxylation reaction of hydroxymandelate synthase reveal mechanistic complexity. *Biochemistry* **52**, 6097-6107
19. He, P., Conrad, J. A., and Moran, G. R. (2010) The rate-limiting catalytic steps of hydroxymandelate synthase from Amycolatopsis orientalis. *Biochemistry* **49**, 1998-2007
20. Purpero, V. M., and Moran, G. R. (2006) Catalytic, noncatalytic, and inhibitory phenomena: kinetic analysis of (4-hydroxyphenyl)pyruvate dioxygenase from Arabidopsis thaliana. *Biochemistry* **45**, 6044-6055
21. Ryle, M. J., Koehntop, K. D., Liu, A. M., Que, L., and Hausinger, R. P. (2003) Interconversion of two oxidized forms of taurine/alpha-ketoglutarate dioxygenase, a non-heme iron hydroxylase: Evidence for bicarbonate binding. *Proceedings of the National Academy of Sciences of the United States of America* **100**, 3790-3795
22. Ryle, M. J., Liu, A., Muthukumaran, R. B., Ho, R. Y., Koehntop, K. D., McCracken, J., Que, L., Jr., and Hausinger, R. P. (2003) O2- and alpha-ketoglutarate-dependent tyrosyl radical formation in TauD, an alpha-keto acid-dependent non-heme iron dioxygenase. *Biochemistry* **42**, 1854-1862

23. Liu, A., Ho, R. Y., Que, L., Ryle, M. J., Phinney, B. S., and Hausinger, R. P. (2001) Alternative Reactivity of an alpha-Ketoglutarate-Dependent Iron(II) Oxygenase: Enzyme Self-Hydroxylation. *J Am Chem Soc* **123**, 5126-5127

24. Purpero, V., and Moran, G. R. (2007) The diverse and pervasive chemistries of the alpha-keto acid dependent enzymes. *J Biol Inorg Chem* **12**, 587-601

25. Pavel, E. G., Zhou, J., Busby, R. W., Gunsior, M., Townsend, C. A., and Solomon, E. I. (1998) Circular Dichroism and Magnetic Circular Dichroism Spectroscopic Studies of the Non-Heme Ferrous Active Site in Clavaminate Synthase and Its Interaction with alpha-Ketoglutarate Cosubstrate. *J. Am. Chem. Soc.* **120**, 743-753

26. Neidig, M. L., Kavana, M., Moran, G. R., and Solomon, E. I. (2004) CD and MCD Studies of the Non-Heme Ferrous Active Site in (4-Hydroxyphenyl)pyruvate Dioxygenase: Correlation Between Oxygen Activation in the Extradiol and alpha-KG Dependent Dioxygenases. *J Am Chem Soc* **126**, 4486-4487

Personal:

Name: Dhara D. Shah
Address: Department of Chemistry and Biochemistry,
UW-Milwaukee, 3210 N. Cramer Ave.,
Milwaukee, WI – 53201.

Education:

PhD in Biochemistry: 2009 to current.
Department of Chemistry and Biochemistry, University of Wisconsin-Milwaukee
Dissertation: Mechanism of the hydroxylation reactions catalyzed by 4-Hydroxyphenylpyruvate Dioxygenase and Hydroxymandelate Synthase.

Masters degree in Biochemistry: 2006-2008.
Department of Biochemistry, The Maharaja Sayajirao University of Baroda, India
Dissertation: Characterization of antibiotic biosynthesis cluster deletion mutant of '*Streptomyces flavisclerotic*us'.

Undergraduate degree: 2003-2006.
Major: Biochemistry
Gujarat University, Gujarat, India.

Publications:

1. **Dhara D. Shah** and Graham R. Moran (2014). 4-Hydroxyphenylpyruvate Dioxygenase and Hydroxymandelate Synthase: 2-Oxo Acid-Dependent Oxygenases of Importance to Agriculture and Medicine. *2-Oxoglutarate-Dependent Oxygenases (Schofield C. J. and Hausinger R. P. Eds.), In press.*

2. Brett A. Beaupre, Brenton R. Carmichael, Matthew R. Hoag, **Dhara D. Shah** and Graham R. Moran (2013) Renalase is an α-NAD(P)H Oxidase/Anomerase. *J. Am. Chem. Soc. 135,13980-13987. (Article featured in JACS spotlights 18 September 2013)*

3. **Dhara D. Shah**, John A. Conrad and Graham R. Moran (2013) Intermediate Partitioning Kinetic Isotope Effects for the NIH shift of 4-Hydroxyphenylpyruvate Dioxygenase and the Hydroxylation Reaction of Hydroxymandelate Synthase Reveal Mechanistic Complexity. *Biochemistry 52,6097-6107*.

4. **Dhara D. Shah**, John A. Conrad, Brian Heinz, June M. Brownlee and Graham R. Moran (2011) Evidence for the Mechanism of Hydroxylation by 4-Hydroxyphenylpyruvate Dioxygenase and Hydroxymandelate Synthase from Intermediate Partitioning in Active Site Variants. *Biochemistry 50,7694-7704.*

5. Matthew R. Hoag, **Dhara D. Shah**, Brenton R. Carmichael and Graham R. Moran. Characterization of Renalase Active Site Variants. *Manuscript in preparation.*

6. Karen Crozier-Reabe, **Dhara D. Shah** and Graham R. Moran. Evidence for Proton Movements in the Catalytic Cycle of Kynurenine-3-monooxygenase from *Pseudomonas aeruginosa. Manuscript in preparation.*

Poster Presentations:

1. On the Mechanism of Hydroxylation in the Two-Substrate alpha-Keto Acid Dependent Oxygenases.
Dhara D. Shah, John A. Conrad and Graham R. Moran. Presented at the 33rd Midwest Enzyme Conference, Loyola University Chicago, IL, Oct. 2013. **(Selected as the best poster at MECC 2013)**

2. On the Mechanism of Hydroxylation in the Two-Substrate alpha-Keto Acid Dependent Oxygenases.
Dhara D. Shah, Brett A. Beaupre, John A. Conrad and Graham R. Moran. Presented at the 32nd Midwest Enzyme Conference, University of Illinois-Chicago, IL, Oct. 2012.

3. The Mechanism of Hydroxylation by Two-Substrate Alpha-Keto Acid Dioxygenases from Intermediate Partitioning in Active Site Variants.
Dhara D. Shah, John A. Conrad, Brian Heinz, June M. Brownlee and Graham R. Moran Presented at the Gordon Isotopes in Biological & Chemical Sciences Conference, Galveston, TX. Feb. 2012.

4. Evidence for the Mechanism of Hydroxylation by 4-Hydroxyphenylpyruvate Dioxygenase and Hydroxymandelate Synthase from Intermediate Partitioning in Active Site Variants.
Dhara D. Shah, John A. Conrad, Brian Heinz, June M. Brownlee and Graham R. Moran Presented at the Enzymes, Coenzymes, and Metabolic Pathways, Zing Conference, Cancun, Mex. Dec 2011.

5. Evidence for the Mechanism of Hydroxylation by 4-Hydroxyphenylpyruvate Dioxygenase and Hydroxymandelate Synthase from Intermediate Partitioning in Active Site Variants.
Dhara D. Shah, John A. Conrad, Brian Heinz, June M. Brownlee and Graham R. Moran Presented at the 31st Midwest Enzyme Conference, University of Illinois, Chicago, IL, Oct. 2011.

6. Evidence for the Mechanism of Hydroxylation by 4-Hydroxyphenylpyruvate Dioxygenase and Hydroxymandelate Synthase from Intermediate Partitioning in Active Site Variants.
Dhara D. Shah, John A. Conrad, Brian Heinz, June M. Brownlee and Graham R. Moran. Presented at the Enzymes, Coenzymes, and Metabolic Pathways Gordon Conference,

Waterville, NH. July 2011.

7. Functional Assignment of the N245 Residue of 4-Hydroxyphenylpyruvate Dioxygenase from Streptomyces avermitilis: A Key Residue in Hydroxylation Regiospecificity.
June M. Brownlee, **Dhara D. Shah** and Graham R. Moran. Presented at The 22nd Enzyme Mechanism Conference, St. Petes Beach, FL, 2011.

Awards/honors:

1. Best Poster Award, Midwest Enzyme Chemistry Conference, Chicago, IL. 2013
2. McFarland Graduate Research Award for the Department of Chemistry and Biochemistry awards day, University of Wisconsin-Milwaukee. 2013
3. Keulks Graduate Research Award for the Department of Chemistry and Biochemistry awards day, University of Wisconsin-Milwaukee. 2011
4. UW-Milwaukee Graduate School Travel award. 2011
5. UW-Milwaukee Chancellors Graduate award. 2009-present.
6. Junior Research Fellowship and National Eligibility Test (JRF/NET) from Council for Scientific and Industrial Research (CSIR), India. 2009.

Teaching and Organizational Experience:

- Graduate teaching Assistant, UW-Milwaukee. Courses taught:

CHEM 103 (Discussion & Lab): Survey of Biochemistry. Summer 2013.
CHEM 603 (Lab): Introduction to Biochemistry Laboratory. Spring 2014, Spring 2013, Spring 2012, Fall 2012, Spring 2010.
CHEM 105 (Discussion & Lab): General Chemistry for Engineering. Fall 2010.
CHEM 102 (Discussion & Lab): General Chemistry. Fall 2013, Fall 2009.

- Officer for Chemistry & Biochemistry Graduate Student Council. Fall 2011 to Spring 2012.
- Mentor for teaching assistants, Department of Chemistry & Biochemistry, UW-Milwaukee. Fall 2013, Spring 2014.